ELECTRICAL CHARACTERISTICS OF MONOPOLE ANTENNAS ABOVE A RECTANGULAR PRISM

Charles Thomas Ristorcelli

Report Number NPS52Ab75121

NAVAL POSTGRADUATE SCHOOL
Monterey, California

THESIS

ELECTRICAL CHARACTERISTICS
OF MONOPOLE ANTENNAS
ABOVE A RECTANGULAR PRISM

by

Charles Thomas Ristorcelli

December 1975

Thesis Advisor: R. W. Adler

Approved for public release; distribution unlimited.
Prepared for: Naval Ship Engineering Center
Hyattsville MD 20782
and Naval Electronics Laboratory Center
San Diego, CA 92152

Electrical Characteristics of Monopole Antennas Above a Rectangular Prism

by

Charles Thomas Ristorcelli
Lieutenant, United States Navy
B.S., Northrop Institute of Technology, 1968

Submitted in partial fulfillment of the requirements for the degree of

ELECTRICAL ENGINEER

from the

NAVAL POSTGRADUATE SCHOOL
December 1975

UNCLASSIFIED
SECURITY CLASSIFICATION OF THIS PAGE *(When Data Entered)*

REPORT DOCUMENTATION PAGE		READ INSTRUCTIONS BEFORE COMPLETING FORM
1. REPORT NUMBER NPS-52Ab75121	2. GOVT ACCESSION NO.	3. RECIPIENT'S CATALOG NUMBER
4. TITLE *(and Subtitle)* Electrical Characteristics of Monopole Antennas Above a Rectangular Prism		5. TYPE OF REPORT & PERIOD COVERED Final Report 1 Feb 75 - 1 Dec 75 6. PERFORMING ORG. REPORT NUMBER
7. AUTHOR(s) Charles Thomas Ristorcelli in conjunction with Richard William Adler		8. CONTRACT OR GRANT NUMBER(s)
9. PERFORMING ORGANIZATION NAME AND ADDRESS Naval Postgraduate School Monterey, California 93940		10. PROGRAM ELEMENT, PROJECT, TASK AREA & WORK UNIT NUMBERS
11. CONTROLLING OFFICE NAME AND ADDRESS Naval Ship Engineering Center Hyattsville, MD 20782; and Naval Electronics Laboratory Center, San Diego		12. REPORT DATE December 1975 13. NUMBER OF PAGES 124
14. MONITORING AGENCY NAME & ADDRESS *(if different from Controlling Office)* CA 92157.		15. SECURITY CLASS. *(of this report)* Unclassified 15a. DECLASSIFICATION/DOWNGRADING SCHEDULE
16. DISTRIBUTION STATEMENT *(of this Report)* Approved for public release; distribution unlimited.		
17. DISTRIBUTION STATEMENT *(of the abstract entered in Block 20, if different from Report)*		
18. SUPPLEMENTARY NOTES		
19. KEY WORDS *(Continue on reverse side if necessary and identify by block number)* Surface Charge and Current Distribution. Monopole Admittance. Monopole Electrical Characteristics		

20. ABSTRACT *(Continue on reverse side if necessary and identify by block number)*

A scaled model of an idealized superstructure was used to support an electrically thin radiating monopole antenna. The surface charge and current distributions on the antenna were measured, and with the resulting data, the antenna's apparent admittance was calculated. The procedures for measurements of surface distributions on antennas were then modified to permit similar measurements on flat metallic surfaces, and with the

DD FORM 1 JAN 73 1473 EDITION OF 1 NOV 65 IS OBSOLETE
S/N 0102-014-6601 |
(Page 1)

UNCLASSIFIED
SECURITY CLASSIFICATION OF THIS PAGE *(When Data Entered)*

(20. ABSTRACT Continued)

modified techniques the surface charge and current distributions were obtained for the vertical sides of the model superstructure.

The results of the measurements provide benchmark data for use in connection with the application of numerical techniques for the analysis of geometrical configurations similar to the model used in the experiment.

NAVAL POSTGRADUATE SCHOOL
Monterey, California

Rear Admiral Isham W. Linder
Superintendent

Jack R. Borsting
Provost

This thesis was prepared in conjunction with research supported in part by project numbers NAVSEA WR-52221 and NELC WR-00116.

ABSTRACT

A scaled model of an idealized ship superstructure was used to support an electrically thin radiating monopole antenna. The surface charge and current distributions on the antenna were measured, and with the resulting data, the antenna's apparent admittance was calculated. The procedures for measurements of surface distributions on antennas were then modified to permit similar measurements on flat metallic surfaces, and with the modified techniques the surface charge and current distributions were obtained for the vertical sides of the model superstructure.

The results of the measurements provide benchmark data for use in connection with the application of numerical techniques for the analysis of geometrical configurations similar to the model used in the experiment.

TABLE OF CONTENTS

ACKNOWLEDGMENT

I wish to express my most sincere admiration and thanks to Mr. Frank Abbe and ETl Thomas Nowak, of the Naval Postgraduate School staff, for their efforts in machining the equipment required to conduct the measurements incident to this research. I can truly say they made the seemingly impossible appear almost routine.

Finally I wish to dedicate this thesis to my wife Elinor. She assisted me during all the data acquisition, proofread the manuscript, and without her love, support, and devotion this research would never have been so personally rewarding.

I. INTRODUCTION

A. PROBLEM DEFINITION

The research effort described in this thesis was conducted with two fundamental objectives. First was the introduction to the Naval Postgraduate School of the machining techniques and instrumentation requirements necessary to pursue the measurement of the electrical characteristics and the surface current and charge distributions, on antennas and their supporting structures. Second was to experimentally measure the admittance and relative magnitude and phase of the axial distribution of current and charge on transmitting monopole antennas and on the vertical sides of a metallic box supporting the antenna.

B. MOTIVATION FOR THE EXPERIMENT

The analytical solution for the electrical characteristics of antennas relies heavily upon geometrical simplifications to attain mathematical answers in closed form. In the most direct approach, and relative to the operating wavelength, antenna supporting platforms are considered infinitely large, whereas the radiating monopole is considered infinitely thin, allowing a "filament of current" to replace the antenna.

In the majority of naval applications, antennas are located aboard ship in a geometrical configuration where the above simplifications are no longer applicable when attempting to mathematically analyze the antenna characteristics. To

quantify the shipboard geometry consider the following typical ship dimensions relative to an operating frequency of 6 MHz [Reference 1]:

USS Schofield (FFG-3):	Length	126.3 m (2.52 λ)
	Beam	13.5 m (0.27 λ)
USS Exultant (MSO-441):	Length	57.3 m (1.15 λ)
	Beam	12.0 m (0.24 λ)

A significant effort is presently underway to develop numerical techniques which, when applied in conjunction with large digital computers, will provide solutions for the electrical characteristics of antennas located aboard ship.

In order to obtain experimental measurements of electrical characteristics of an antenna in an environment similar to that described above, a scaled model of a radiating monopole antenna located aboard ship was constructed with dimensions which are explained later in this report. Because the structure chosen as a model necessarily ignores the problems of mutual coupling between several antennas, as well as between the ship's superstructure and any antenna under consideration, it was understood that the measurements resulting from this experiment, although not directly applicable to a particular shipboard geometry, would nevertheless yield the correct values for a configuration sufficiently

arbitrary to be of particular interest for analysis by a numerical solution method.

In addition to the antenna measurements, it was of interest to obtain an initial measure of the distribution of surface charge and current on the sides of the box supporting the driven monopoles, as very little is known about the effects the sharp edges found on this structure will have upon these distributions, especially in the vicinity of the driving point. The information resulting from these measurements would be of help in understanding the conditions that must be satisfied for the analytical solution of the electric fields associated with similar geometries.

C. APPLICATIONS

The measurements obtained in this experimental effort have two principal applications. First, the measured admittance of the monopole antennas above the box provides a quantitative check for the result of admittance calculations on similar structures using existing numerical techniques. And second, the measured surface charge and current distributions on the sides of the box supporting the driven antenna will provide insight into the conditions that must be resolved in the development of numerical analysis techniques for the solution of electrical characteristics of antennas associated with arbitrary geometrical structures.

II. EXPERIMENTAL SET-UP

A. IMAGE PLANE

The development of the equipment to pursue the measurements of interest was coincidental with the construction of an image plane at the Naval Postgraduate School. This image plane is a 10 meter square aluminum surface which serves as roof for a room in which the measuring equipment is located, providing isolation between the antenna undergoing measurement and the associated instrumentation. The image plane and final model for the measurements is shown in Figure 1.

The importance of a well designed image plane can best be understood by considering the effect of the ocean surface in the analysis of shipboard antennas. At the frequencies of principal interest (2-32 MHz) sea water skin depth is less than 0.5% the wavelength. The surface of the ocean then appears as an image plane with respect to a shipboard mounted antenna, and this analogy is preserved in the model chosen for measurement.

On the image plane surface, slightly offset from the center, is an 8" diameter circular aperture, which can accomodate antennas whose electrical characteristics are to be experimentally determined, or else provides access to structures placed above the image plane. Offsetting the aperture insures that the possibility of resonances along the image plane surface is minimized, especially in the

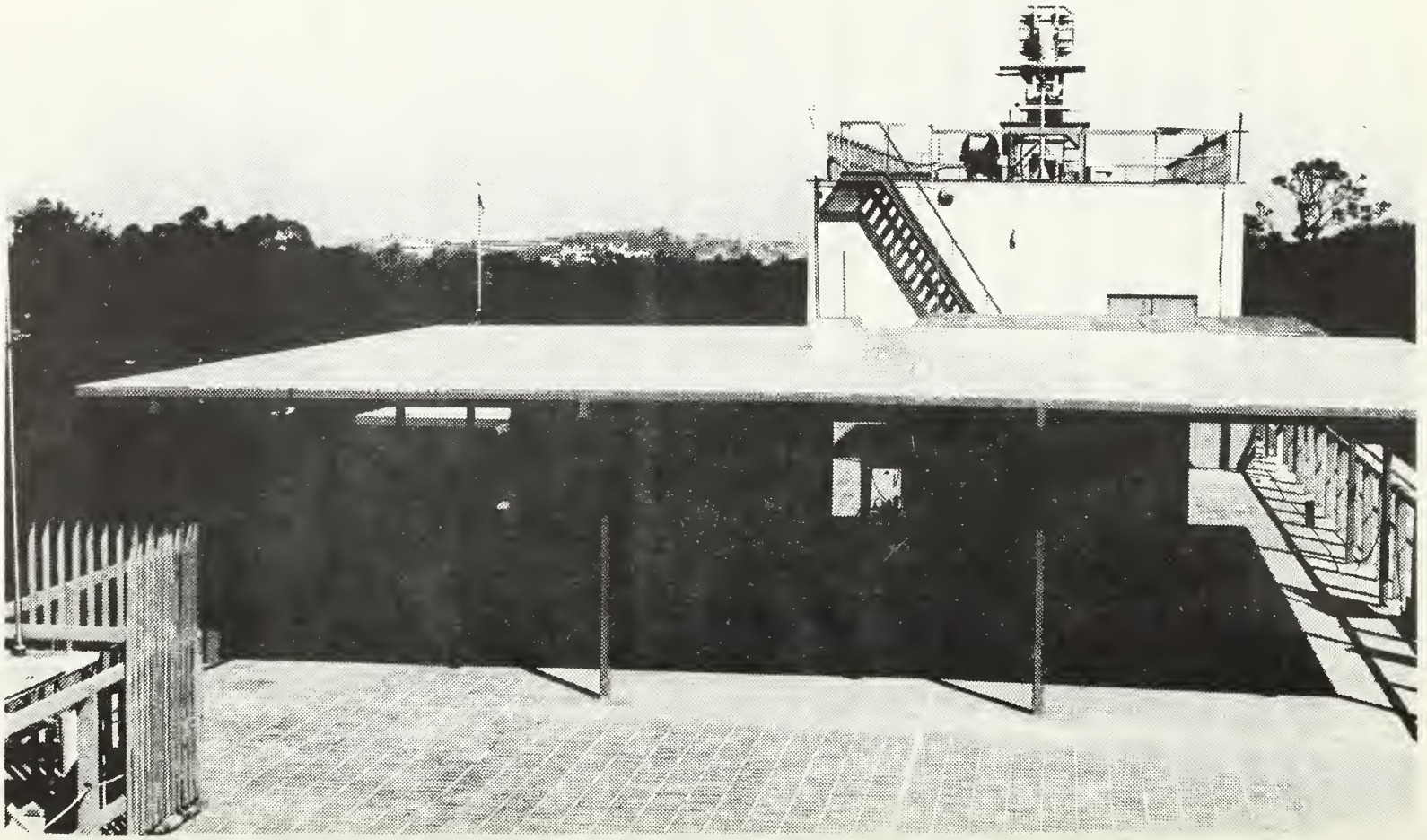

FIGURE 1. Image Plane with Measurement Model

event that measurements are performed on antennas whose feed line is connected directly to and is flush with the image plane aperture, as would be the case with a base driven monopole.

B. SUPPORTING STRUCTURE

In designing the box to support the monopoles to be measured, the decisions for the box dimensions were motivated by several considerations. It was necessary to preserve dimensions relative to measurement wavelength which would approximate "typical" shipboard sizes, while simultaneously providing an object easily machinable by the facilities existing at the Naval Postgraduate School. It was also desirable to examine a configuration which would be closely related to a numerical study. A consultation with the Naval Electronics Laboratory Center indicated that such a study of a radiating monopole (35' whip antenna) located above a patrol gunboat (PPG) was in progress. The gunboat had been modeled by a wire grid box of dimensions 60' x 20' x 16' at an operating frequency of 6 MHz. This model was chosen for the experimental investigation, scaling all the dimensions in wavelength relative to a frequency of 100 MHz.

The box was constructed of 3/4" aluminum sheets on the sides, and 1/4" aluminum on the top, with twenty slots machined in two of the vertical sides. The resulting model dimensions in wavelengths relative to the frequencies of

operation in this experiment are given in Table I, and a simplified drawing of the model is shown in Figure 2.

Box Dimension (inches)	Frequency (MHz)		
	200	300	400
L - 43.11	0.73 λ	1.1 λ	1.46 λ
H - 11.51	0.2 λ	0.29 λ	0.39 λ
W - 14.39	0.24 λ	0.37 λ	0.48 λ

TABLE I. Measurement Model Dimensions

The slots in the box sides were designed to accomodate the surface charge and current measuring probes chosen for this experiment. Twenty slots were machined in the sides nearest the antenna, with two slots as near one corner of the box as possible, one slot on each side, and the remaining eighteen slots separated at an arbitrarily chosen distance of three inches. Figure 3 shows detail dimensions of the box sides, top, and measuring slots.

Two advantages were expected to result from the lack of symmetry found in the final configuration. First, by placing the slots as near the antenna feed point as possible, it was believed the generation of fields of sufficient magnitude to be detected by the surface charge and current probes was assured. This consideration was important because little knowledge existed with which to predict how well these probes would operate in their chosen configuration. And

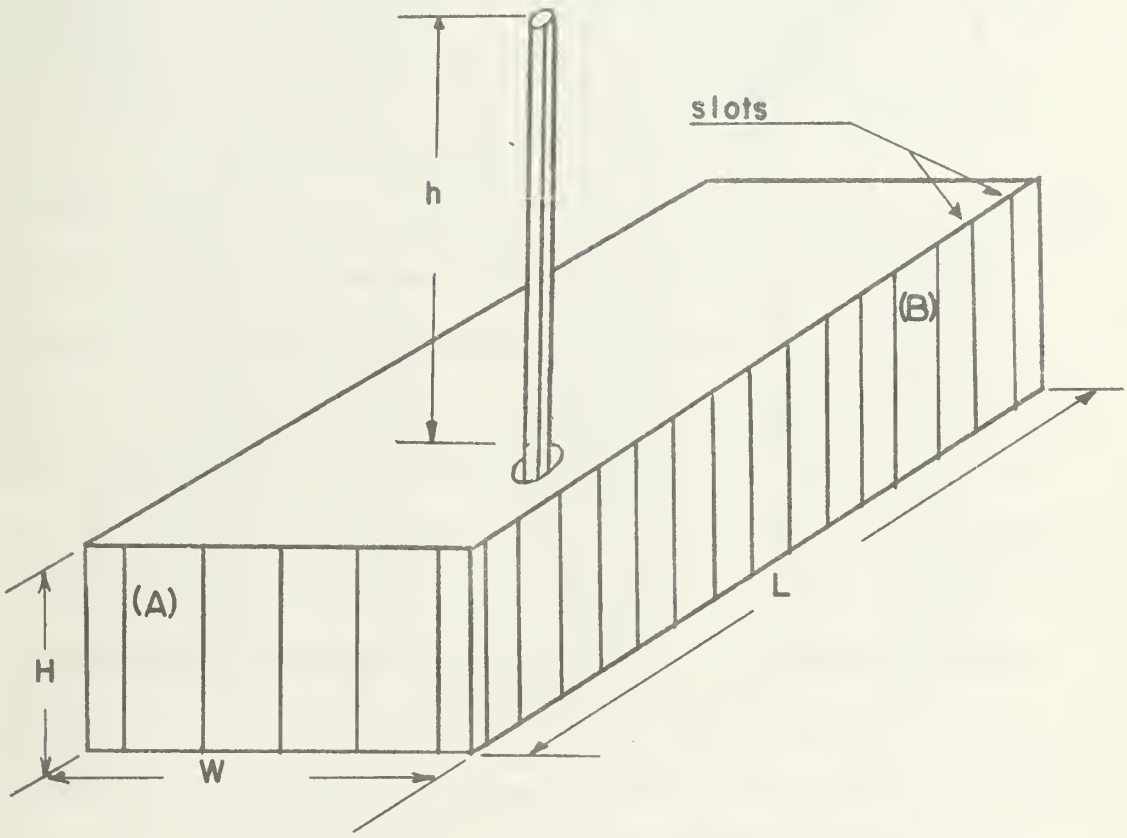

FIGURE 2. Experimental Model

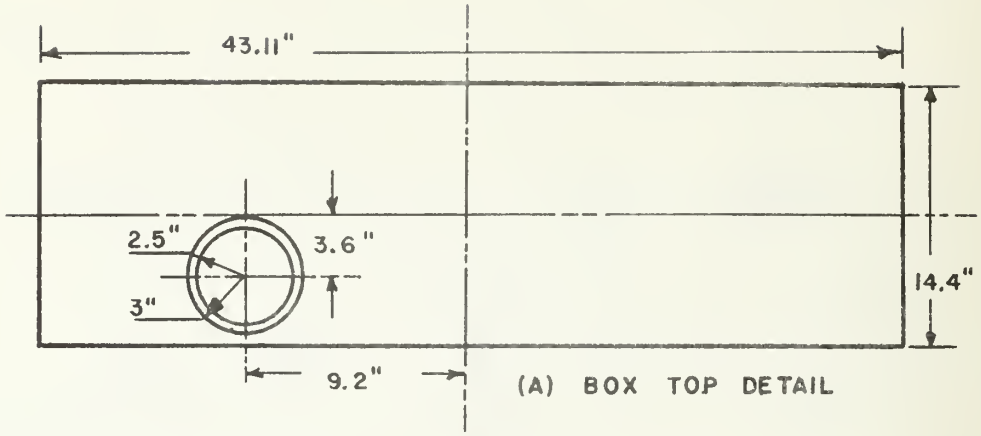

(A) BOX TOP DETAIL

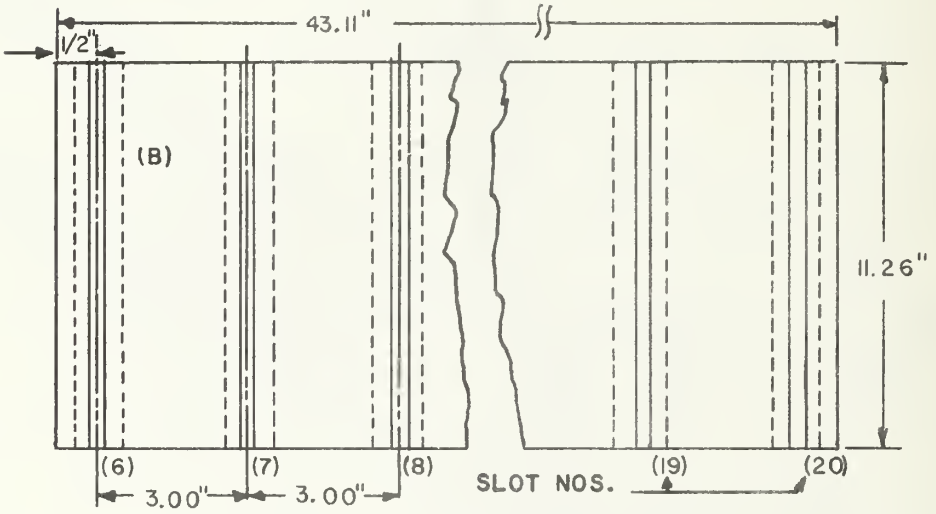

(B) BOX SIDE DETAIL (SIDE B)

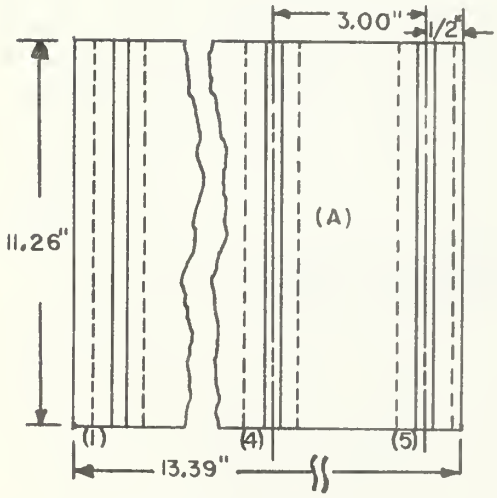

(C) BOX SIDE DETAIL (SIDE A)

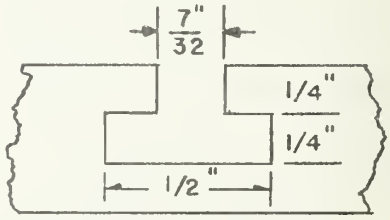

(D) SLOT DETAIL

FIGURE 3.

second, because it was hoped that results of the measurements would provide insight to the validity of numerical method solutions, an asymmetrical case would provide the most meaningful benchmark data for comparison purposes. The final construction model is shown in Figure 4.

C. COAXIAL LINE AND MONOPOLE CONSTRUCTION

The antennas that were of primary interest in this study were base driven monopoles fed by a coaxial line.

The conventional laboratory procedure for determining the field distributions in a coaxial line, and from this the characteristics of the antenna terminating the line, consists of probing the fields with a detection device, inserted through the outer conductor of the coaxial cable. Because it was desired to measure the charge and surface current distribution on the monopole itself, the procedure just described would involve the undesirable presence of a probe supporting mechanism as well as the observer in the very near field of the antenna. To eliminate this difficulty a mechanism similar to that described in Reference 2 was constructed. It consists of a coaxial line formed by concentric brass pipes, with one end shorted by a brass plate and the other end flared out into a brass ring which serves as a support for the coaxial line when it is suspended from the image plane, as well as the connection of the outer conductor to the plane itself. The structure and dimensions of this line are shown in Figures 5 and 6.

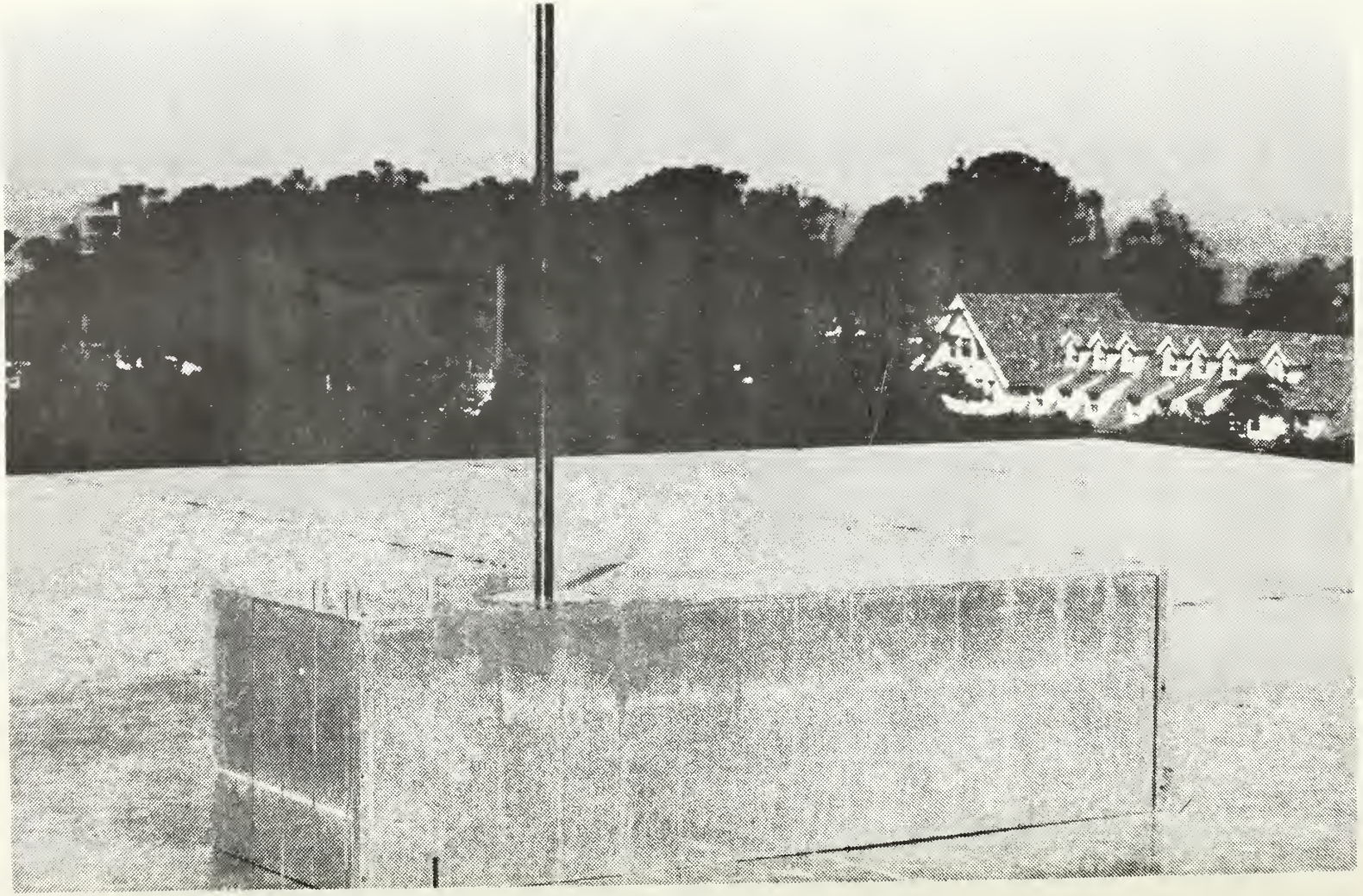

FIGURE 4. Detail of Final Model

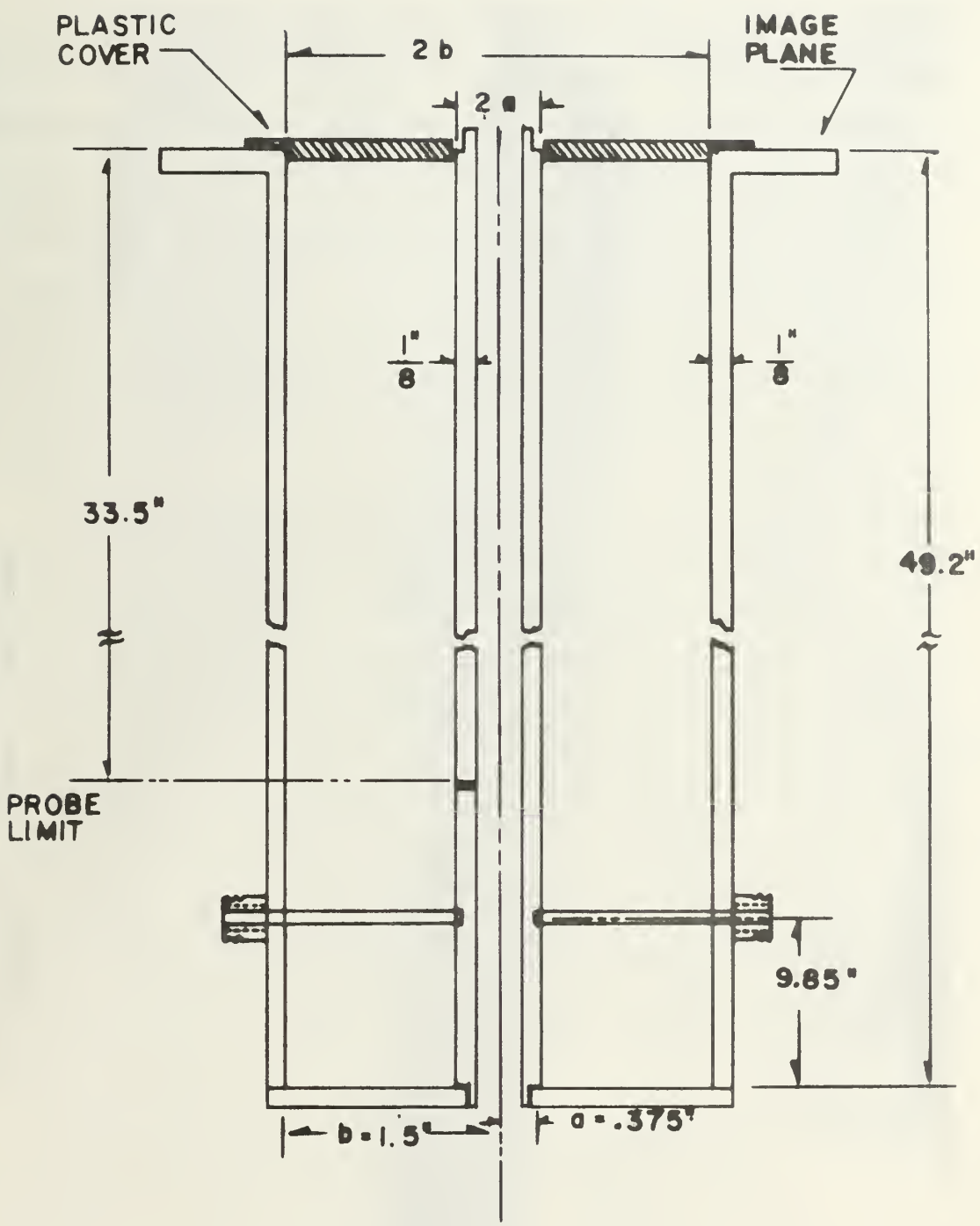

FIGURE 5. Coaxial Feed Line Detail

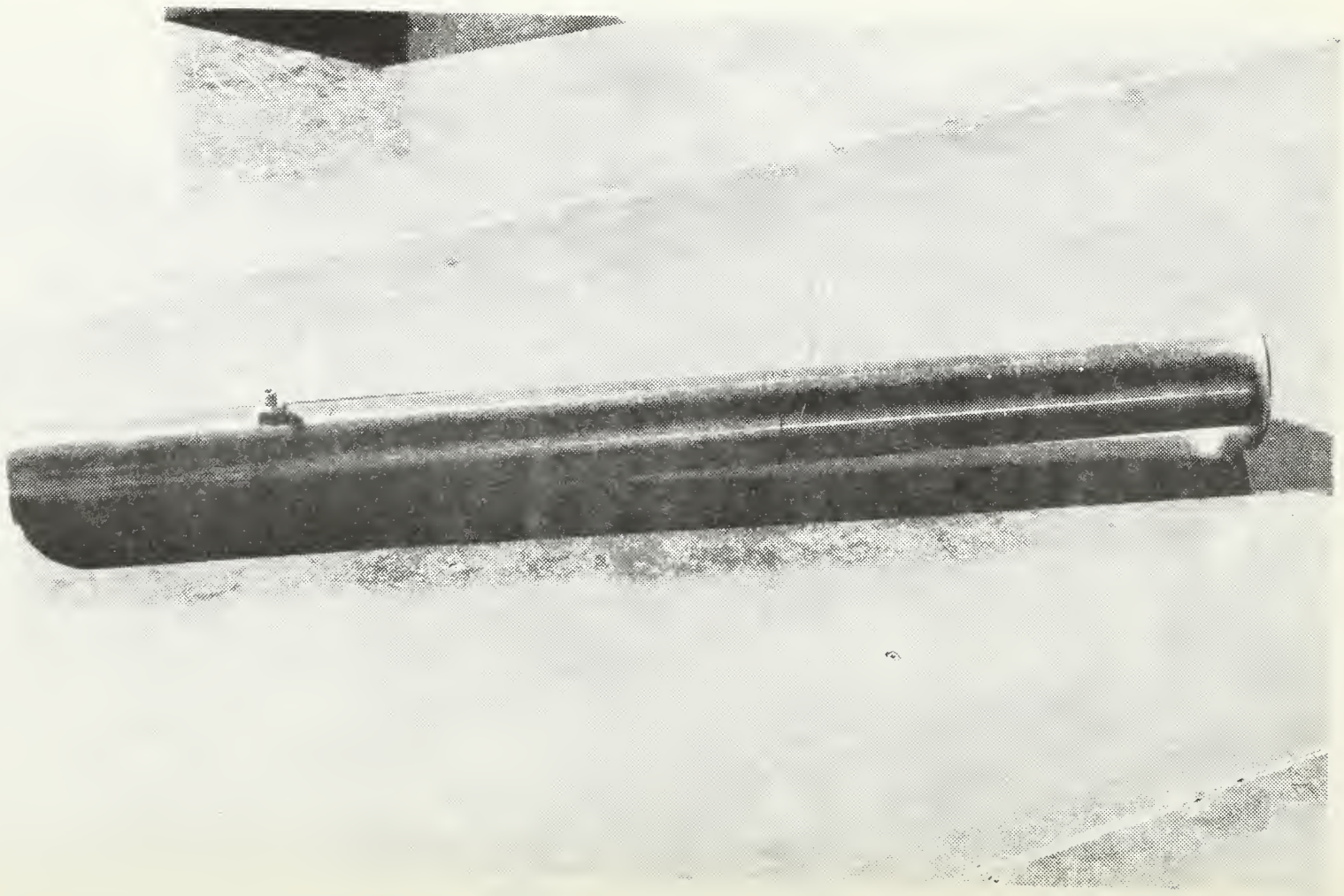

FIGURE 6. Coaxial Feed Line

A rack and pinion mechanism was designed which, when attached to the bottom of the coaxial line shorting plate, allowed positioning the field measuring probes anywhere along the axial line and antenna. The center conductor of the coaxial feed line extended above the feed aperture a distance of 1 inch. This section was machined to allow variable lengths of brass tubing to be placed above the feed point, permitting the study of monopoles of diverse lengths.

The inner conductor of the coaxial feed line and the monopole antennas were longitudinally slotted to permit the measuring probes to travel the length of the system. These probes were supported above a 1/8 inch brass tube placed inside the coaxial center conductor, extending beneath the coaxial line shorting plate and connected to the rack and pinion positioning mechanism. The configuration permitted the routing of the transmission line from the probe back to the measuring equipment through the supporting tube, thus eliminating any possible coupling between the electromagnetic fields and the measuring equipment.

The dimensions of the coaxial line constructed for the experiment were:

Outer conductor diameter	4 in.
Inner conductor diameter	3/4 in.
Wall thickness	1/8 in.

Because air served as the dielectric, these dimensions lead to the following characteristic impedance calculation:

$$Z_c = \frac{138}{\sqrt{\epsilon_r}} \log \frac{b}{a} = 96.45 \text{ ohms},$$

where "a" and "b" are the inner and outer conductor radii respectively.

Monopoles of three lengths were constructed for placement above the feed line aperture. The lengths were 25 cm, 50 cm, and 64 cm, this last length corresponding to the 35' whip antenna used in the numerical study after scaling to a frequency of 100 MHz.

For the measurement of surface current and charge on the sides of the box it was necessary to move the box (in relation to the image plane aperture) in order to reach all the side slots. Because the brass coaxial feed system extended through the image plane when an antenna was located above the box, lateral movement in such a situation was not possible. Consequently a 50 ohm tapered coaxial feed was designed with a longitudinal dimension that permitted its containment within the box, requiring only a flexible coaxial cable for connection to the signal generator beneath the image plane.

D. PROBE DESIGN AND CONSTRUCTION

The measurement of relative magnitude and phase of surface charge and current distributions on antennas is, in general, accomplished by using probes which sample the

electromagnetic fields associated with the antenna. The construction of the probes must meet several requirements. The probing element must be very loosely coupled to the antenna, that is, its presence must not alter the near field electromagnetic distributions. Additionally, the probe dimensions should be small relative to the operating wavelength (ideally a point probe), and it must be located very near the antenna [Reference 2].

To satisfy these requirements for measurement on the cylindrical monopoles here considered, a linear monopole charge probe and a singly loaded circular loop current probe (Figures 7 and 8) were constructed based on the theory and experimental results described by Whiteside in Reference 3.

The probing element was constructed of solid shield coaxial cable (UT-20) of 0.02 in. o.d., with a 0.005 in. o.d. center conductor and a Teflon dielectric. In the case of the charge probe, the outside conductor was stripped from the section protruding from the probe support, leaving only the dielectric and center conductor to extend above the surface of the monopole antenna under measurement. For both probes the center conductor was led back to a Microdot 31-59 connector which served as the junction to the transmission line leading back to the measuring equipment, while at the same time providing a mechanical joint to the 1/8 inch brass tube which positioned the probes along the coaxial feed line and monopole.

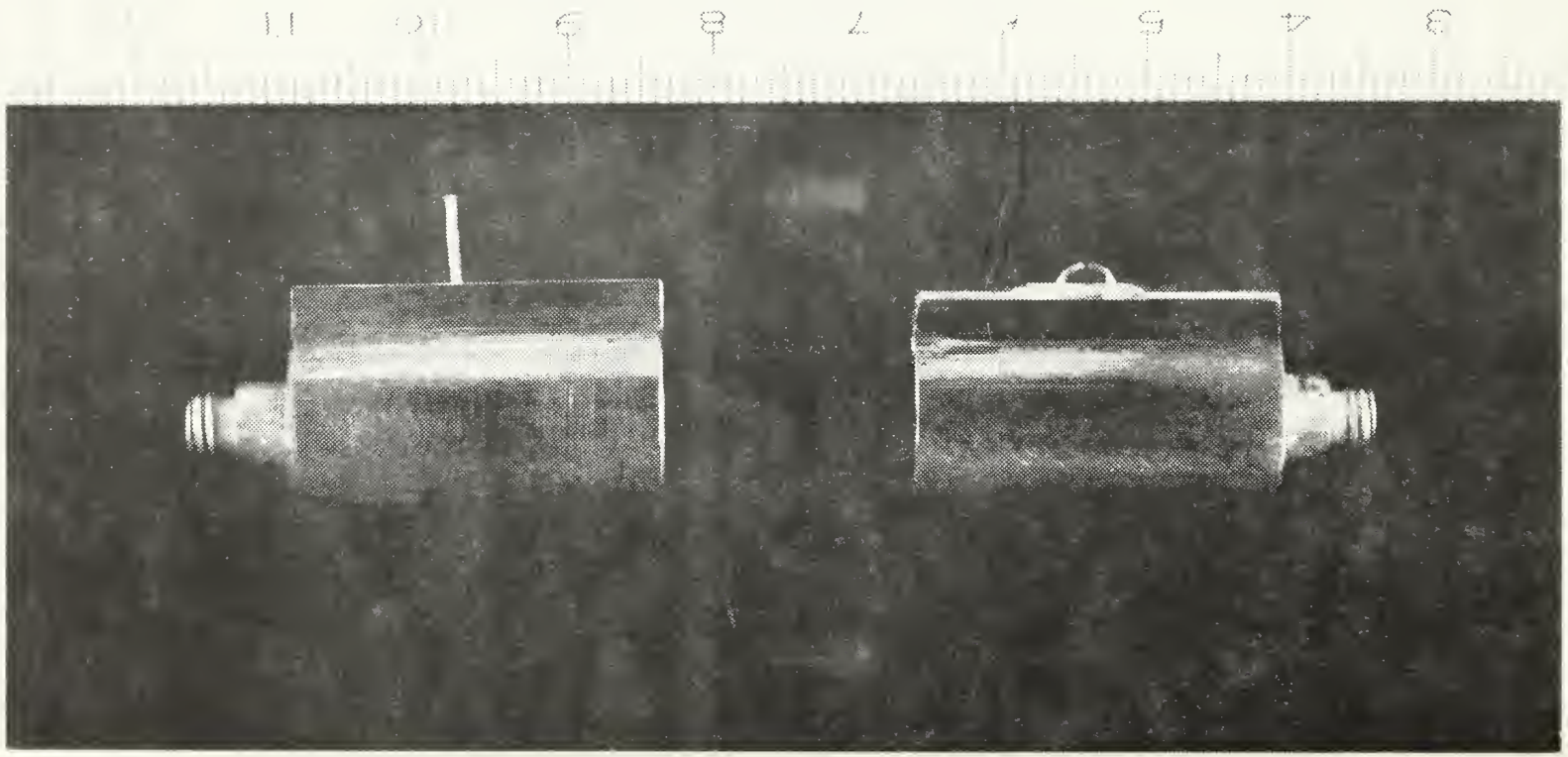

FIGURE 7. Monopole Probes

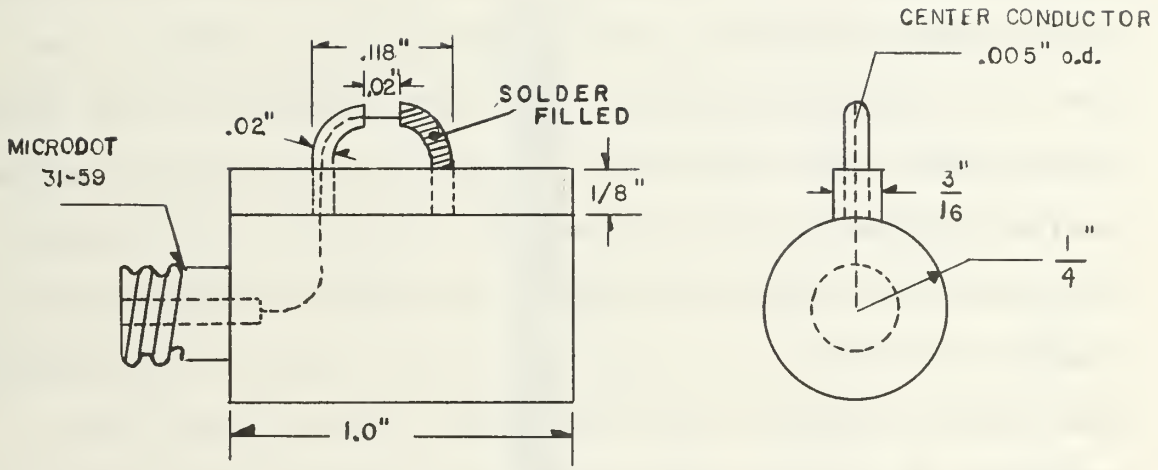

(A) Current Probe

(B) Charge Probe

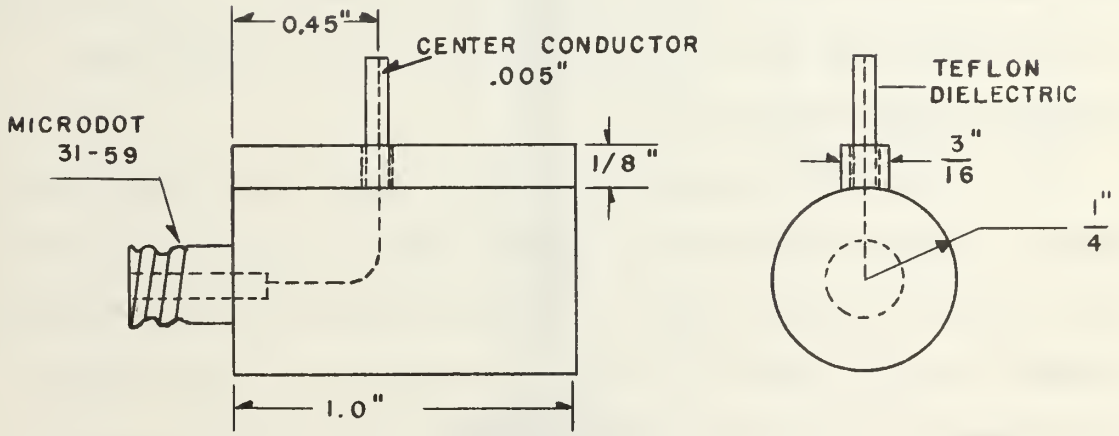

FIGURE 8. Monopole Probes

For the measurements on the vertical sides of the box, charge and current probes of similar construction to the above were made an integral part of an aluminum bar machined in the form of a 'T' to fit the slots in the side of the box. In this case however, a pair of concentric loops were constructed, one inside and orthogonal to the other, as the surface currents in this case will decompose into longitudinal and transverse components, and both of these must be measured to obtain the complete surface current distribution. Each probe located on the bar leads to a Microdot 31-59 connector at the bar base providing separate connections to the detecting equipment located beneath the image plane. The details of the probes and of the supporting bar are shown in Figures 9 through 11.

The rack and pinion limited the range of positions to which the probes had access. In the case of the monopole probes, measurements were possible from a point 85 cm beneath the junction of the coaxial line and antenna to 1.39 cm and 1.23 cm from the end of the monopole for the charge and current probes respectively.

For the surface current probes an additional difficulty arose. It was noticed that as the bar was positioned with the rack and pinion system, contact irregularities existed between the bar and the slot causing erratic measurements. To eliminate the problem, a small beryllium copper spring plate was fastened beneath the probes, serving to clamp the

FIGURE 9. Surface Measurement Probe (T-BAR)

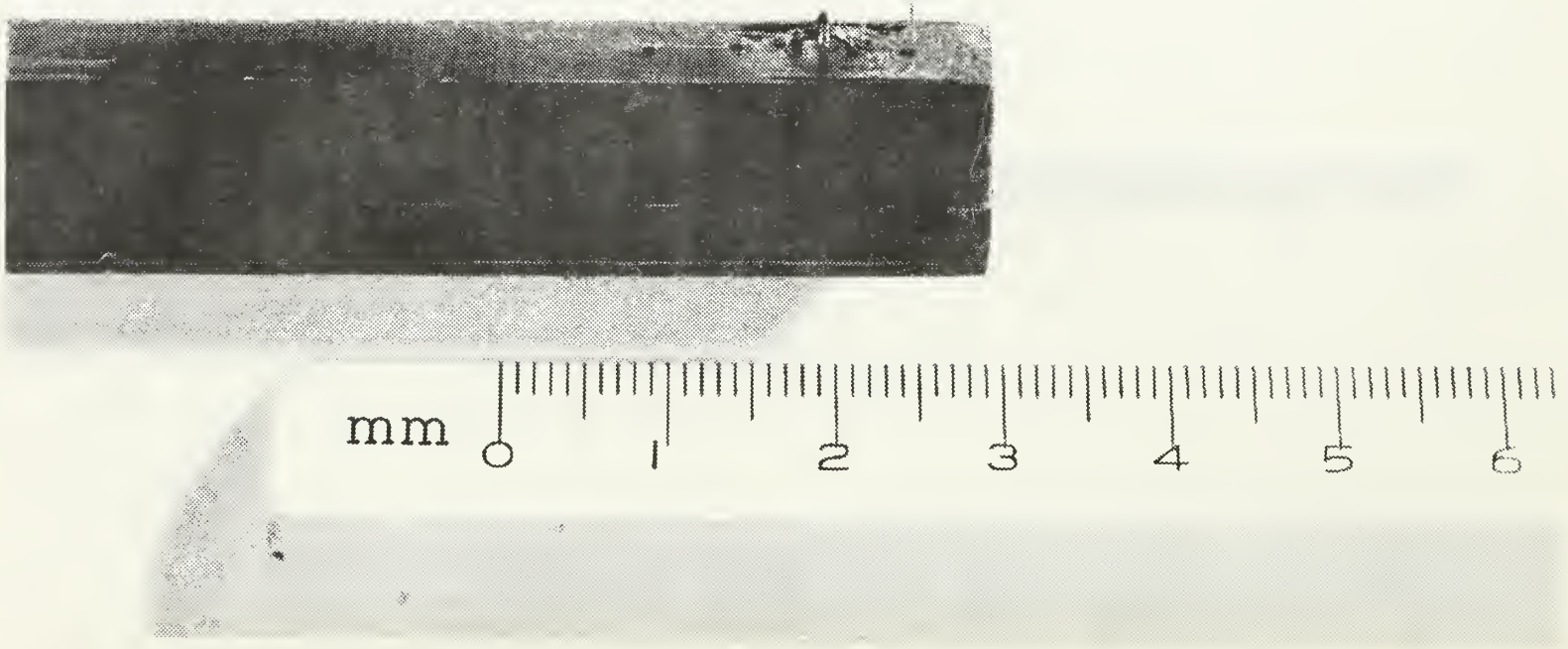

FIGURE 10. Surface Probe (T-BAR) Detail

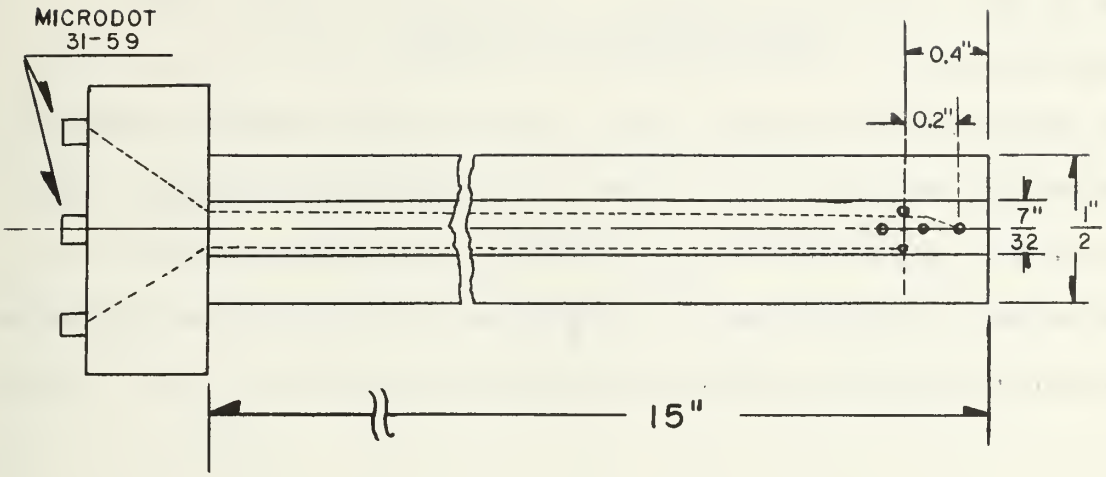

(A) "T-BAR" Dimension

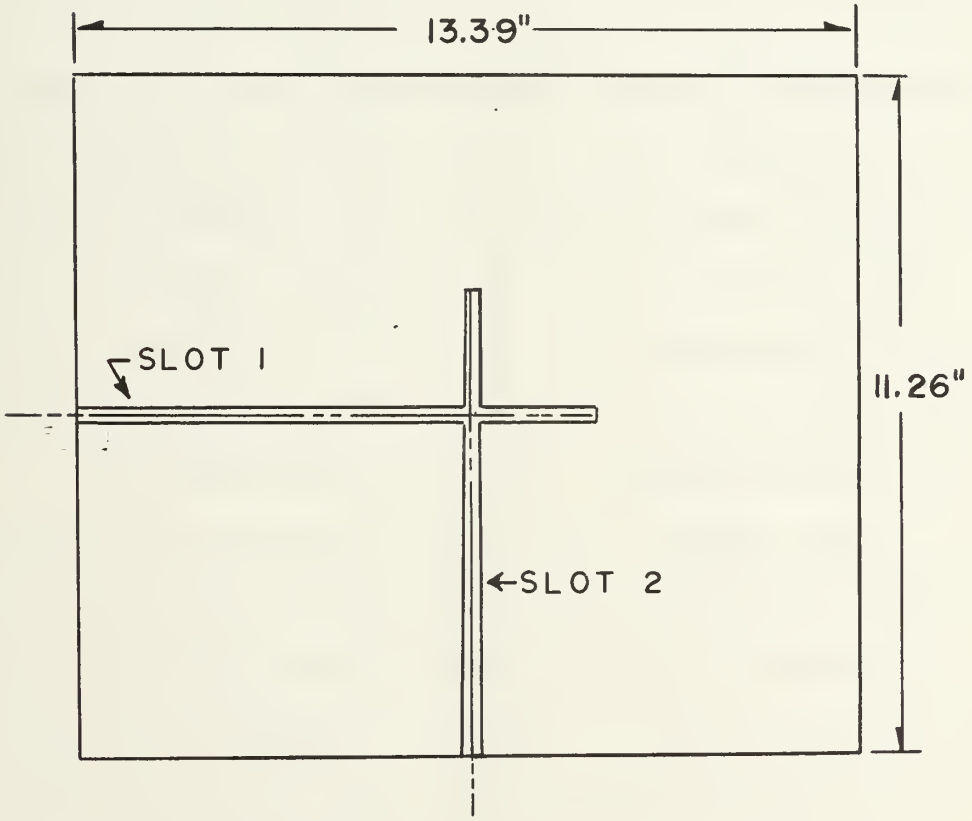

(B) Surface Probe Calibration Slots

FIGURE 11. Surface Measurement Hardware

bar to the surface of the box. This limited the lower position to which the probes had access as the clamp could not penetrate the image plane aperture when the bar reached the bottom of the slot. Thus the longitudinal positioning of the bar was restricted to 4.16 cm and 3.66 cm from the bottom edge of the box, to 0.5 cm and 1 cm from the top edge for the charge and current probes respectively.

III. THEORY AND MEASUREMENTS

A. GENERAL CONSIDERATIONS

1. Antenna Definitions

The purpose of a transmitting antenna is to allow periodically varying distributions of current and charge to radiate significant electromagnetic fields at points distant from the antenna. Reference 2 indicates that the generation of these fields results from the current distributed on the antenna and its supporting structure, and furthermore, that it is likely the current found only on certain portions of the antenna will have the greatest effect on the properties of the radiated electromagnetic fields. Because of this relationship between the supporting structure and the antenna current and charge distributions, it is of interest to determine whether variations of the supporting structure significantly affect the antenna electrical characteristics.

The transmitting antennas studied here are electrically thin monopoles,base fed by a coaxial line. The monopole consists of a highly conducting rod or tube of diameter 2a which acts as an extension of a coaxial line above the feed aperture, with its axis at a distance b/2 from the edge of the feed point aperture (Figure 5).

2. Antenna Characteristics

The measurements performed in this study were carried out to obtain a quantitative description of the admittance

of monopole antennas as well as the surface charge and current distribution on the antenna and on its supporting structure. These three quantities describe the electrical characteristics of a transmitting monopole [Reference 4].

The general definition of admittance is given by:

$$Y = \frac{I}{V} = G + jB \qquad (1)$$

where I and V are respectively complex current and voltage, resulting in a complex value of admittance with two components: conductance (G) and susceptance (B).

The approach taken here to obtain the quantities necessary for application of equation (1) was to design a measuring system which would make use of the fundamental concepts of transmission line theory, relating the electromagnetic field distributions on the transmission line and monopole to the surface charges and currents, and to the load admittance terminating the feed line.

Initially measurements were made of monopole antennas placed above the image plane in order to verify the measuring accuracy of the experimental design. The admittance measured at a point $\lambda/2$ from the coaxial line aperture, referred to as the apparent admittance of the load, was compared with existing analytical solutions which apply to monopole geometries where the aperture satisfies the relation:

$$\frac{b - a}{h} \ll 1 \qquad (2)$$

This restriction is necessary because transmission line theory based on the TEM mode of propagation is not applicable at the junction region between the antenna and coaxial line feed aperture. This is a result of the effects of the aperture edges on the TEM field configuration. However, as long as the restriction is satisfied the assumption of TEM mode along the entire structure does not significantly alter the theoretical results [Reference 4].

The analytical results used for comparison apply to electrically thin antennas where the following inequalities are satisfied:

$$k_o a \ll 0.06$$

$$a/\lambda \ll 0.01$$

where $k_o a = 2\pi/\lambda$ and λ is the free space wavelength.

Correspondence between these restrictions and the monopoles used for measurement is shown in Table II as a function of the frequencies at which measurements were performed.

A consideration of the physical implications of the term "electrically thin antenna" can provide justification for the measurements in the one case listed that does not strictly meet the restrictions.

f (MHz)	200	300	400
$k_o a$	0.039	0.059	0.079
a/λ	0.00635	0.009525	0.0127
(b-a)/h	0.0254	0.0381	0.0508

Table II. Geometrical Properties of Experimental Monopoles

To characterize an antenna as electrically thin is to relate its physical thickness to the wavelength of incident plane wavefronts. If the antenna is electrically thin, then the distribution of surface currents resulting from the incident wave may be considered circumferentially uniform. In the cases measured in this experiment, transmitting vice receiving antennas were investigated, and the physical characteristics of the feed system as well as its geometrical symmetry insured the circumferentially uniform distribution. Consequently the case which does not strictly meet the restrictions earlier mentioned was considered a valid measurement situation relative to the experimental accuracy expected.

One additional consideration is necessary in order to interpret the measurement results. Reference 4 shows that the analytical solutions used as reference values for this study are valid in the case of finite length monopoles which meet the restriction:

$$\frac{b - a}{h} \ll 1.$$

Furthermore, it is also shown that the analytical calculation of conductance, G, is a function of $k_o a$ only, whereas the calculation of susceptance, B, is a function of $k_o a$ as well as the ratio $\frac{b}{a}$, a ratio that will depend on the feed line geometry. Therefore, the conductances measured in this experiment provide the best comparison to the theoretical values, as the parameter $k_o a$ can be controlled through variation of the frequency, whereas the ratio $\frac{b}{a}$ is fixed, generating susceptances which are feed line dependent.

B. MONOPOLE MEASUREMENTS

1. Data Acquisition and Analysis

The experimental procedures described below follow from the transmission line theory applicable to lines in which TEM mode of propagation exists.

The surface charge and current probes (explained in the following section) develop voltages which are proportional to the $\bar{E}$ and $\bar{B}$ fields present at the probe position. Let the generated voltages be designated by:

$$V_I \propto \bar{B} \triangleq \text{Current Probe generated voltage}$$

$$V_Q \propto \bar{E} \triangleq \text{Charge probe generated voltage}$$

By sequentially recording the magnitude and relative phase of the voltage output from the probes as a function of their position along the entire system, a description of the standing

wave patterns results. By noting the values and position relative to the feed line aperture of the maxima and minima associated with the charge probe the following relations relative to the voltage distribution on the line can be applied to the system [Reference 5]:

$$SWR = \frac{\left|V_{Q_{max}}\right|}{\left|V_{Q_{min}}\right|} = \frac{\left|V_{I_{max}}\right|}{\left|V_{I_{min}}\right|} \tag{3}$$

$$Y_n(z) = \frac{1 - |\Gamma_r| e^{j\zeta}}{1 + |\Gamma_r| e^{j\zeta}} \tag{4}$$

where $Y_n(z)$ is the normalized line admittance as a function of line position,

$$\zeta = (\rho + 2\beta z) = \begin{cases} 0 & \text{at voltage maximum} \\ \pi & \text{at voltage minimum} \end{cases}$$

and ρ is the phase angle between the incident and reflected voltage wave at the load.

The magnitude of the voltage reflection coefficient can be shown to be given by:

$$|\Gamma_r| = \frac{VSWR - 1}{VSWR + 1} \tag{5}$$

By introducing the distance z from the minimum to the junction of the monopole and the coaxial line (feed aperture) the apparent normalized admittance of the antenna is obtained directly from equation (5). This equation is the mathematical representation of the fundamental relationship governing the transmission line Smith chart, and thus allows mathematical or graphical solution procedures for the apparent admittance to be applied to the experimentally measured values.

2. Monopole Probes

The electromagnetic field probes (Figures 7 and 8) used for the monopole antenna measurements are the essential element for sampling the coaxial line fields, and with the data thus gathered, one can obtain the description of the antenna's electrical characteristics. The design and construction of these probes is based on the theoretical and experimental results presented in Reference 3.

It is apparent that the charge probe will generate an EMF directly proportional to the $\bar{E}$ field parallel to the probe wire element, and other than the necessity of making the probe as small as possible to avoid disturbing the fields under measurement, few other criteria exist for choosing this probe configuration. In all respects the charge probe itself appears as a small monopole antenna, with the coaxial feed line center conductor as a ground plane, and its analysis in this fashion is readily available.

The choice of surface current probe configuration does provide occasion for alternative configurations. For the desired measurements, a means of generating an EMF proportional to the surface current on the coaxial center conductor and monopole is required. By providing a circuit element which reacts to the $\overline{B}$ field concentric to the center conductor and monopole, the surface current is measured as a result of the following relation:

$$\overline{J} = \hat{n} \times \overline{H}$$

The physical construction of the coaxial feed line would suggest that a wire loop with a plane orthogonal to the magnetic field would be best suited for the generation of the required EMF. However, as the current is also to be measured on the monopole antenna, the presence of $\overline{E}$ field components parallel to the monopole axis will also generate a response from the loop probe causing erroneous relative magnitude measurements. Reference 3 demonstrates that use of a singly loaded circular loop such as that chosen for this experiment eliminated this problem provided the loop diameter satisfies the inequality:

$$\frac{d}{\lambda} < 0.01$$

That the current probes constructed for this experiment satisfy this inequality is demonstrated by the information tabulated in Table III.

f (MHz)	200	300	400
d/λ	0.002	0.003	0.004

Table III. Monopole Current Probe Characteristics

As a final comment related to the surface measurements of interest, it must be pointed out that these field probes will only be strictly accurate in their measurement of surface charge and current at distances less than 5d (1.5 cm) from the ends or base of the antenna, because the fields at these locations are strictly proportional to the charge and current only at the antenna surface, and an infinitesimally small probe would be required for their measurement.

3. Monopole Probe Calibration

The axial distribution of surface charge and current is described in terms of magnitude and phase, and for the cases of interest here a relative phase measurement is to be achieved. An early analysis of the electromagnetic field probes (Appendix A) showed that erroneous amplitude and phase measurements would result unless the probes underwent some form of calibration. Amplitude calibration would not be necessary as the magnitude of the distributions was to be normalized through the measured monopole admittance.

The easiest calibration procedure would be the use of a matched load termination on the end of the coaxial line leading to a known field distribution, however the line characteristic impedance prevented this alternative.

A further consideration of transmission line theory provided the calibration procedure necessary for the experimental set up. The theory predicts that in a lossless transmission line, the positions at which voltage and current are respectively maximum and minimum, and vice-versa, are locations at which zero relative phase exists between these quantities.

It was decided to conduct measurements of admittance and surface current and charge distributions on monopoles located above the image plane, a geometry for which extensive theoretical results already exist. With this data and the use of equation (4) the measured conductance was compared with the theoretical solutions tabulated in Reference 4. As was explained earlier the conductance is independent of the ratio $\frac{b}{a}$ and for this reason it is used as a measure of the calibration in this experiment. A simple graphical interpolation routine was used to obtain the conductance values for the cases $\frac{h}{\lambda} = 1/6$ and 0.64 as these cases were not listed directly. This calibration procedure provided the 6% error bound on the measured values, which was considered sufficient for experimental purposes.

The data collected was plotted as a function of field probe position. A simple computer algorithm was

developed to determine the phase factor required to insure the charge and current plotted "in-phase" at the positions of magnitude maxima and minima. The phase calibration factors were determined at the three frequencies chosen for measurement.

The accuracy of the resulting phase calibration factors was determined by consideration of the phase plots.

The admittance angle calculated from the field magnitude and position data depended principally on the accuracy with which the probe position was known, and the probe positioning mechanism was measured accurate to within 0.1 % of the coaxial line length. Therefore, it was expected that the correlation between the calculated admittance angle and the relative phase angle plotted at $\frac{\lambda}{2}$ from the feed plane aperture would provide one indication of calibration accuracy.

The admittance angle is given mathematically by:

$$\angle Y = \tan^{-1} \frac{B}{G}$$

It has already been pointed out that the susceptance is a function of the ratio $\frac{b}{a}$, a quantity associated with the line characteristic impedance. The theoretical admittance values tabulated in Reference 4 and used in the calibration procedure for reference purposes were calculated for a line of 100 ohm characteristic impedance. It was considered that the difference between the theoretical and experimental line characteristic impedance was sufficiently negligible to warrant comparing

the theoretical and experimentally measured admittance angles for an indication of any significant anomalies in measurement system performance.

The calibration data is summarized in Table IV. Because the phase angle is a periodic function, it is clear that the maximum angular error possible in measurement is 360°. Thus the percent error for the phase measurement has been calculated relative to the maximum possible error. As indicated earlier, calibration data for the cases not directly available was obtained through a graphical interpolation routine on the data listed in Reference 4.

4. Monopole Measurement Procedure

The equipment set up for both the calibration and the monopole measurements above the box is shown in Figure 12.

The coaxial feed line with the superimposed monopole was supported, depending on the configuration of interest, by the image plane or the box aperture. The Hewlett-Packard HP8640A signal generator output was applied to the coaxial feed line through a bi-directional coupler. The coupled output was attenuated and applied to the reference channel (Channel A) of the HP8405 Vector Voltmeter and to the Taktronix DC-502 frequency counter. These two connections served to monitor the stability of the applied signal. The level of attenuation was chosen in order to insure that the level of the reference signal was the same as the signal level produced by the electromagnetic field probe at the input to Channel B.

$\frac{h}{\lambda}$	$\frac{a}{\lambda}$	Theoretical Value		Measured Value			% Error	
		G	$\angle Y$	G	$\angle Y_{calc}$	$\angle Y_{plot}$	G	$\angle Y^*$
$\frac{1}{6}$	0.00635	4.0	73.77°	4.15	74.77°	76°	3.75	0.2
$\frac{1}{4}$	0.009525	17.16	-24.0°	16.38	-25.5°	-25°	4.5	0.3
0.64	0.009525	4.15	68.43°	3.90	69.62°	65°	6.0	0.3
$\frac{1}{3}$	0.0127	----	-----	5.10	-19.9°	-19°	----	----

Table IV. Calibration Data
Admittance of Monopoles Above Image Plane
(Theoretical Values from Reference 4).

*Angular percent error between calculated and plotted admittance angle, relative to 360°

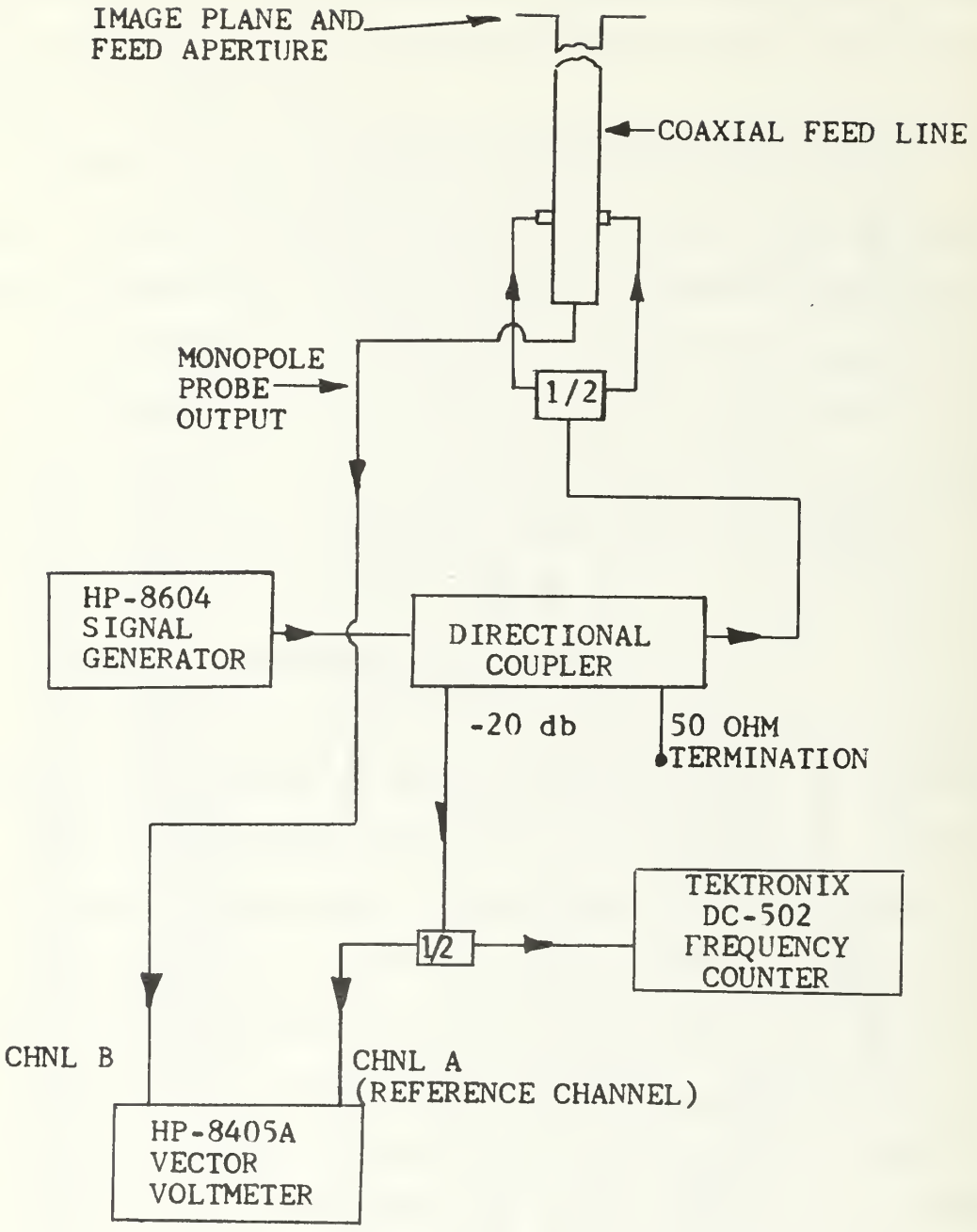

FIGURE 12. Monopole Measurement System

This requirement was necessary in order to meet the ± 1.5° phase measuring accuracy of the vector voltmeter.

The surface charge and current probes were sequentially run through the coaxial line and monopole antenna, and at 1 cm intervals, the magnitude and phase of the probe generated signal detected by the vector voltmeter was recorded on a HP9821 programmable calculator for additional data processing.

5. Measurement Results

Table V is a compilation of the measured admittance of the monopoles above the box. The general parameters of interest, $\frac{a}{\lambda}$, $\frac{h}{\lambda}$, and $k_o h$ varied as a result of using three different frequencies with the three antenna lengths earlier described. Also listed for comparison are the admittance values for similar monopoles located above an image plane. The angular values indicated are those resulting from the VSWR calculation as well as obtained from the relative phase plot at a distance of $\lambda/2$ from the feed plane aperture.

Figures 13 through 16 show the surface current and charge distributions on the monopoles above the image plane measured incident to the monopole probe calibration, and Figures 17 through 25 are the result of the measurements conducted on the monopoles located above the box.

The distributions are plotted as a function of axial displacement along the feed line and monopole, from a position 85 cm beneath the feed aperture to a point 1.39 cm and 1.23 cm

$Y = G + jB$ (millimhos)

f (MHz)	$\frac{a}{\lambda}$	$\frac{h}{\lambda}$	$k_o h$	Theory Above Image Plane $Z_c = 100\Omega$ G	Theory Above Image Plane $Z_c = 100\Omega$ B	Measured Above Box $Z_c = 96.45\Omega$ G	Measured Above Box $Z_c = 96.45\Omega$ B	$\angle Y_{calc.}$	$\angle Y_{plot.}$
200	0.00635	$\frac{1}{6}$	1.047	4.0	13.75	2.72	12.72	77.92°	78.0°
		$\frac{1}{3}$	2.094	3.8	- 2.75	5.86	- 3.25	-29.0°	-30.0°
		0.427	2.68	2.3	0.5	2.67	0.26	5.56°	11.0°
300	0.009525	$\frac{1}{4}$	1.57	17.16	- 7.64	14.19	- 9.65	-34.22°	-33.5°
		$\frac{1}{2}$	3.142	2.30	2.93	1.81	3.93	64.11°	64.0°
		0.64	4.021	2.15	10.50	4.46	10.43	66.85°	67.2°
400	0.0127	$\frac{1}{3}$	2.094	----	-----	5.27	- 2.20	-22.65°	-20.5°
		$\frac{2}{3}$	4.188	----	-----	8.29	13.86	59.20°	54.2°
		0.853	5.361	----	-----	4.78	- 0.91	-10.77°	- 8.0°

Table V. Admittance Values of Electrically Thin Monopoles

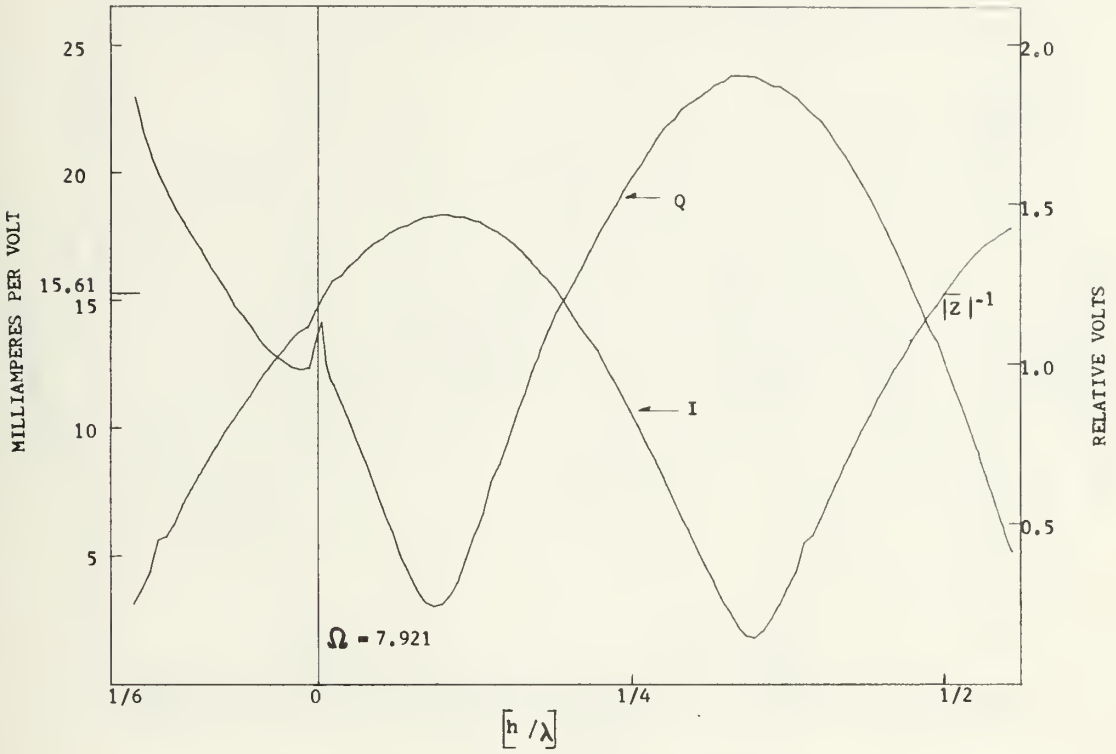

FIGURE 13.- Surface charge and current distribution on a monopole above an image plane. (h = 25 cm., λ = 150 cm.)

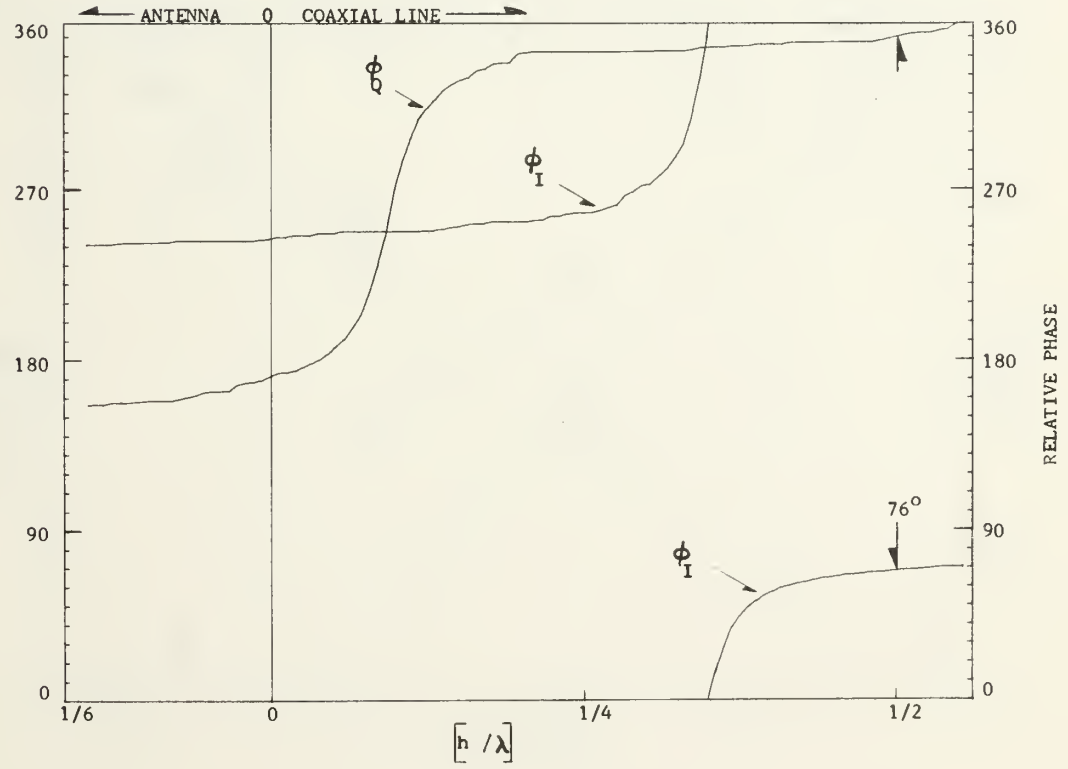

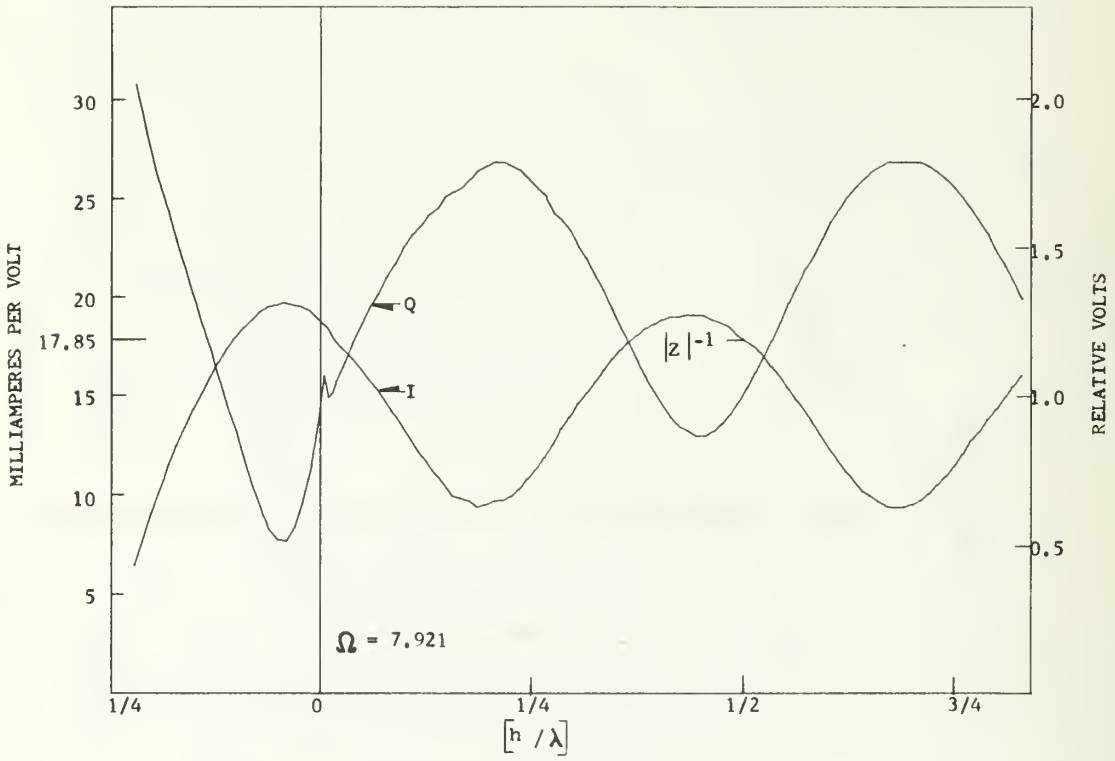

FIGURE 14.- Surface charge and current distribution on a monopole above an image plane. (h = 25 cm., λ = 100 cm.)

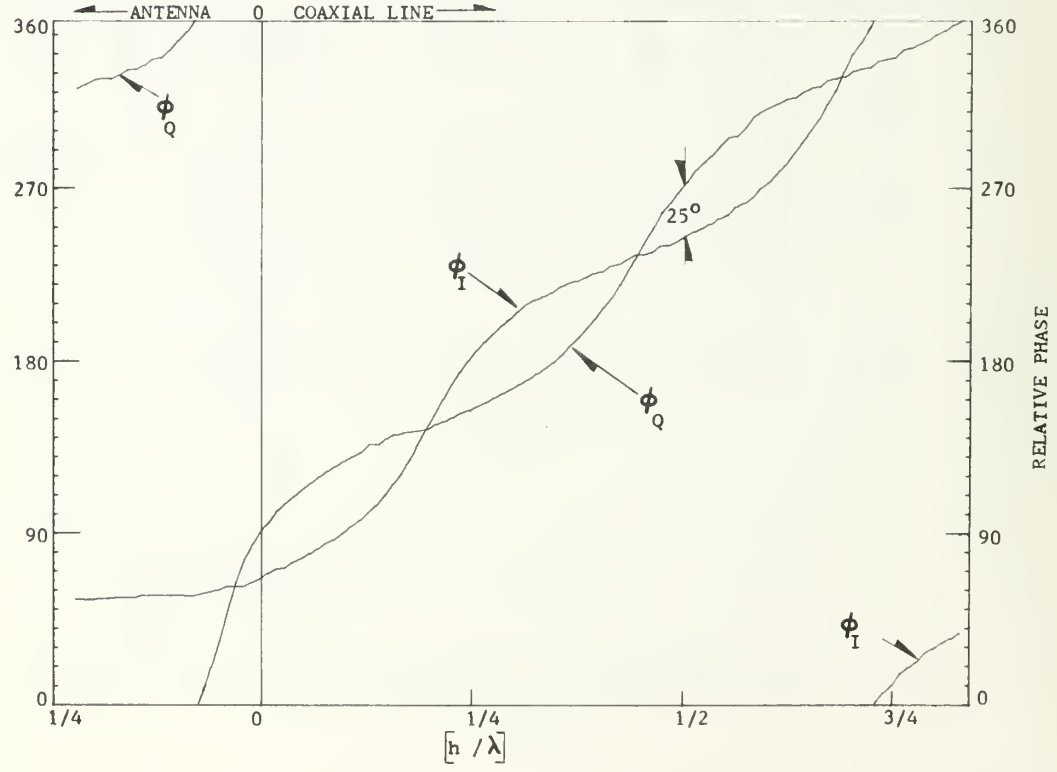

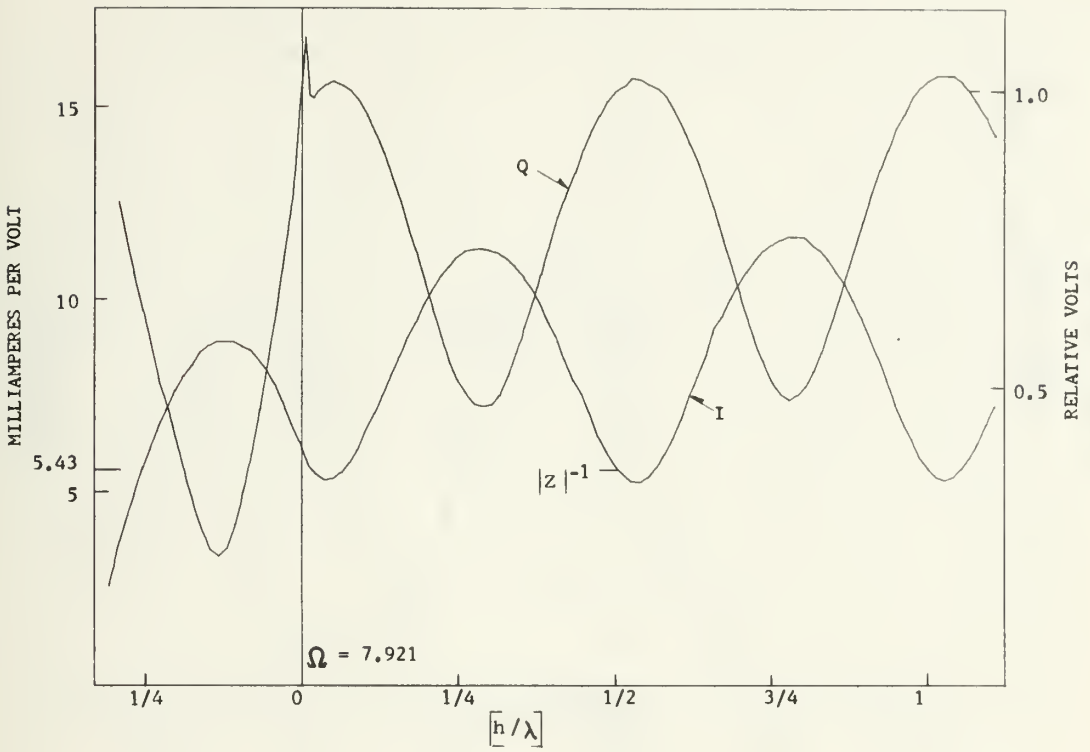

FIGURE 15.- Surface charge and current distribution on a monopole above an image plane. (h = 25 cm., λ = 75 cm.)

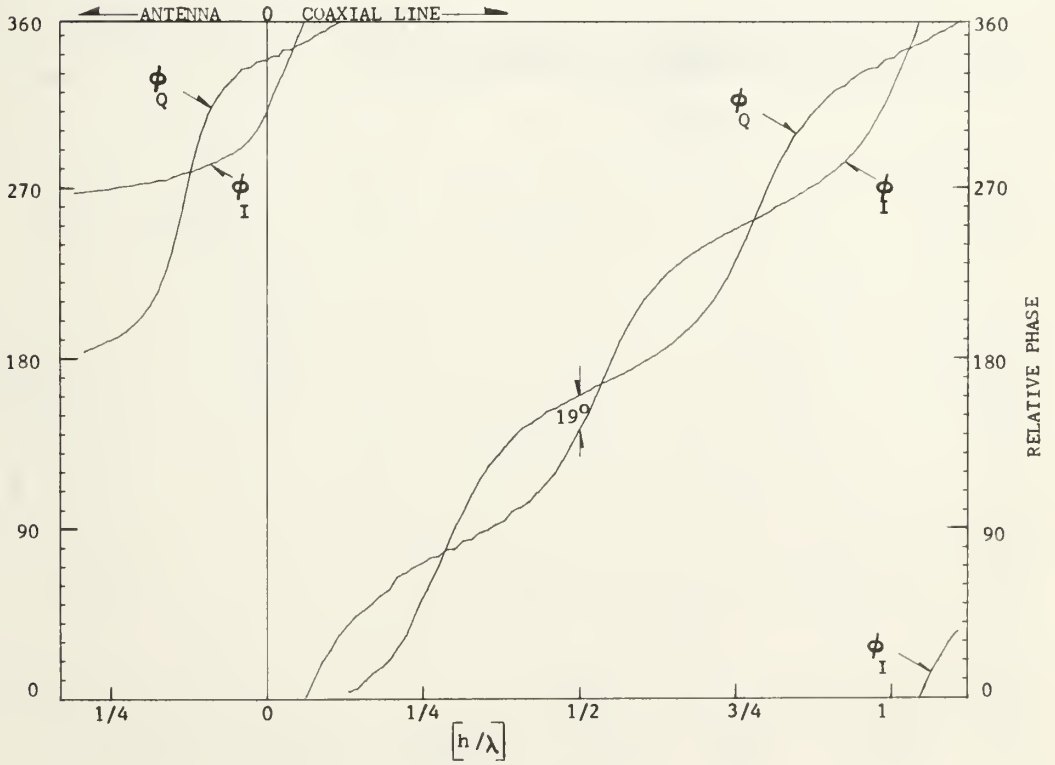

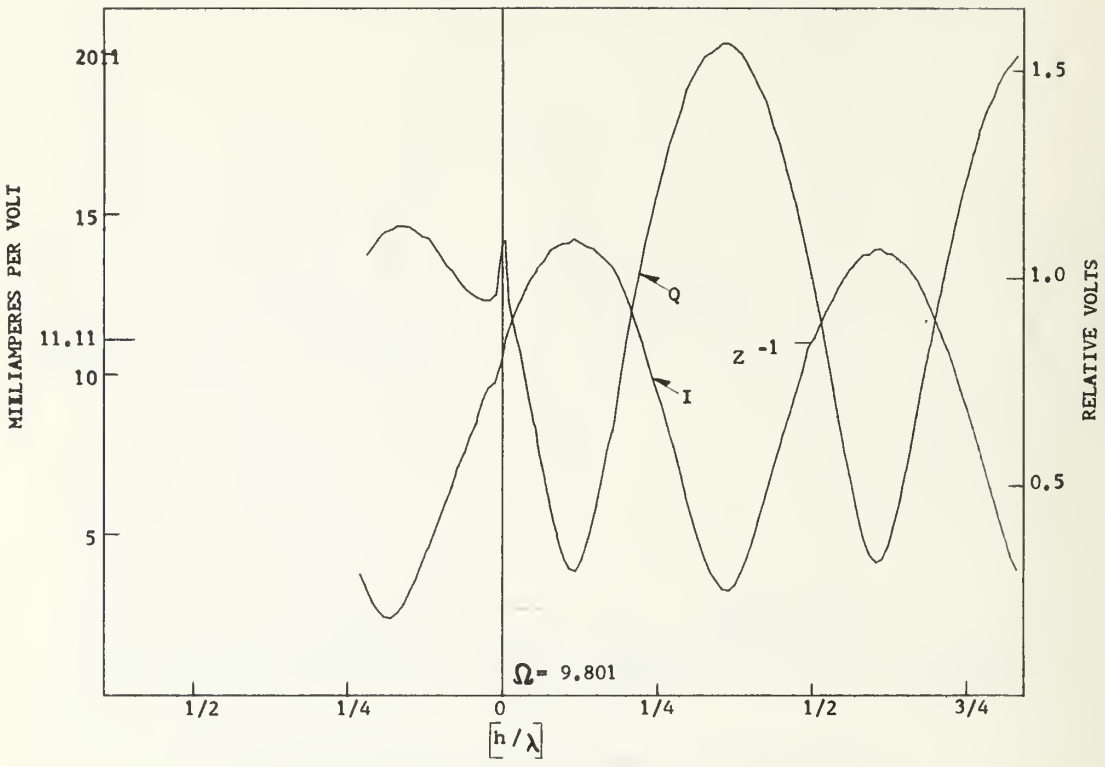

FIGURE 16.- Surface charge and current distribution on a monopole above an image plane.
(h = 64 cm., λ = 100 cm.)

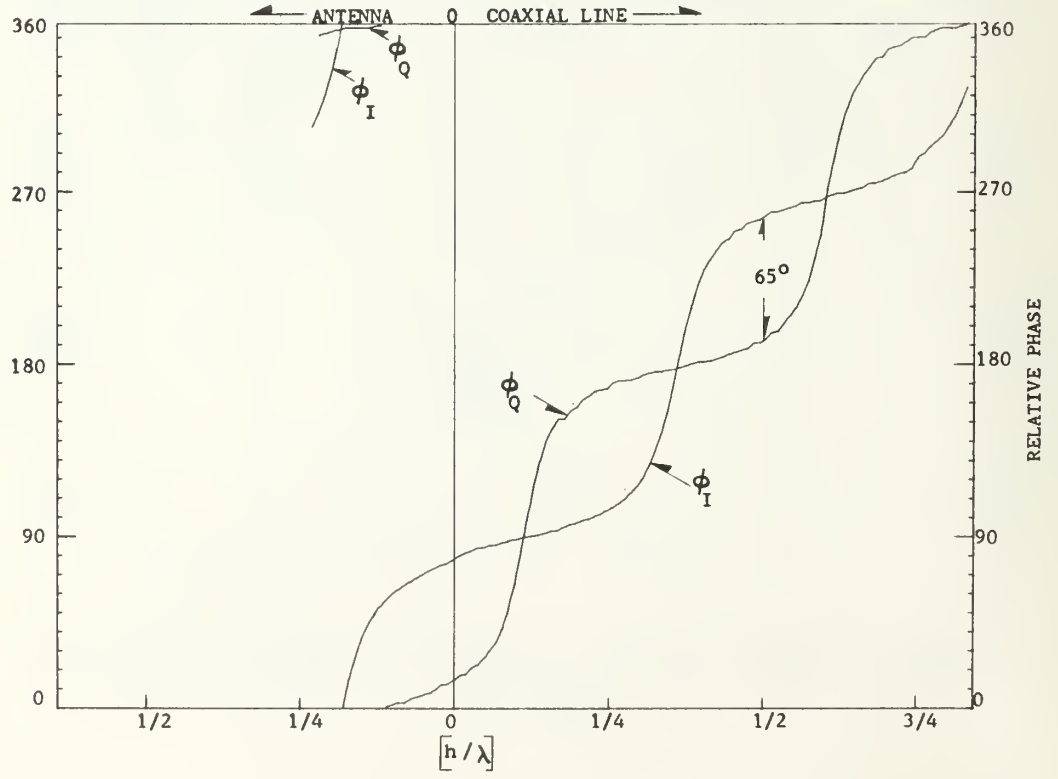

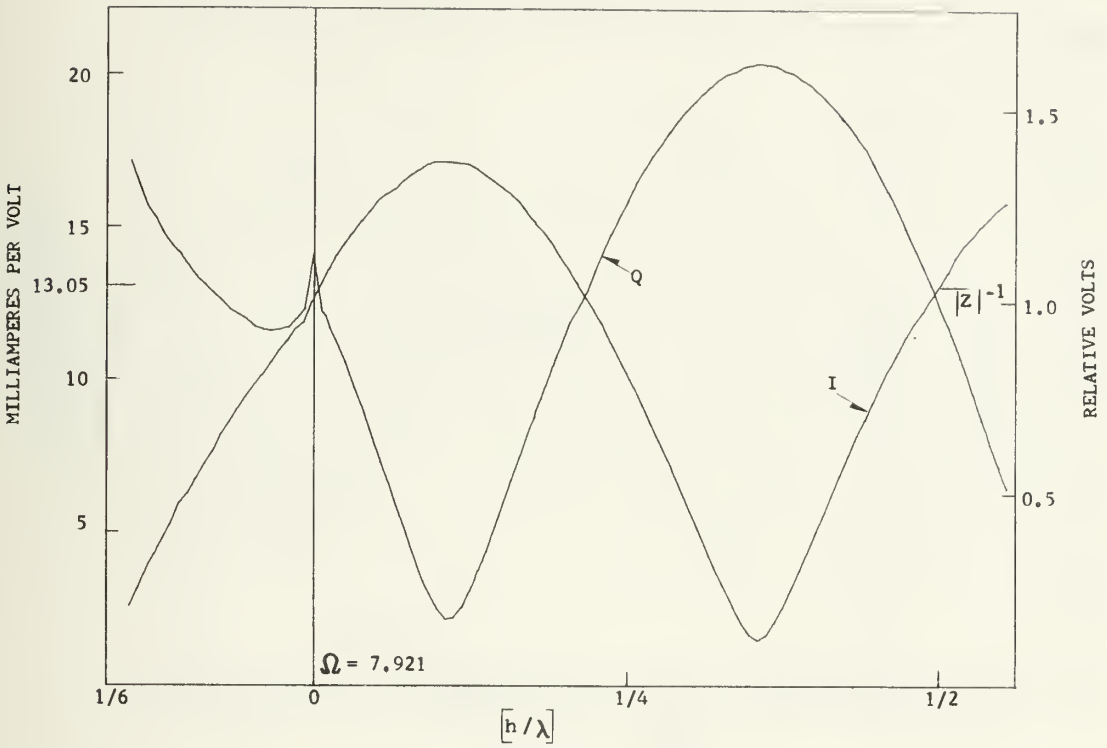

FIGURE 17.- Surface charge and current distribution on a monopole above a box.
(h = 25 cm., λ = 150 cm.)

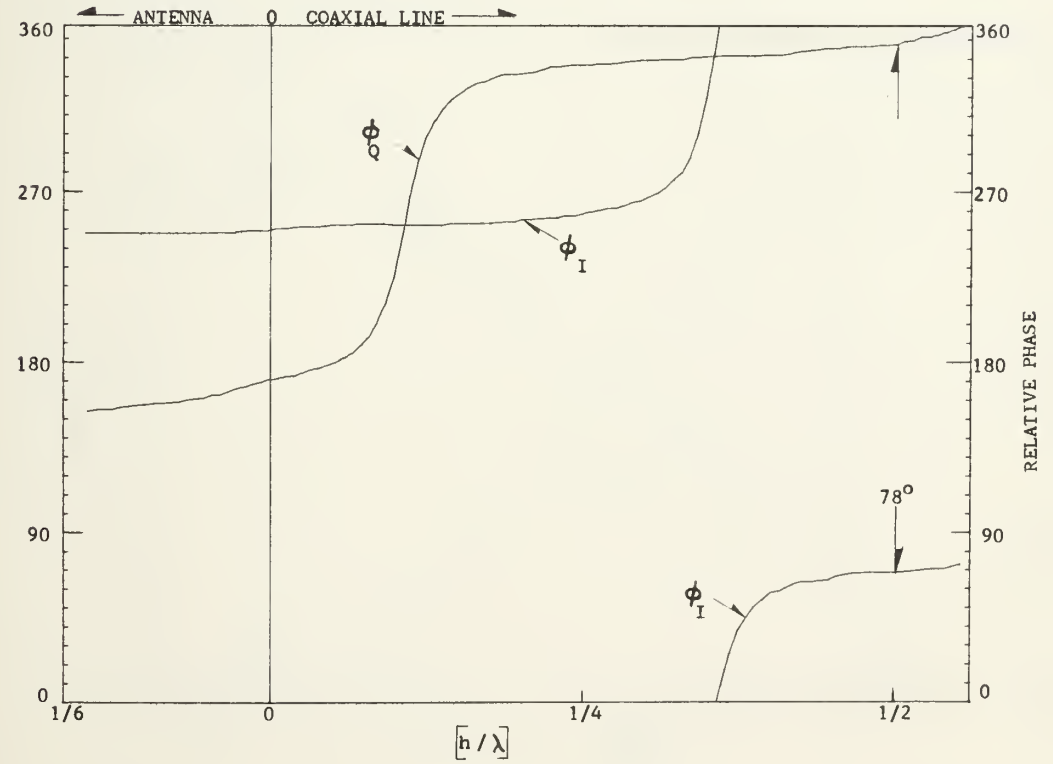

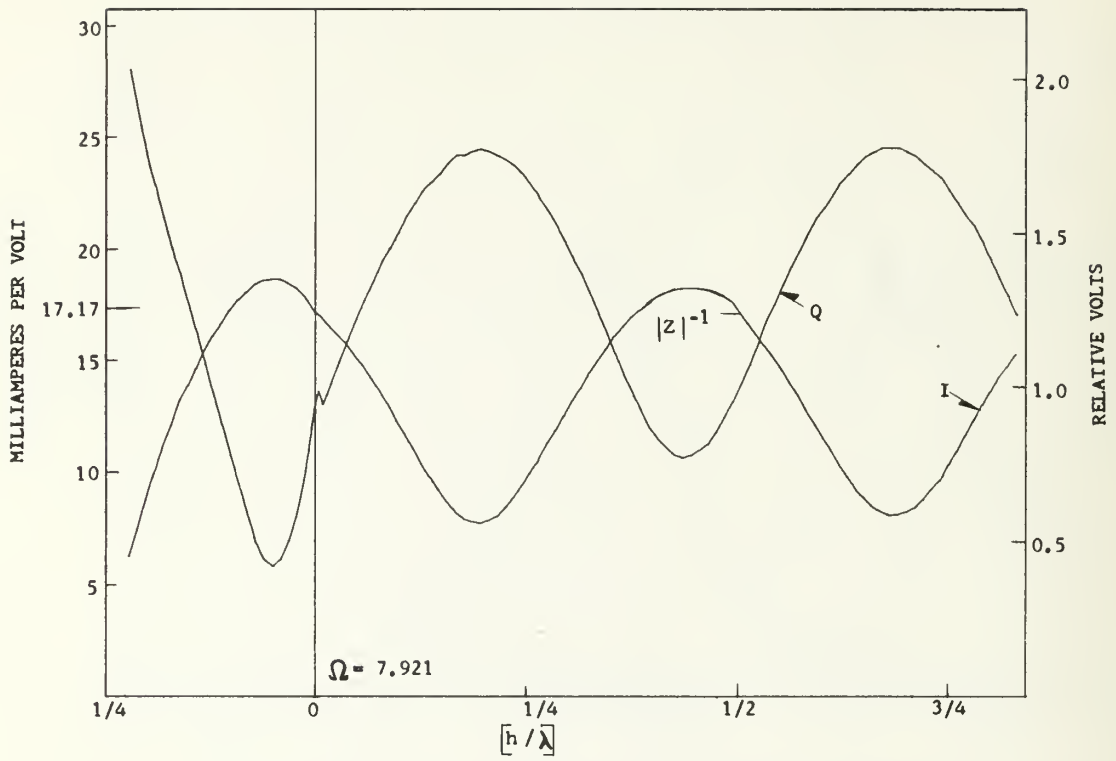

FIGURE 18.- Surface charge and current distribution on a monopole above a box.
(h = 25 cm., λ = 100 cm.)

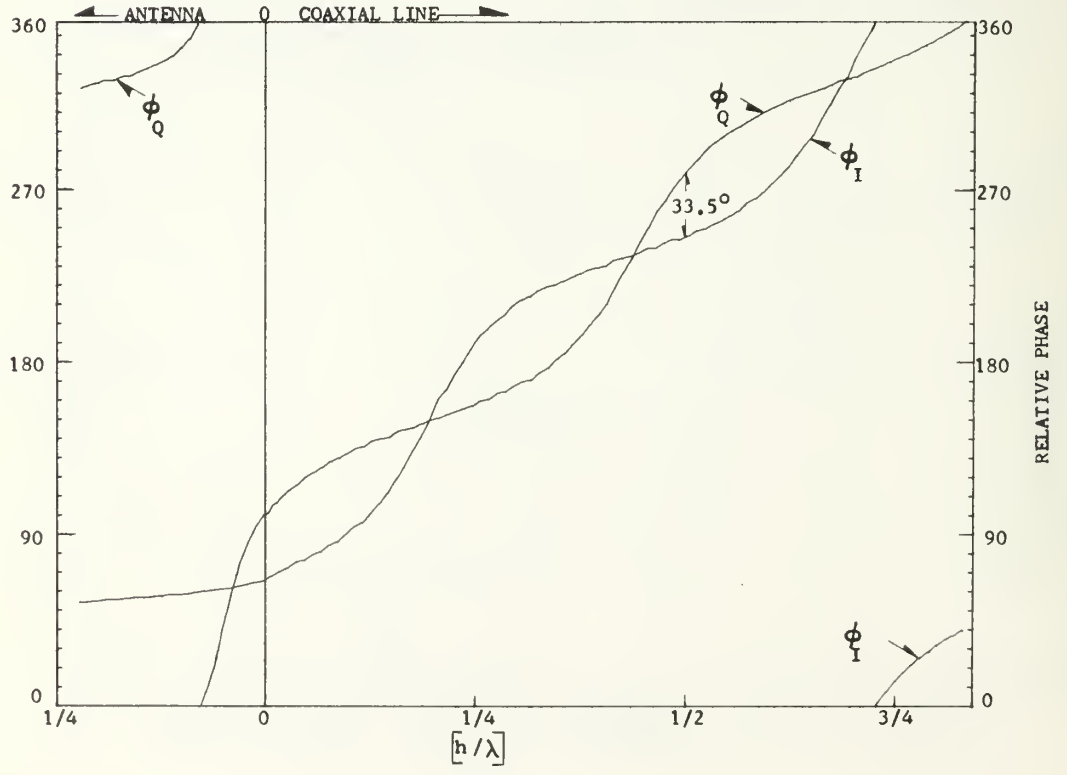

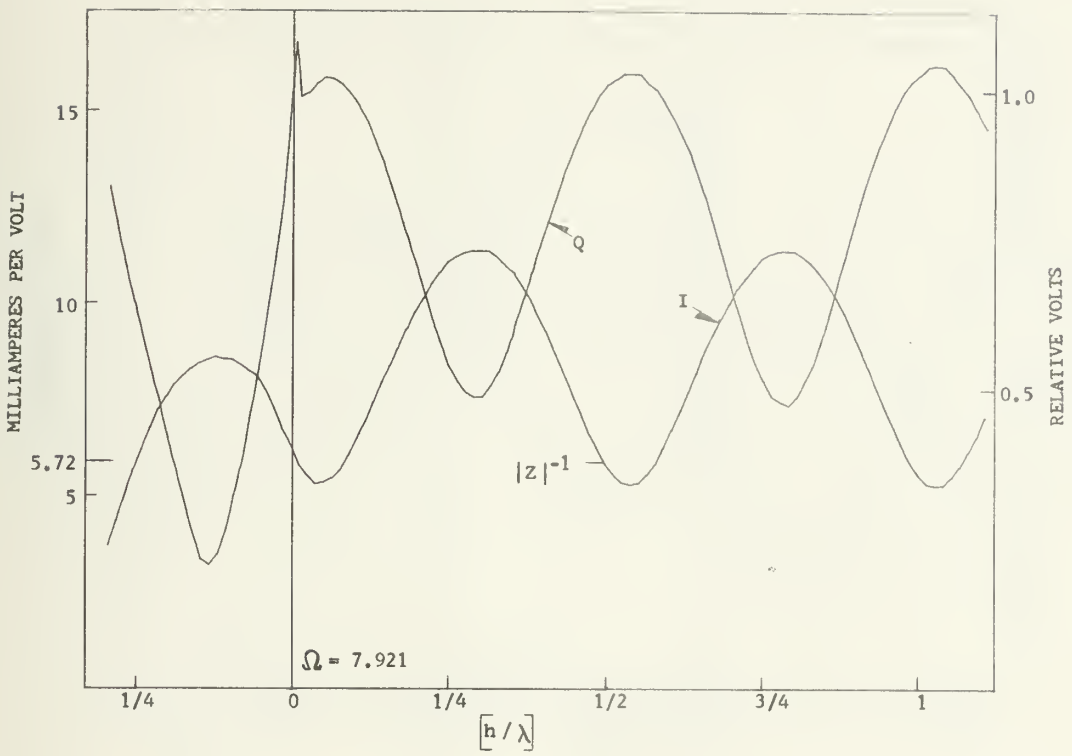

FIGURE 19.- Surface charge and current distribution on a monopole above a box.
(h = 25 cm., λ = 75 cm.)

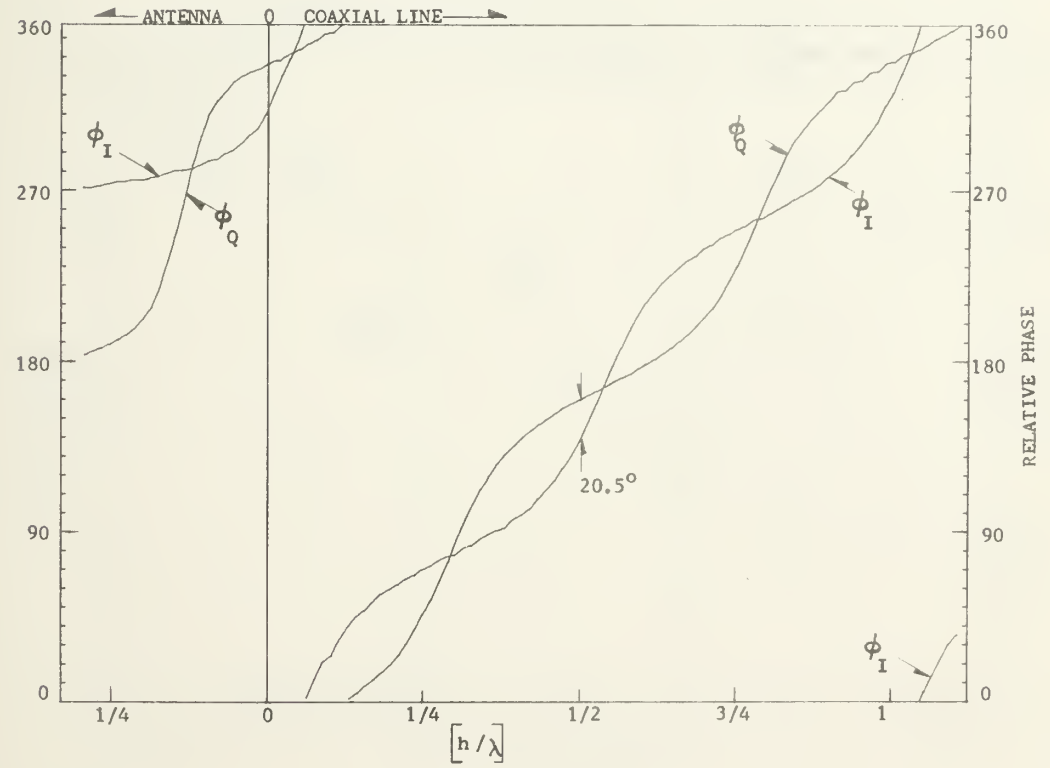

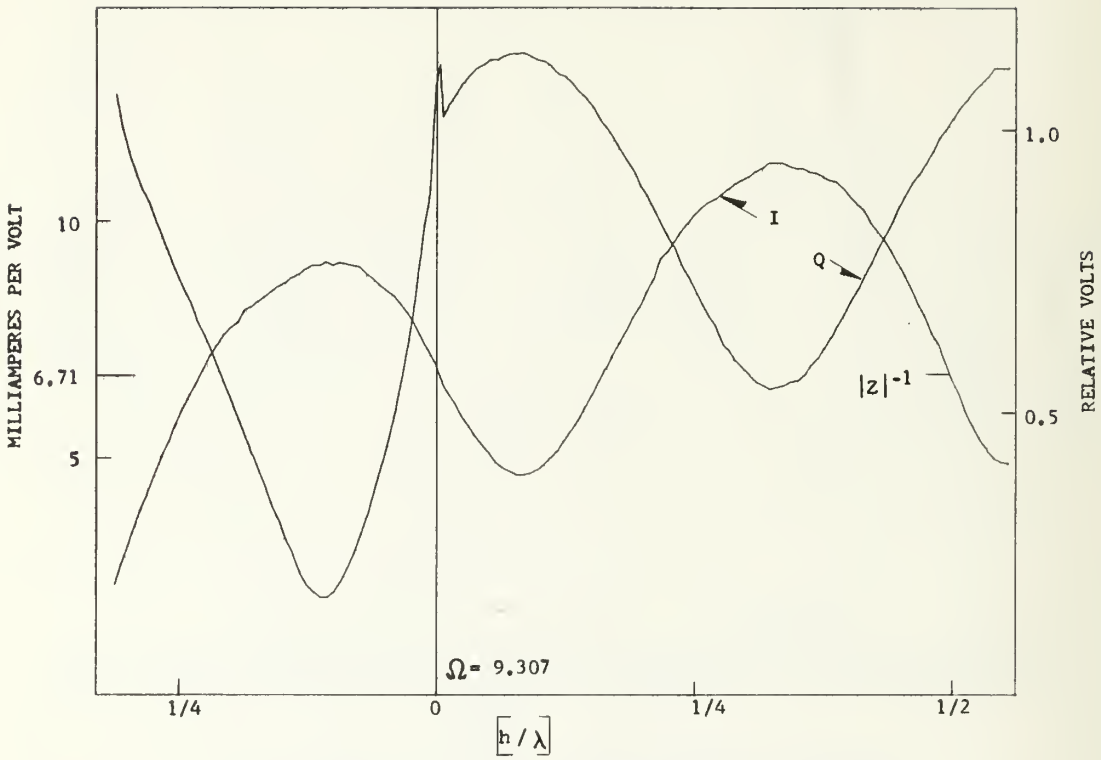

FIGURE 20.- Surface charge and current distribution on a monopole above a box.
(h = 50 cm., λ = 150 cm.)

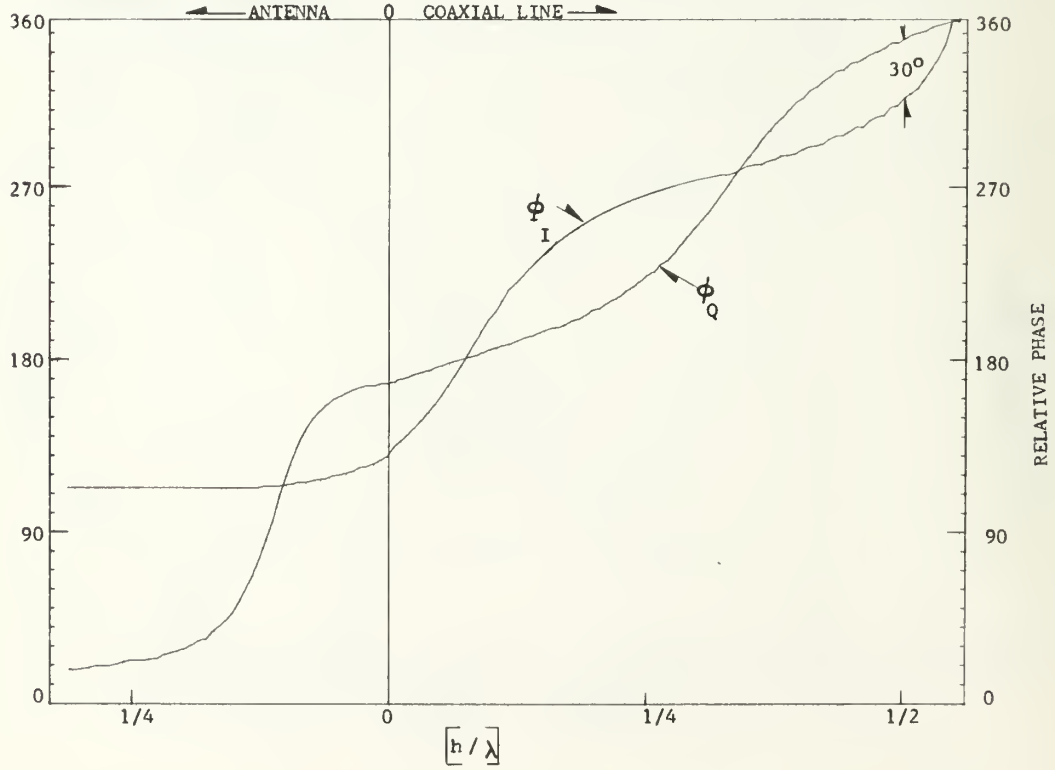

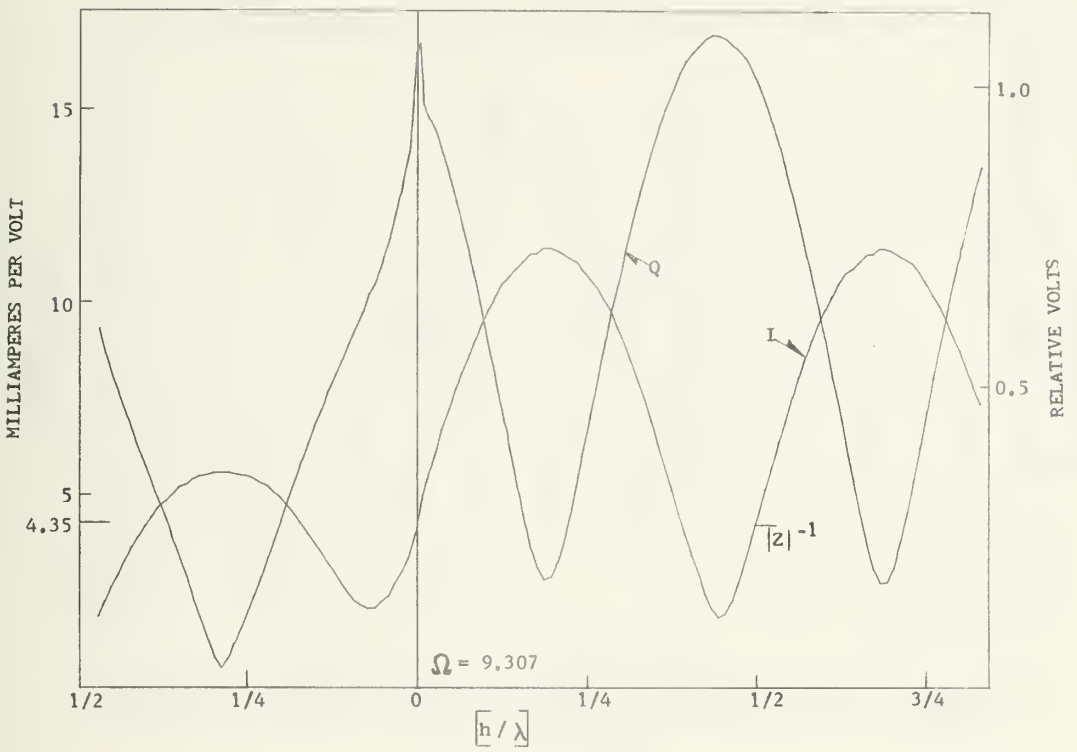

FIGURE 21.- Surface charge and current distribution on a monopole above a box.
(h = 50 cm., λ = 100 cm.)

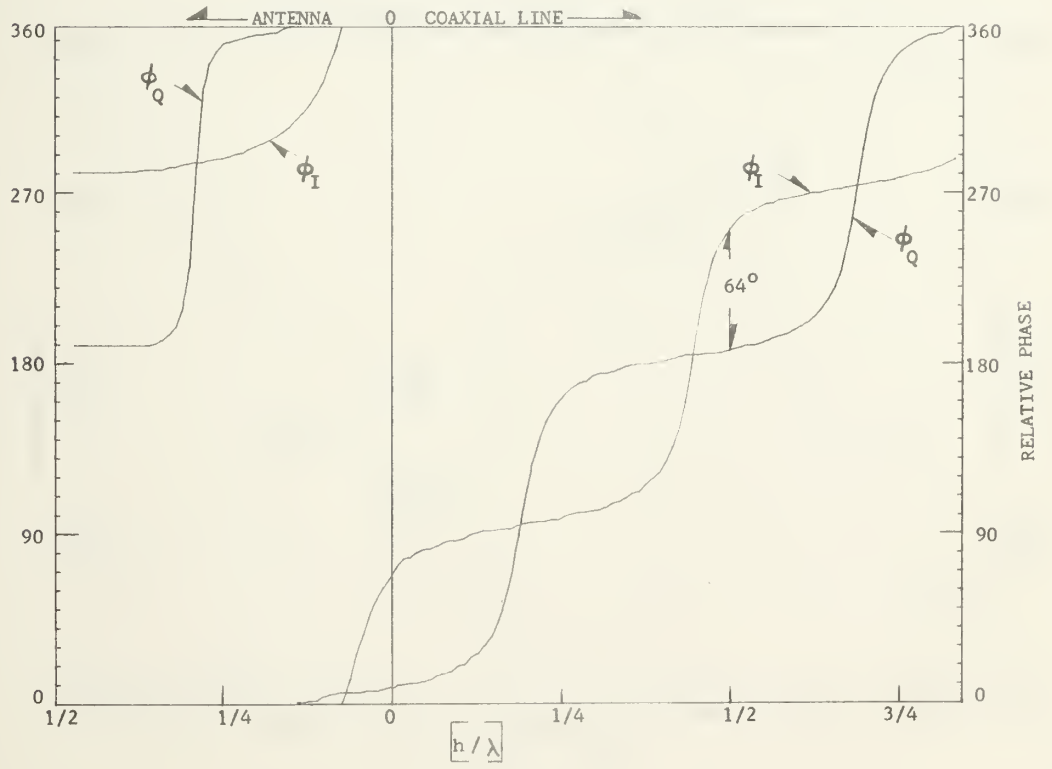

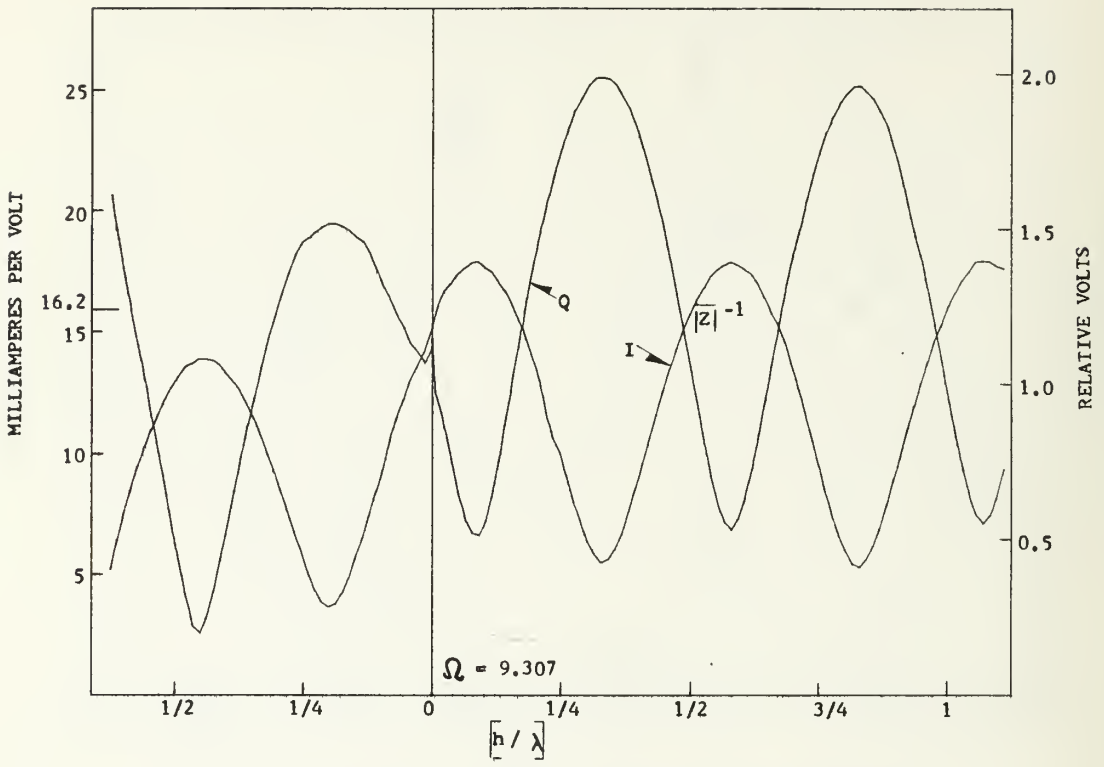

FIGURE 22.- Surface charge and current distribution on a monopole above a box.
(h = 50 cm., λ = 75 cm.)

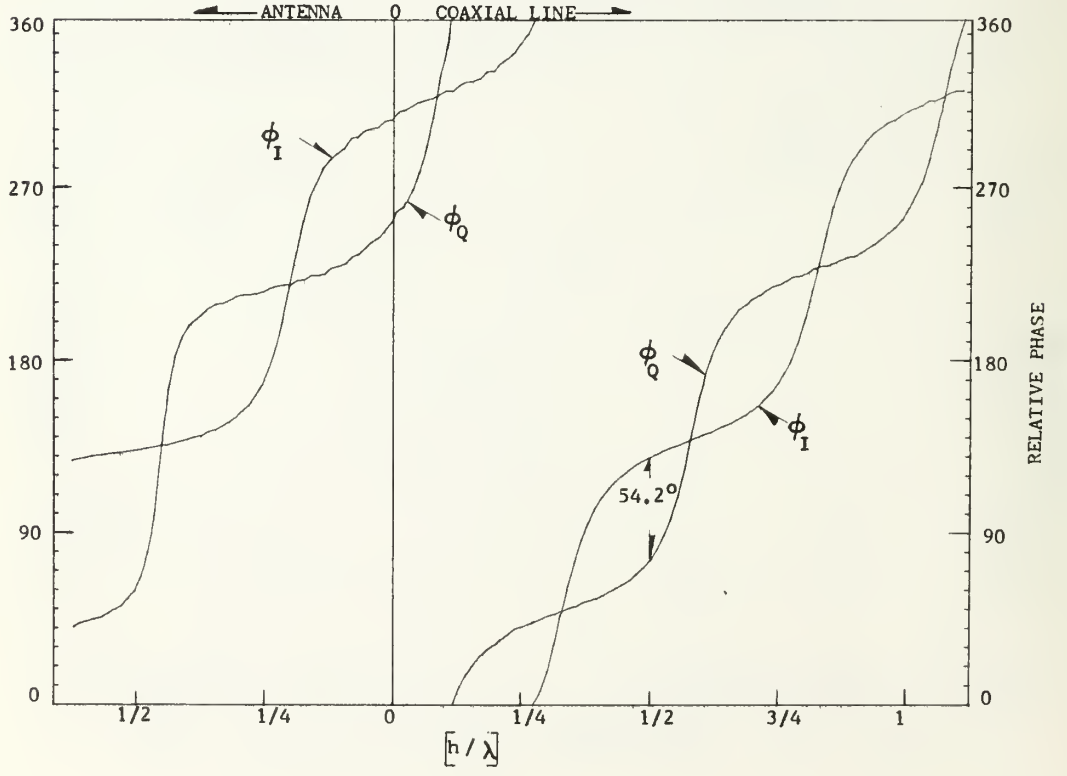

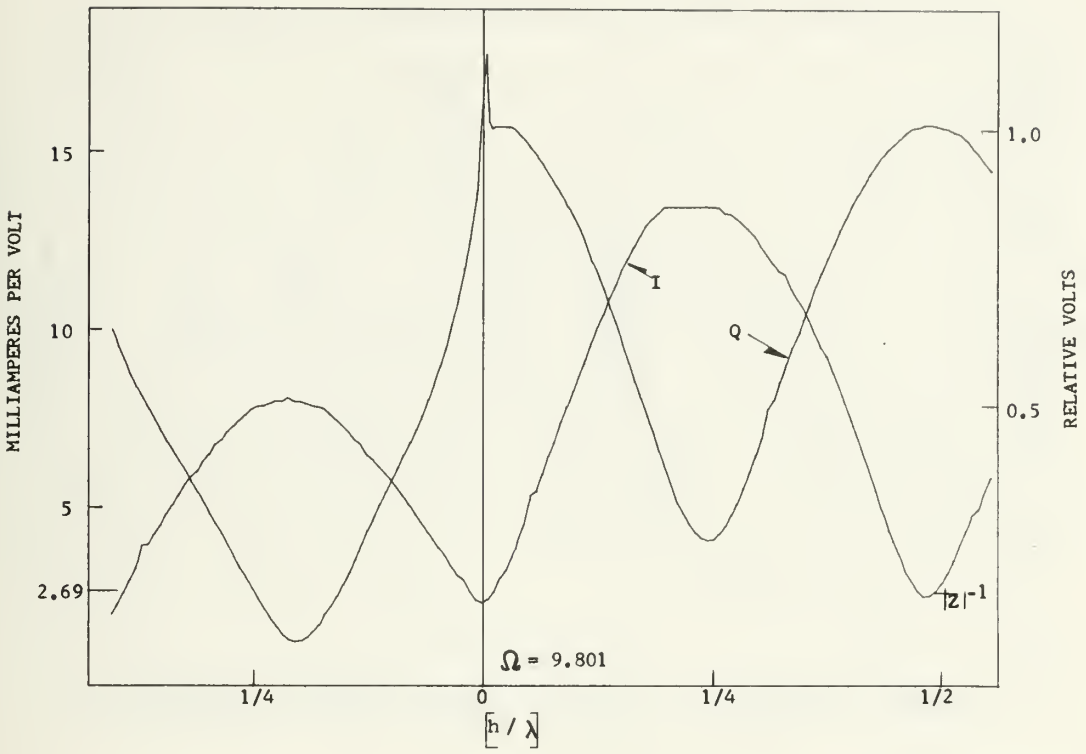

FIGURE 23.- Surface charge and current distribution on a monopole above a box.
(h = 64 cm., λ = 150 cm.)

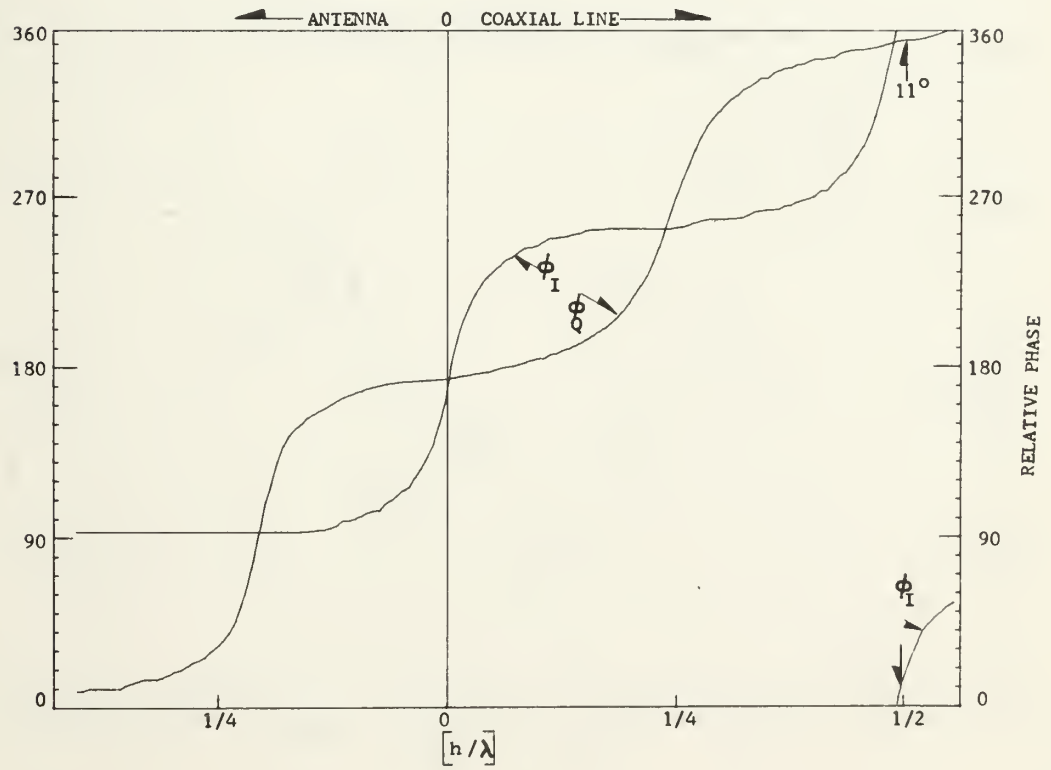

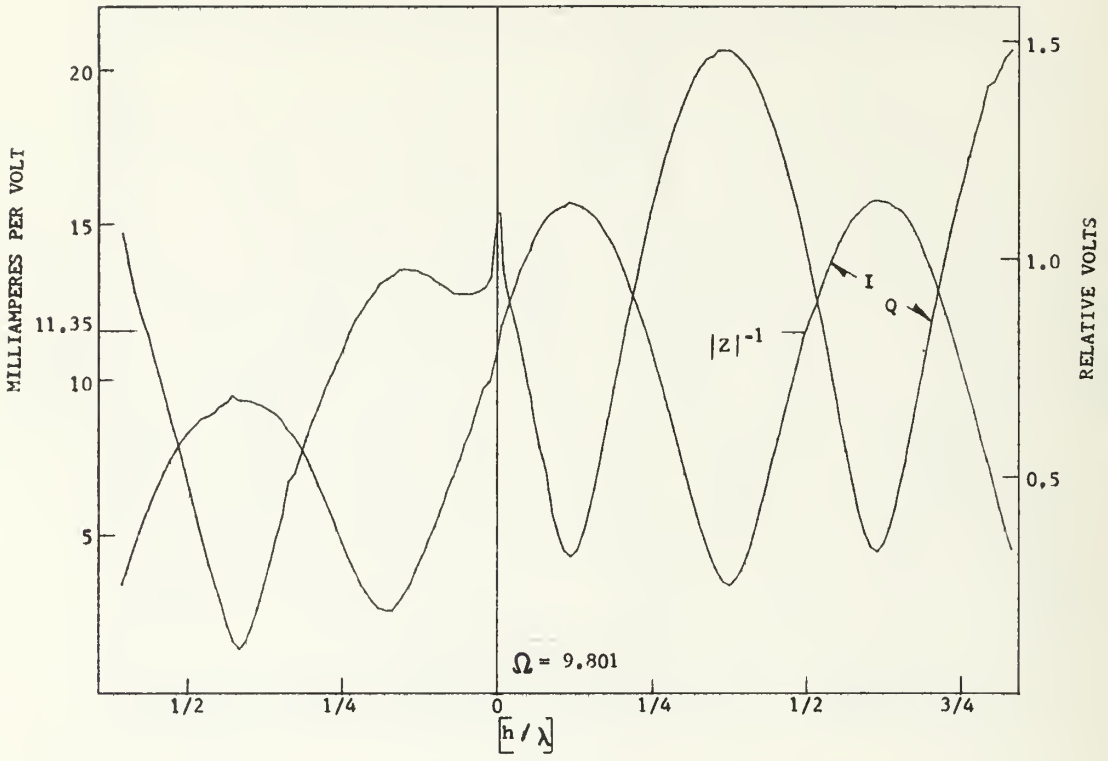

FIGURE 24.- Surface charge and current distribution on a monopole above a box.
(h = 64 cm., λ = 100 cm.)

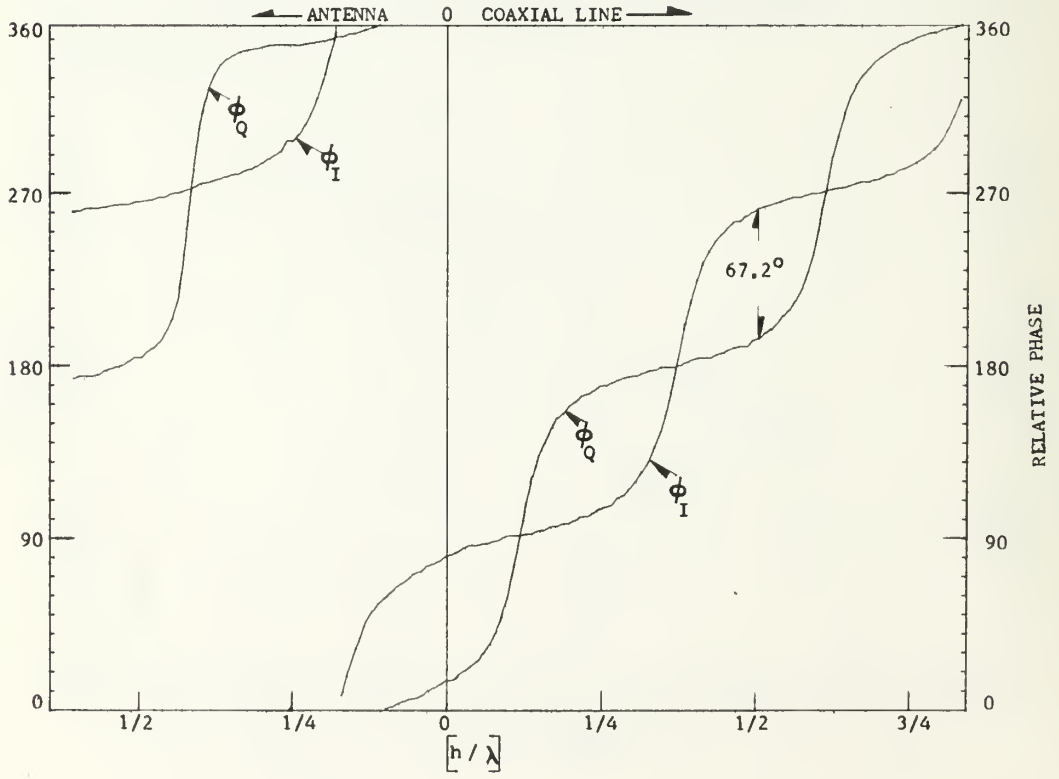

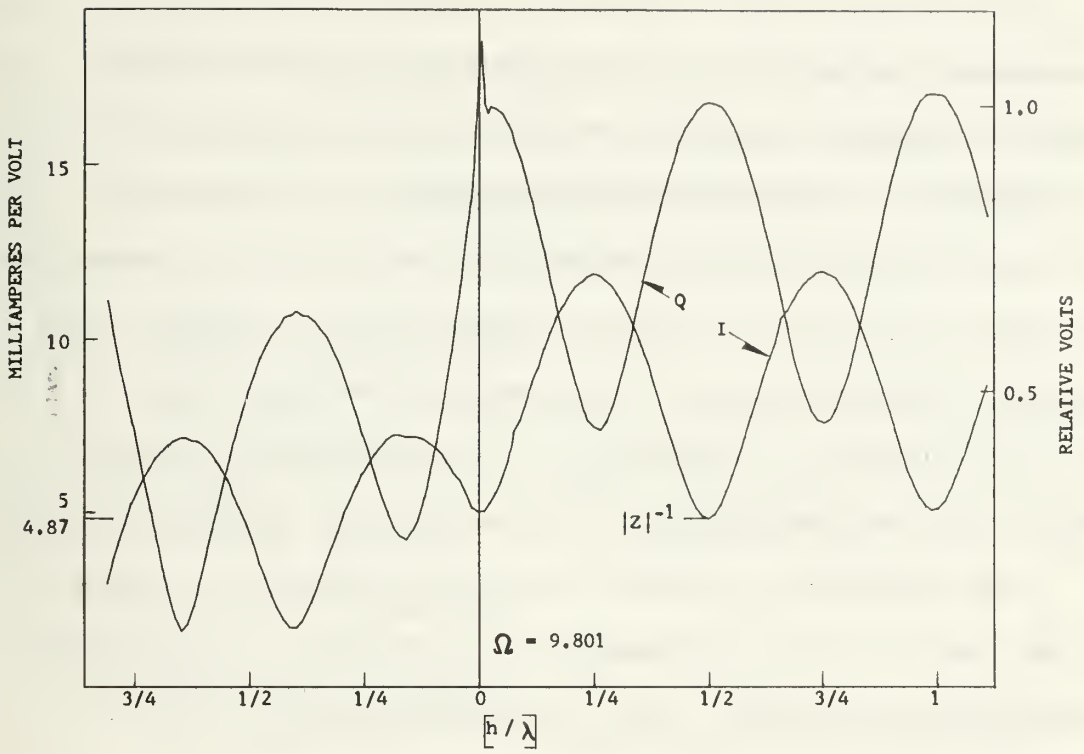

FIGURE 25.- Surface charge and current distribution on a monopole above a box.
(h = 64 cm,, λ = 75 cm.)

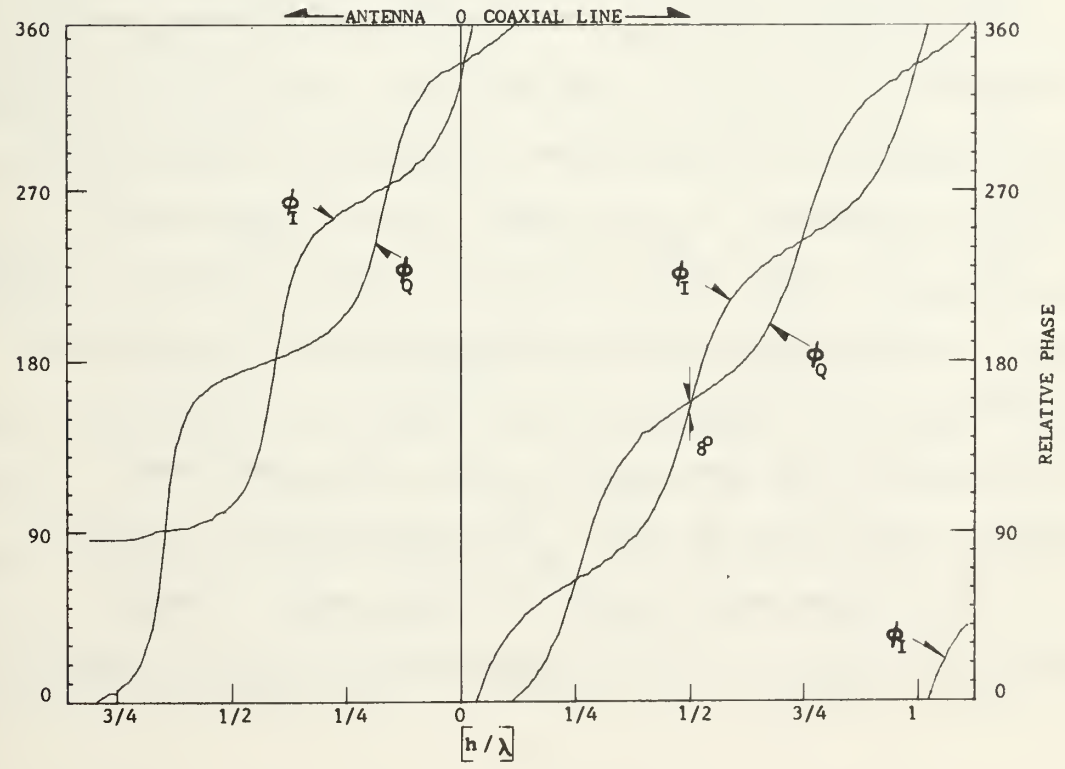

measurements respectively (corresponding to the maximum extension along the monopole of the respective probes). One exception to this description appears in Figure 16, where the probe positioning mechanism did not allow measurements along the entire monopole because of its length. The information obtained inside the coaxial feed line and accessible portion of the monopole was sufficient however to permit the determination of its electrical characteristics.

The parameter Ω shown in all the figures is a description used by King [Reference 4] to provide an indication of the monopole thickness, and is mathematically given by:

$$\Omega = 2 \ln (2h/a)$$

The relative phase plot shows the admittance angle at a distance $\lambda/2$ from the feed aperture. This is the angle resulting directly from the phase measurements detected by the vector voltmeter. A calculated negative admittance angle plots as a case where the charge phase leads the current phase. The admittance scale in milliamps/volt was derived by assuming an arbitrary relative voltage of 1 volt at a half wavelength from the aperture, and using the VSWR calculated admittance to obtain the corresponding current.

It is important to note that the peak of charge distribution found in all the magnitude plots at the feed

plane aperture is not due to the TEM mode discontinuity, but instead reflects the presence at the aperture of a plexiglass cover used to provide lateral support for the center conductor, also preventing moisture from entering the coaxial feed system.

C. BOX SURFACE MEASUREMENTS

Once the monopole antenna measurements were completed, the measurement of surface current and charge distributions on the box sides generated by a transmitting monopole located above the box was undertaken.

1. Surface Probe Theory

The theoretical considerations earlier described concerning measurement of charge distributions using a small monopole probe remain valid for this case. The dimensions of the probe and the manner in which it was constructed remain unchanged, with the only difference being how it is supported and positioned for the data acquisition. The resulting probe configuration, including the current probes, was shown in Figures 9 through 11, and owing to the support geometry will hereafter be referred to as the "T-BAR" probe.

Because of the geometrical configuration of the vertical surfaces of the box, the measurement of surface current distribution presented a complication not found on the monopole surfaces. On a cylindrical structure of small diameter relative to the wavelength of incident or transmitted electromagnetic energy, the distribution of surface currents will

be entirely in the axial direction. On the box surfaces however, the current distribution will be axial with respect to the measurement slots (hereafter referred to as longitudinal current), as well as in quadrature to the slot axis (which will be referred to as transverse current). In order to describe the overall current distribution, both of these components must be measured either sequentially or simultaneously.

The simplest arrangement for these measurements was provided by the construction of two current probes of the same dimensions as used in the monopole measurements, and so arranged that the planes of the coaxial cable loops were orthogonal to one another.

Several other complications arose in connection with the box surface measurements. Owing to the presence of the measurement slots, surface discontinuities exist which could affect the distribution of the transverse surface current. Consequently "filler bars" were machined to be placed in all the slots other than the one undergoing measurement, preserving a smooth surface geometry in the area adjacent to the slot being measured. It also appeared likely that the empty slot area immediately above the T-BAR could pose a field disturbance problem. Therefore one of the "filler bars" was cut into 1 cm lengths for use as a filler above the probe. Measurements were to proceed from the slot bottom at 1 cm intervals, after removal of the filler piece sequentially appearing at the top of the slot, preventing

coupling from the transmitting antenna directly to the probes. Suffice it to say that a complete set of measurements with, and without the 1 cm filler pieces resulted in no measurable differences, and their use was discontinued.

One final comment must be made to complete the description of the measurement procedure. It was observed that, owing to minor irregularities in the dimensions of the machined slots and T-BAR, a chatter existed as the bar was positioned using the rack and pinion, causing very erratic measurements. As a remedy a small beryllium copper clamp was fastened to the probe surface, drawing the T-BAR against the slot and serving to insure positive contact between the probes and the slot while resolving this situation.

2. Probe Calibration

As in the case of the monopole probes, the ideal procedure for calibration of the T-BAR probes would be the construction of a device such as a resonant cavity to provide a deterministic electromagnetic field configuration for calibration. Because of time limitations this was not a tractable alternative. It was decided, therefore, to limit the presentation of the charge data to a magnitude contour plot with no further calibration of the charge probe, as it appeared such a description would confirm the intuitive expectations of the charge distribution.

For the description of the surface current distribution a localized vectorial sum of the longitudinal and

transverse current components was desired, and this required at least a relative calibration of one probe to the other. This relative calibration was accomplished by placing them sequentially in the same electromagnetic field and recording their outputs as obtained from the vector voltmeter. It was theorized that, provided the electromagnetic field remained unchanged, the EMF induced in one probe should be the same as that induced in the orthogonal probe after the T-BAR had been rotated 90° in the field.

When the measurements of the surface distribution on the vertical sides of the box were completed, a pair of mutually orthogonal slots were machined in one side (Figure 11(b)). With a signal fed to the monopole antenna above the box, the probes were inserted sequentially in the two slots in such a manner that the circular probes were colinear with the center line crossing point of the slots, and their outputs recorded for both orientations. Great care was taken to maintain exactly the same experimental conditions for all the measurements. It was noticed that when the probe was inserted in slot No. 1 the possibility existed of currents being generated on the T-BAR as a result of direct coupling to the monopole. To prevent this an aluminum sheet was fastened to the box top, in order to shield the probe bar from the monopole, and this configuration was maintained for all the measurements.

With cases 1 and 2 representing positioning of the probe in the numerically corresponding slot, let

V_{L_2} and V_{L_1} = Complex voltage from longitudinal probe.

V_{T_1} and V_{T_2} = Complex voltage from transverse probe.

where as before the terms longitudinal and transverse are with respect to the measurement slot. It is expected that if the probes are identical, and under constant field conditions:

$$V_{L_1} = V_{T_2} \quad \text{and} \quad V_{L_2} = V_{T_1}$$

A calibration factor for one probe relative to the other is then given by:

$$\frac{V_{L_1}}{V_{L_2}} = |V_{cal}| \quad V_{cal}$$

The calibration procedure was carried out at four different frequencies to obtain an average magnitude calibration factor, while the phase calibration factor was obtained for the two frequencies at which surface distribution data for the box was to be measured. The results of the calibration are given in Table VI.

f (MHz)	$\lvert V_{cal} \rvert$	$\angle V_{cal}$
300	2.73	19.5°
400	2.73	-54.0°

Table VI. Surface Current Probe Calibration Data

One estimate of the validity of the calibration results from the following consideration. The EMF output from a circular loop in a varying magnetic field is directly proportional to the area of the loop. It may be seen in Figure 11 that, owing to the mutual orthogonality of the surface current probes, one loop is slightly larger than the other. A careful measurement of the loops provided an approximate area ratio of 2.54 which is near the value of the magnitude calibration factor indicated in Table VI, an intuitively gratifying result.

3. Measurement Procedure

The equipment set-up for the measurements of the surface distributions on the box sides was very similar in detail and purpose to that used for the monopole measurements and is shown in Figure 26. The only significant difference in this set-up is the use of the Boonton 230A power amplifier to boost the signal level of the output from the HP8640A generator, and the consequent need for greater attenuation in the reference channel to the vector voltmeter.

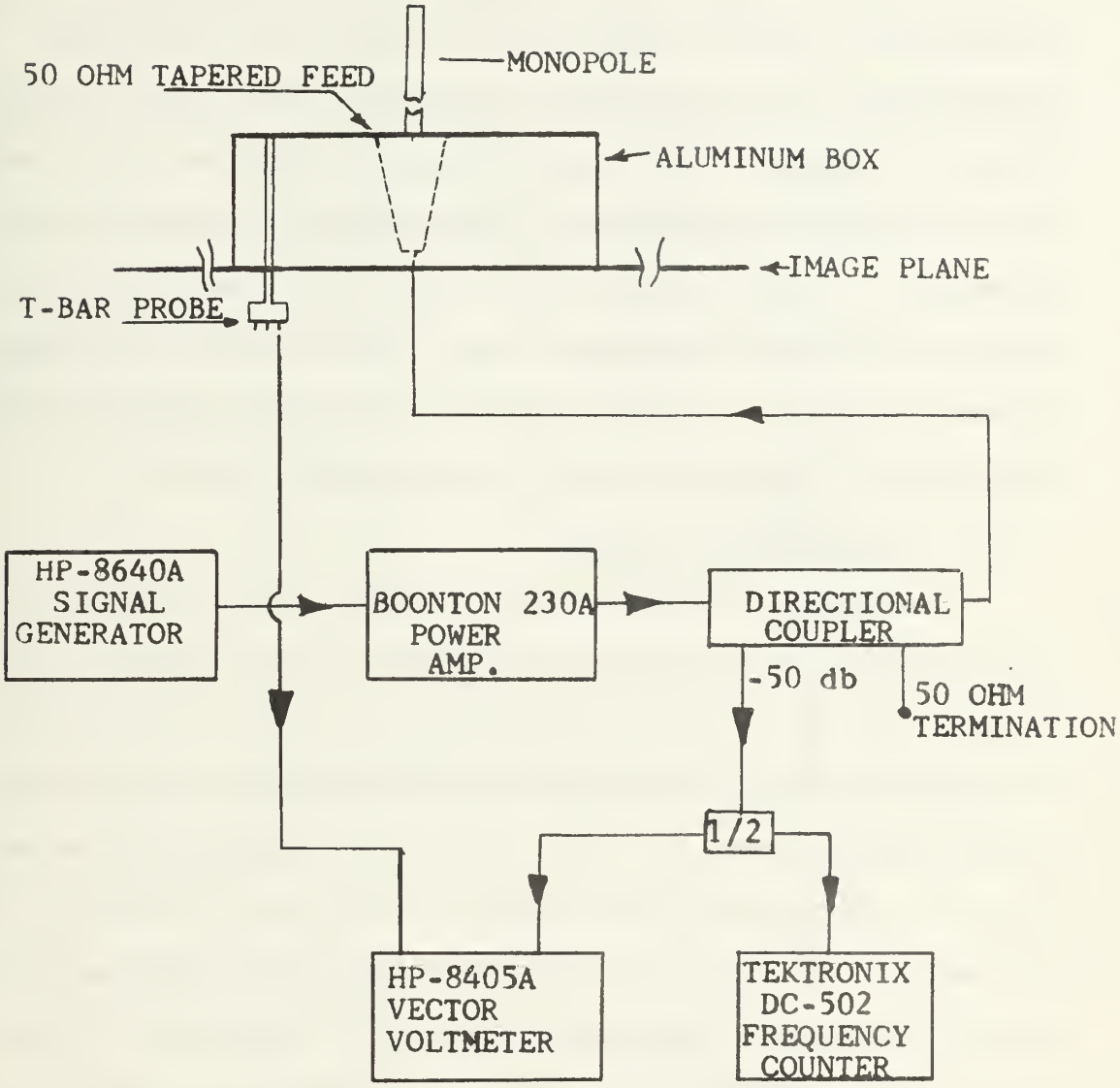

FIGURE 26. Box Surface Distribution Measurement System

The T-BAR probe was sequentially positioned in each measurement slot and the voltage (magnitude and phase) generated by each probe was recorded as displayed by the vector voltmeter. All the information gathered as a result of the surface distribution measurements is tabulated in Appendix B. The minimum height above the image plane, to which the probes had access, was a function of the probe element position on the T-BAR and the copper clamp mentioned earlier in connection with the measurement set-up.

4. Measurement Results

Figures 27 and 29 show selected current distribution information. The ellipses displayed in the figures show a description of the surface current in terms of the elliptically polarized components associated with a travelling electromagnetic wave. The orientation of the ellipse major axis is indicative of the spatial direction of current flow whereas the magnitude of the minor axis shows the amount of phase differential between the current components. This manner of presenting the surface current is the result of a development due to R.W.P. King of Harvard University, and R.W. Burton of the Naval Postgraduate School.[1]

The ellipses were plotted using the magnitude and phase of the voltage generated by the surface current

---

[1]A complete description of this development is scheduled for publication subsequent to the writing of this thesis.

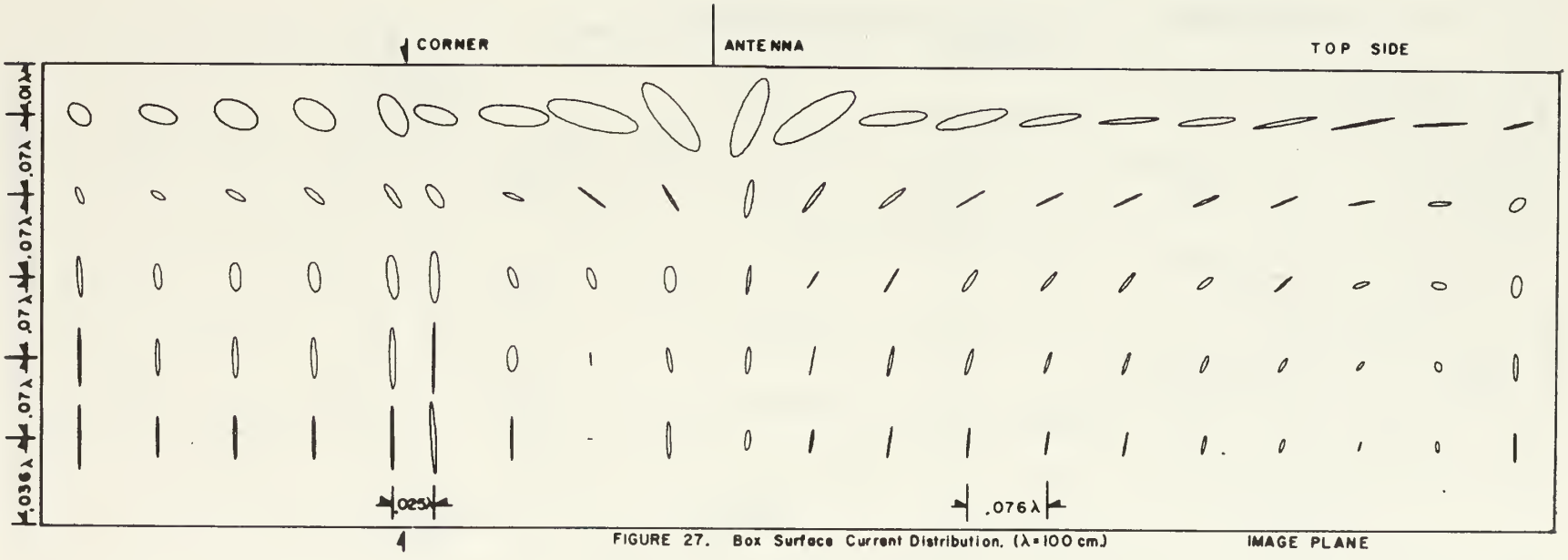

FIGURE 27. Box Surface Current Distribution. (λ=100 cm.)

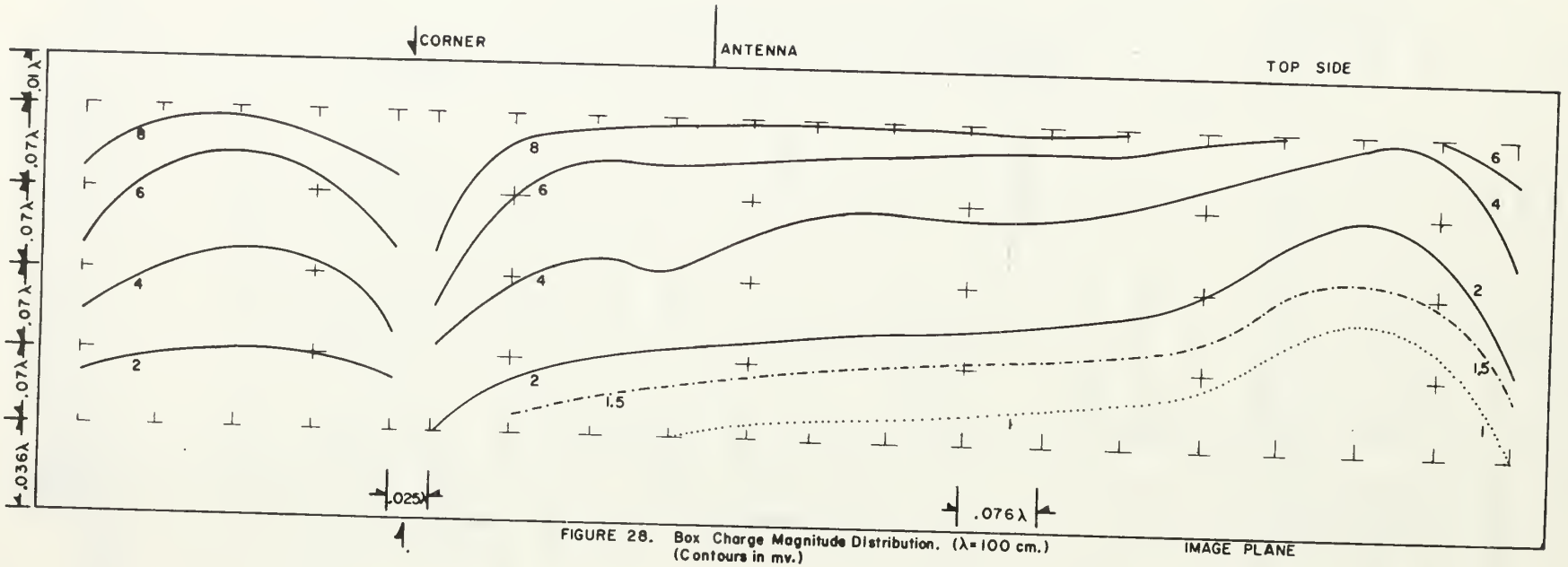

FIGURE 28. Box Charge Magnitude Distribution. (λ= 100 cm.)
(Contours in mv.)

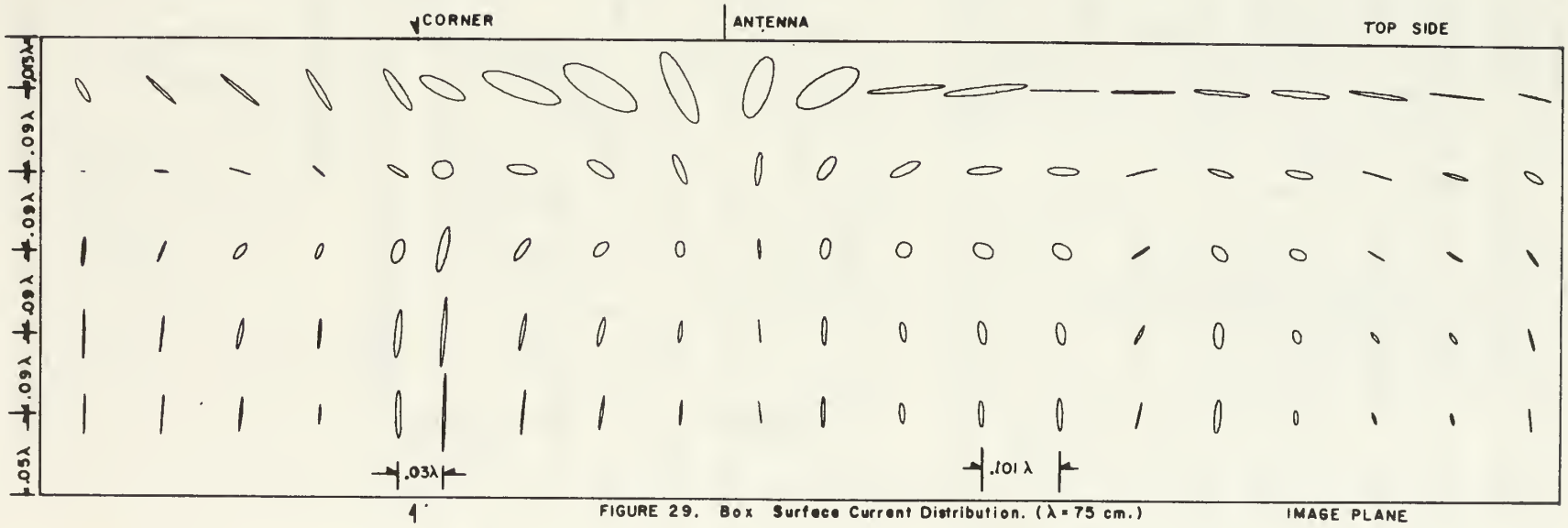

FIGURE 29. Box Surface Current Distribution. (λ = 75 cm.)

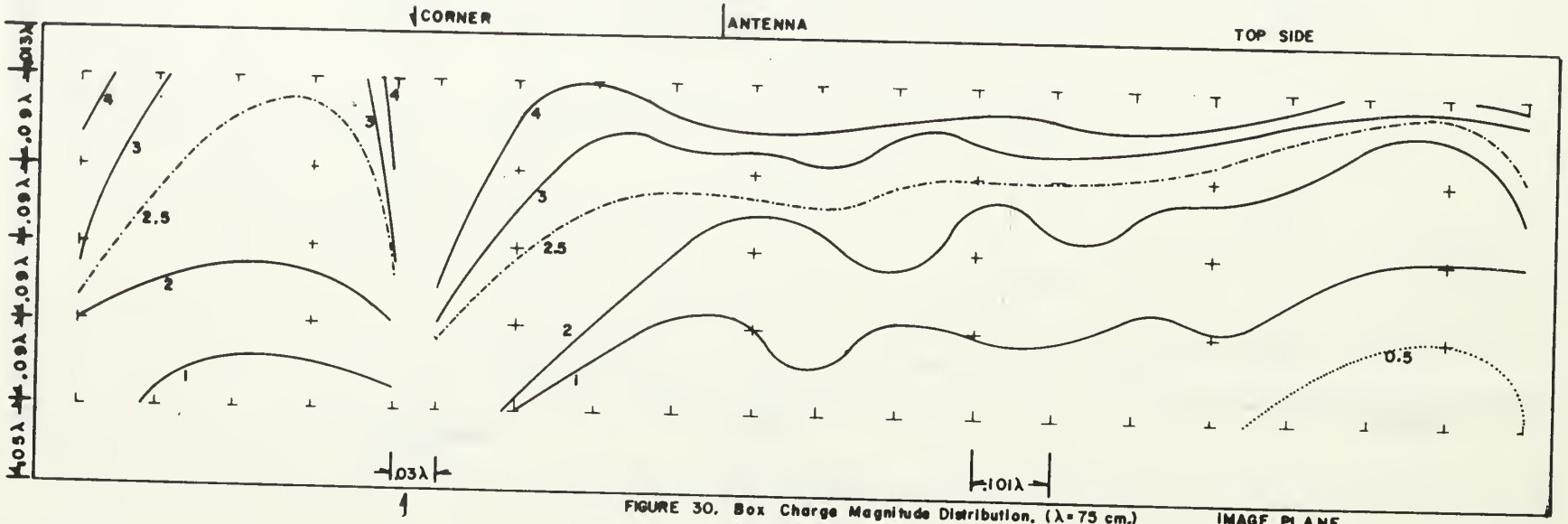

FIGURE 30. Box Charge Magnitude Distribution. (λ = 75 cm.)
(Contours in mv.)

measuring loops at positions 7 cm apart along each measurement slot. The vertical separation thus chosen preserved the dimensional symmetry relative to the horizontal separation of the measuring slots. Superimposed on the figures is an idealized presentation of the location of the principal geometrical features on the box as seen from the side.

Because a calibration of the charge probe (either absolute or relative) was not available, it was decided to plot the charge magnitude data in the form of equipotential contour lines in a manner that would at least permit a correlation with the intuitive expectations of the charge distribution.

The charge data (magnitude and phase) is tabulated in Appendix B. The equipotential contour plots were generated using linear interpolation among the charge magnitude values obtained along the measuring slots. The resulting graphical information is shown in Figures 28 and 30 in relation to the sides of the box. In addition to the features of interest, a grid is included which establishes the slot locations on the box sides', as well as the positions at which current data was plotted, providing one additional means of correlation between the two measurements.

IV. CONCLUSIONS AND RECOMMENDATIONS

1. The procedures for measurement of surface current and charge distributions on antennas were successfully modified to conduct similar measurements on antenna supporting structures. The techniques subsequently developed resulted in the measurement of the distributions of current and charge on the surfaces of the box supporting the radiating monopole, and are presently in use at the Naval Postgraduate School in experimental research for measurement of similar distributions originated by the scattering of electromagnetic plane waves incident on flat metallic surfaces.

2. In the cases studied of the radiating monopole antennas located above the image plane, the excellent correlation between the experimentally measured and theoretically predicted electrical characteristics proved the measurement procedures were of significant accuracy. Therefore, the results of the measurements conducted on the radiating monopoles located above the box are believed representative of the typical effects the chosen model geometry has on the antenna characteristics.

Although the experimental results given in Table V on the average do not show radical admittance changes, variations of admittance alone can not provide indication of the overall effect that the box (ship's superstructure) has on the monopole electrical characteristics. As mentioned earlier,

coupling between the monopole and additional structures located above the box remains to be investigated. In addition to the possible effects of coupling, a study of the changes in the far field radiation characteristics of the monopole is needed to complete the description of the electrical characteristics associated with this structure.

3. The measurement procedures followed in the research were relatively simple and their improvement to facilitate further research is desirable. Of greatest benefit would be the design of a feed line with a characteristic impedance which would allow the line's termination in a known precision load. This would greatly simplify the monopole probe calibration. In the event a general study of admittance (impedance) variations of monopoles above the model structure is of interest, construction of a feed line with electromagnetic probes fixed at a particular location as described in Reference 6 would simplify the measurement efforts.

4. The adaption to the T-BAR of the singly loaded circular current loop used successfully in the monopole surface measurements provides a very reliable means of measuring the surface current on the box sides.

The presentation of the measured surface current distribution shown in Figures 27 and 29 shows the elliptical polarization associated with the electromagnetic wave radiated from the box as a result of this surface current. The primary significance of this data lies in the benchmark it

provides for further analytical development. A numerical solution technique which yields transverse and longitudinal current components, of magnitude and phase which agree relatively with the measured data, will provide the correct solutions to the electrical characteristics of the antenna supported by the structure.

The single factor necessary for the measured data to exactly represent the surface current distribution is the accurate calibration of the probes. Such a calibration could be accomplished by construction of a cavity which provides a deterministic electromagnetic field to be measured by the probes, and is recommended for further research. However, a consideration of the measured data by itself again shows that any numerical analysis technique which generates solutions in agreement with the data here measured will of itself produce the necessary calibration factor.

5. The data obtained from the charge probe is also in need of calibration. The presentations of Figures 28 and 30 serve, however, to confirm the intuitive expectations of the charge distribution. It is seen that charge accumulation takes place on the structure corners, as well as near the antenna feed point. Similarly an absence of charge is noticed in the middle of the vertical sides, as well as at the contact region between the box and the image plane.

The calibration of the charge probe relative to the current probes could be a result of the cavity measurements

recomended earlier, or, given a numerical solution for the current, could be obtained by satisfying the equation of continuity on the box surfaces.

APPENDIX A

Mathematical Analysis of Monopole Probes [1]

The following mathematical derivation provides a basis for understanding the probe characteristics that create the requirement for calibration of the probes. The equivalent circuits for the monopole probes are shown in Figure A1.

1. Current Probe Analysis:

The following definitions apply to the quantities presented in the current probe equivalent circuit:

r_1	=	Coaxial Line outer conductor radius.
A_p	=	Current probe area.
V_g	=	Generator voltage.
Z_{of}	=	Feed line characteristic impedance.
$Z_A^{(in)}$	=	Antenna impedance transformed through feed line to probe position.
V_f	=	Feed line voltage at probe position.
I_f	=	Feed line current at probe position.
L_p	=	Probe inductance.
$Z_p^{(in)}$	=	Input Impedance to probe line.
V_i	=	Voltage induced in probe by feed line field.

---

[1] This development was suggested by Dr. J. B. Knorr, of the Naval Postgraduate School.

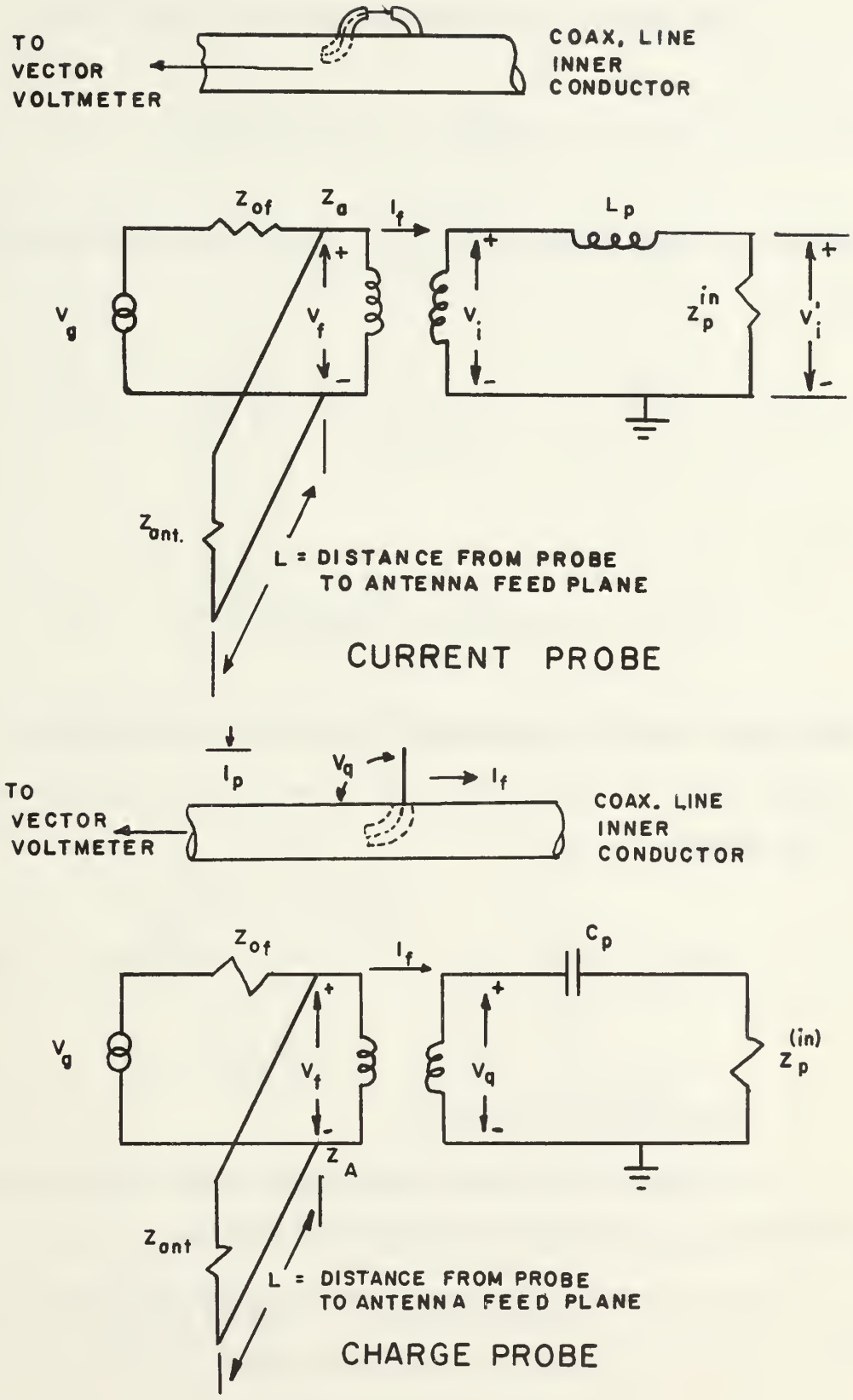

FIGURE A1. PROBE ANALYSIS

The field at the probe position is:

$$H_\phi = \frac{I_f}{2 \pi r}$$

and the voltage induced in the current probe by this field is:

$$V_I = \pm \frac{d\Phi}{dt} = \pm j\omega \iint_{probe} \mu_o \bar{H} \cdot \hat{n} \, da$$

or

$$V_I = \pm j\omega \left(\frac{I_f}{2 \pi r_1}\right) \mu_o A_p$$

where the ± applies depending upon the orientation of the current probe in the feed line. The voltage at the input to the probe line is:

$$V_I' = V_I \frac{Z_p^{(in)}}{Z_p^{(in)} + j \omega L_p} = \pm j\omega\mu_o \left(\frac{I_f}{2 \pi r_1}\right) A_p \times \frac{Z_p^{(in)}}{Z_p^{(in)} + j\omega L_p}$$

2. Charge Probe Analysis

Let the following definitions apply to the quantities presented in the probe equivalent circuit:

V_q = Voltage induced in charge probe.

C_p = Charge probe capacitance.

l_p = Charge probe length.

V_q' = Voltage at input to charge probe line.

The field at the position of the probe is:

$$E_r = \frac{V_f}{r \ln (r_2/r_1)} \qquad (r_2, r_1, = \text{feed line radii}).$$

and the voltage induced in the charge probe by this field is:

$$V_q = - \int_{\text{probe}} \bar{E} \cdot \overline{dl}$$

or,

$$V_q = \frac{V_f \, l_p}{r_1 \ln (r_2/r_1)}$$

The voltage at the input to the charge probe line is:

$$V_q' = V_q \frac{Z_p^{(in)}}{Z_p^{(in)} - j(\frac{1}{\omega C_p})}$$

$$= [\frac{V_f \, l_p}{r_1 \ln (r_2/r_1)}] \cdot [\frac{Z_p^{(in)}}{Z_p^{(in)} - j(\frac{1}{\omega C_p})}]$$

Assuming the input impedance to the probe line, $Z_p^{(in)}$, is the same for both probes (a valid assumption since the equipment set-up remains unchanged for the sequential use of the probes) then the ratio of charge to current induced

voltages, which is equivalent to the impedance at the probe position, is expressible as:

$$\frac{V'_q}{V'_I} = \left[\frac{V_f \, l_p}{\ln (r_2/r_1) \left(Z_p^{(in)} - j\frac{1}{\omega C_p}\right)}\right] \cdot \left[\frac{2\pi Z_p^{(in)} + j\omega l_p}{\pm j \omega \mu_o I_f}\right]$$

where input impedance to probe line, Z_p^{in}, is assumed the same for both probes.

$$\frac{V_f}{I_f} = Z_A^{(in)} = \text{Antenna input impedance at probe position,}$$

so

$$\frac{V'_q}{V'_I} = Z_A^{(in)} \left[\frac{(Z_p^{(in)} + j\omega L_p)}{\pm j(Z_p^{(in)} - j\frac{1}{\omega C_p})}\right] \cdot \left[\frac{l_p/A_p}{\omega \mu_o \frac{1}{2\pi} \ln r_2/r_1}\right]$$

Since

$$\omega \mu_o = \omega\sqrt{\mu_o \varepsilon_o \frac{\mu_o}{\varepsilon_o}} = \frac{2\pi}{\lambda} \eta$$

and

$$Z_{of} = \frac{1}{2\pi} \eta \ln r_2/r_1,$$

the above expression may be written as:

$$\frac{V'_q}{V'_I} = Z_A^{(in)} \left(\frac{Z_p^{(in)} + j\,\omega\,L_p}{\pm\, j\left(Z_p^{(in)} - j\,\frac{1}{\omega\,C_p}\right)} \right) \cdot \left(\frac{l_p}{A_p\,2\pi\,Z_{of}} \right)$$

It is clear from this expression that the angle of $\frac{V'_q}{V'_I}$ will not be the angle of the transformed antenna impedance, $Z_A^{(in)}$, but will be offset from it by the angle of the first bracketed term. Since both the charge probe and the current probe drive the vector voltmeter through the same probe line length (sequentially), the additional phase shift introduced into the vector voltmeter reading due to this source may be neglected.

Conclusion: A plot of relative phase will not show V'_q and V'_I in phase at the same point where V_f and I_f are in phase unless the probes are calibrated to take into account the angle offset factor.

APPENDIX B

Surface Distribution Data On Vertical Sides Of The Box. (Magnitudes in millivolts of EMF generated by surface probes. Relative Phase Angle in degrees. Height in cm above the image plane.)

	MEASUREMENT SLOT NUMBER						
h (cm)	1	2	3	4	5	6	7
28.76	14.8	11.0	10.4	10.9	14.8	20.0	12.4
27.76	11.8	9.0	8.5	8.6	11.0	15.3	9.6
26.76	10.0	7.7	7.3	7.4	10.0	13.0	8.1
25.76	9.4	7.0	6.6	6.6	9.2	12.2	7.4
24.76	8.8	6.4	6.1	6.1	8.6	11.2	6.8
23.76	8.3	6.0	5.7	5.7	8.1	10.6	6.4
22.76	7.8	5.7	5.4	5.4	7.8	10.2	6.1
21.76	7.5	5.3	5.1	5.2	7.4	9.8	5.7
20.76	7.1	5.1	4.9	4.9	7.0	9.6	5.5
19.76	6.8	4.9	4.6	4.7	6.7	9.0	5.2
18.76	6.5	4.7	4.4	4.5	6.4	8.6	4.9
17.76	6.2	4.5	4.2	4.4	6.2	8.3	4.7
16.76	6.0	4.4	4.0	4.2	5.8	8.1	4.5
15.76	5.6	4.0	3.8	4.0	5.5	7.3	4.3
14.76	5.3	3.8	3.6	3.8	5.2	7.2	4.0
13.76	5.0	3.6	3.4	3.6	4.9	6.5	3.7
12.76	4.7	3.4	3.2	3.6	4.6	6.3	3.5
11.76	4.3	3.1	2.9	3.3	4.2	5.6	3.3
10.76	4.0	2.9	2.8	2.8	4.1	5.3	3.0
9.76	3.6	2.7	2.5	2.5	3.6	4.8	2.8
8.76	3.2	2.4	2.3	2.3	3.2	4.4	2.6
7.76	2.9	2.1	2.0	2.0	2.9	3.9	2.3
6.76	2.5	1.9	1.8	1.8	2.5	3.4	2.1
5.76	2.1	1.6	1.5	1.5	2.2	2.9	1.9
4.76	1.7	1.3	1.2	1.2	1.8	2.5	1.7
4.16	1.5	1.1	1.0	1.0	1.5	2.1	1.3

Charge Magnitude (f = 300 MHz)

	SLOT NUMBER						
h (cm)	8	9	10	11	12	13	14
28.76	10.9	12.2	12.0	11.0	10.6	10.0	8.9
27.76	8.5	9.2	8.9	8.4	7.7	7.9	6.8
26.76	7.2	7.6	7.4	6.8	6.5	6.7	5.7
25.76	6.4	6.7	6.4	5.9	5.8	5.8	5.0
24.76	5.8	6.0	5.8	5.4	5.3	5.3	4.6
23.76	5.5	5.7	5.3	5.2	4.9	4.9	4.2
22.76	5.2	5.3	4.9	4.5	4.5	4.6	3.8
21.76	5.0	5.0	4.6	4.3	4.2	4.3	3.6
20.76	4.7	4.8	4.4	4.0	4.0	3.9	3.4
19.76	4.5	4.6	4.1	3.7	3.7	3.8	3.1
18.76	4.3	4.4	3.9	3.7	3.5	3.6	3.0
17.76	4.2	4.3	3.7	3.3	3.3	3.3	2.8
16.76	3.9	4.1	3.5	3.2	3.1	3.1	2.6
15.76	3.8	3.9	3.3	3.0	3.0	3.0	2.4
14.76	3.5	3.7	3.0	2.8	2.8	2.8	2.3
13.76	3.3	3.5	2.9	2.6	2.6	2.6	2.1
12.76	3.2	3.2	2.6	2.4	2.4	2.4	2.0
11.76	2.9	3.0	2.4	2.3	2.2	2.2	1.8
10.76	2.8	2.8	2.3	2.1	2.0	2.0	1.7
9.76	2.5	2.5	2.1	1.8	1.8	1.8	1.5
8.76	2.3	2.0	1.8	1.7	1.6	1.7	1.4
7.76	2.0	1.8	1.6	1.5	1.4	1.4	1.2
6.76	1.8	1.6	1.4	1.3	1.3	1.3	1.0
5.76	1.6	1.4	1.2	1.1	1.1	1.1	0.8
4.76	1.3	1.3	0.9	0.9	0.9	0.9	0.7
4.16	1.2	1.1	0.9	0.9	0.8	0.8	0.6

Charge Magnitude (f = 300 MHz)

	SLOT NUMBER					
h (cm)	15	16	17	18	19	20
28.76	9.9	8.1	7.0	5.5	6.0	10.0
27.76	7.3	6.1	5.1	4.1	4.5	8.0
26.76	6.1	5.1	4.2	3.4	3.8	6.9
25.76	5.4	4.5	3.7	3.0	3.4	6.3
24.76	4.9	4.1	3.3	2.7	3.1	5.8
23.76	4.5	3.8	3.0	2.4	2.9	5.4
22.76	4.1	3.5	2.8	2.2	2.7	5.1
21.76	3.8	3.3	2.6	2.1	2.5	4.8
20.76	3.5	3.1	2.4	1.9	2.3	4.5
19.76	3.3	2.9	2.2	1.8	2.2	4.3
18.76	3.1	2.8	2.1	1.6	2.0	4.1
17.76	2.9	2.6	1.9	1.5	1.9	3.9
16.76	2.7	2.4	1.8	1.4	1.8	3.6
15.76	2.6	2.3	1.6	1.3	1.6	3.4
14.76	2.4	2.1	1.5	1.2	1.5	3.2
13.76	2.2	2.0	1.4	1.1	1.4	3.0
12.76	2.0	1.8	1.3	1.0	1.3	2.8
11.76	1.9	1.6	1.1	0.9	1.2	2.6
10.76	1.7	1.5	1.0	0.8	1.1	2.5
9.76	1.5	1.4	0.9	0.7	1.0	2.2
8.76	1.4	1.2	0.8	0.7	0.9	1.9
7.76	1.2	1.1	0.7	0.5	0.8	1.7
6.76	1.0	1.0	0.6	0.5	0.7	1.5
5.76	0.9	0.9	0.5	0.4	0.6	1.3
4.76	0.7	0.7	0.4	0.3	0.5	1.1
4.16	0.7	0.7	0.4	0.3	0.4	1.0

Charge Magnitude (f = 300 MHz)

	SLOT NUMBER						
h (cm)	1	2	3	4	5	6	7
28.76	23.0	31.0	58.0	91.0	96.0	104.0	136.0
27.76	20.5	27.0	50.0	74.0	94.0	100.0	130.0
26.76	19.0	25.0	46.0	69.0	90.0	98.0	125.0
25.76	18.0	24.0	43.8	65.5	85.0	96.0	122.0
24.76	17.5	23.0	42.0	63.0	84.0	95.0	120.0
23.76	17.0	23.0	40.0	60.5	81.0	94.0	117.0
22.76	16.5	23.0	39.0	60.0	80.0	91.0	115.0
21.76	16.5	22.5	38.0	59.0	79.0	90.5	114.0
20.76	16.0	22.0	38.0	58.0	78.0	90.0	111.0
19.76	16.0	22.0	37.0	57.0	76.0	89.0	110.0
18.76	16.0	22.0	36.0	57.0	75.0	88.5	109.0
17.76	16.0	22.0	36.0	55.0	74.0	87.5	107.5
16.76	16.0	22.0	35.5	54.5	74.0	86.0	107.0
15.76	16.0	21.8	35.0	53.8	74.0	85.5	105.5
14.76	16.0	21.8	35.0	53.0	72.5	85.0	105.0
13.76	16.0	21.8	34.5	52.5	71.0	85.0	105.0
12.76	16.0	21.5	34.0	52.1	71.0	84.0	104.0
11.76	16.0	21.5	34.0	52.0	70.5	84.0	103.5
10.76	16.2	21.5	34.0	51.0	70.0	83.5	103.0
9.76	16.0	20.0	33.8	51.0	70.0	83.5	102.5
8.76	17.0	20.0	33.0	51.0	70.0	83.5	102.5
7.76	17.5	20.0	32.8	51.0	70.0	84.0	101.0
6.76	17.0	20.0	32.0	51.0	70.0	83.0	101.0
5.76	17.0	19.0	31.0	50.0	70.0	85.0	102.0
4.76	16.0	18.0	30.0	50.0	68.0	82.0	97.5
4.16	16.0	18.0	30.0	56.0	68.0	83.0	97.5

Charge Phase (f = 300 MHz)

	SLOT NUMBER						
h (cm)	8	9	10	11	12	13	14
28.76	-180.0	-152.0	-157.0	-180.0	155.0	124.0	90.0
27.76	174.0	-161.0	-164.0	176.0	151.0	120.0	88.0
26.76	166.0	-170.0	-170.0	171.0	149.0	119.0	86.0
25.76	159.0	-178.0	-174.0	167.5	145.0	116.0	85.0
24.76	153.0	178.0	-180.0	163.0	142.5	115.0	85.0
23.76	148.0	171.0	178.0	159.0	140.0	112.0	84.0
22.76	143.0	164.0	174.0	155.0	137.5	110.5	82.5
21.76	138.0	157.5	170.0	151.0	135.0	110.0	80.5
20.76	135.0	153.0	165.0	149.0	131.0	108.5	80.0
19.76	131.0	149.0	160.0	146.0	130.0	107.0	80.0
18.76	129.0	145.0	157.5	145.0	127.5	105.0	80.0
17.76	126.0	140.0	155.0	143.0	125.5	105.0	80.0
16.76	125.0	138.0	152.5	140.0	125.0	104.5	80.0
15.76	121.0	135.0	150.0	139.0	124.0	104.0	78.0
14.76	120.0	131.5	148.0	136.0	120.5	103.5	77.5
13.76	120.0	130.0	145.0	135.0	120.0	102.0	77.5
12.76	118.0	125.0	145.0	135.0	119.0	100.5	77.5
11.76	117.0	125.0	144.0	134.0	116.5	102.5	77.5
10.76	115.5	123.0	142.0	132.5	116.0	100.0	78.0
9.76	115.0	121.0	141.0	132.0	115.0	100.0	77.5
8.76	114.0	119.0	144.0	131.0	115.0	100.5	77.5
7.76	112.0	115.0	142.5	132.0	112.0	102.5	78.0
6.76	110.0	110.0	148.0	135.0	111.0	104.0	78.0
5.76	110.0	107.5	148.0	136.0	115.0	105.0	79.0
4.76	110.0	95.0	155.0	137.5	95.0	105.0	84.0
4.16	110.0	85.0	165.0	133.0	90.0	107.0	84.0

Charge Phase (f = 300 MHz)

	SLOT NUMBER					
h (cm)	15	16	17	18	19	20
28.76	57.0	65.0	40.0	-32.0	-79.0	-120.0
27.76	58.0	61.0	40.0	-32.0	-78.0	-120.0
26.76	56.0	60.5	39.0	-32.0	-78.0	-120.0
25.76	56.0	60.0	39.0	-34.0	-78.0	-120.0
24.76	54.1	59.0	39.0	-34.0	-78.0	-121.0
23.76	53.5	58.0	39.0	-34.0	-78.0	-123.0
22.76	52.5	58.0	38.5	-35.0	-78.0	-123.0
21.76	52.5	57.0	38.0	-35.0	-79.0	-124.0
20.76	52.0	56.0	38.0	-35.0	-80.0	-125.0
19.76	50.0	56.0	38.0	-36.0	-80.0	-125.0
18.76	50.0	56.0	38.0	-36.0	-80.0	-125.0
17.76	49.5	57.0	38.0	-36.0	-80.0	-125.0
16.76	50.0	55.0	38.0	-36.0	-80.5	-125.0
15.76	50.0	56.0	38.0	-36.0	-80.5	-126.0
14.76	48.0	56.0	38.0	-36.0	-82.5	-126.0
13.76	50.0	57.0	37.0	-36.0	-82.5	-127.0
12.76	51.0	58.0	37.0	-36.0	-82.5	-127.5
11.76	50.0	58.0	37.0	-36.0	-80.0	-127.5
10.76	50.0	57.0	37.0	-35.0	-80.0	-128.0
9.76	44.0	56.0	38.0	-35.0	-80.0	-129.5
8.76	46.0	56.0	39.0	-35.0	-80.0	-130.0
7.76	44.0	54.0	39.0	-36.0	-80.0	-130.0
6.76	45.0	53.0	39.0	-36.0	-78.0	-130.0
5.76	40.0	53.0	39.0	-38.0	-77.5	-130.0
4.76	33.0	53.0	39.0	-39.0	-80.0	-131.0
4.16	19.0	48.0	39.0	-40.0	-80.0	-134.0

Charge Phase (f = 300 MHz)

	SLOT NUMBER						
h (cm)	1	2	3	4	5	6	7
28.26	1.2	1.9	2.2	2.1	1.5	2.2	3.6
27.26	0.9	1.5	1.9	1.7	1.3	1.9	2.8
26.26	0.7	1.3	1.6	1.6	1.2	1.6	1.4
25.26	0.6	1.1	1.4	1.3	1.1	1.4	2.0
24.26	0.6	1.0	1.3	1.2	1.1	1.2	1.6
23.26	0.5	0.9	1.1	1.1	1.0	1.1	1.5
22.26	0.5	0.8	1.1	1.0	0.9	1.0	1.3
21.26	0.4	0.7	1.0	1.0	0.9	0.9	1.1
20.26	0.4	0.7	0.9	1.0	0.9	0.9	1.0
19.26	0.4	0.6	0.8	0.9	0.8	0.8	0.9
18.26	0.4	0.6	0.8	0.8	0.8	0.7	0.8
17.27	0.3	0.5	0.7	0.8	0.7	0.7	0.7
16.26	0.3	0.5	0.7	0.7	0.7	0.6	0.7
15.26	0.3	0.5	0.6	0.7	0.7	0.6	0.6
14.26	0.3	0.4	0.6	0.6	0.6	0.5	0.5
13.26	0.3	0.4	0.5	0.6	0.6	0.4	0.5
12.26	0.3	0.4	0.5	0.5	0.6	0.4	0.4
11.26	0.2	0.3	0.4	0.5	0.5	0.3	0.5
10.26	0.2	0.3	0.4	0.4	0.5	0.3	0.5
9.26	0.2	0.3	0.4	0.4	0.4	0.3	0.6
8.26	0.2	0.3	0.3	0.4	0.4	0.2	0.5
7.26	0.2	0.2	0.3	0.3	0.3	0.1	0.5
6.26	0.1	0.2	0.3	0.3	0.3	0.1	0.4
5.26	0.1	0.2	0.2	0.2	0.2	0.1	0.4
4.26	0.1	0.1	0.2	0.2	0.2	0.3	0.2
3.66	0.1	0.1	0.1	0.2	0.2	0.3	0.1

Transverse Current Magnitude (f = 300 MHz)

	SLOT NUMBER						
h (cm)	8	9	10	11	12	13	14
28.26	4.6	3.0	1.9	4.1	3.4	3.6	3.1
27.26	3.7	2.2	1.5	3.0	3.0	2.9	2.8
26.26	3.1	1.7	1.0	2.5	2.6	2.4	2.4
25.26	2.4	1.4	1.0	2.1	2.3	2.2	2.0
24.26	2.1	1.2	0.7	1.8	2.0	1.9	1.8
23.26	1.7	1.0	0.6	1.5	1.7	1.7	1.6
22.26	1.5	0.9	0.5	1.3	1.5	1.6	1.5
21.26	1.4	0.8	0.5	1.1	1.3	1.4	1.3
20.26	1.2	0.8	0.4	1.0	1.2	1.3	1.2
19.26	1.0	0.8	0.4	0.9	1.1	1.2	1.2
18.26	0.9	0.8	0.4	0.8	1.0	1.1	1.1
17.27	0.9	0.7	0.4	0.7	0.9	1.0	1.0
16.26	0.8	0.7	0.3	0.7	0.8	0.9	0.9
15.26	0.7	0.7	0.3	0.6	0.8	0.9	0.9
14.26	0.5	0.6	0.3	0.5	0.7	0.8	0.8
13.26	0.4	0.5	0.3	0.5	0.7	0.7	0.7
12.26	0.4	0.5	0.3	0.5	0.6	0.7	0.7
11.26	0.3	0.4	0.1	0.4	0.5	0.6	0.6
10.26	0.2	0.4	0.2	0.4	0.5	0.6	0.6
9.26	0.2	0.4	0.3	0.3	0.4	0.5	0.5
8.26	0.3	0.3	0.3	0.4	0.4	0.5	0.4
7.26	0.1	0.3	0.3	0.3	0.3	0.4	0.4
6.26	0.1	0.2	0.3	0.3	0.3	0.4	0.3
5.26	0.5	0.1	0.3	0.2	0.3	0.3	0.3
4.26	0.4	0.2	0.3	0.2	0.3	0.3	0.2
3.66	0.2	0.2	0.3	0.2	0.3	0.1	0.2

Transverse Current Magnitude (f = 300 MHz)

	SLOT NUMBER					
h (cm)	15	16	17	18	19	20
28.26	3.0	2.9	3.3	3.3	2.7	1.5
27.26	2.6	2.5	2.5	2.7	2.2	1.4
26.26	2.4	2.3	2.2	2.3	2.0	1.2
25.26	2.0	2.0	2.0	2.0	1.8	1.1
24.26	1.8	1.8	1.8	1.8	1.6	1.0
23.26	1.6	1.6	1.7	1.6	1.5	0.9
22.26	1.5	1.4	1.5	1.4	1.3	0.8
21.26	1.4	1.3	1.4	1.3	1.2	0.8
20.26	1.3	1.2	1.3	1.3	1.1	0.7
19.26	1.2	1.1	1.2	1.2	1.1	0.7
18.26	1.1	1.0	1.1	1.1	1.0	0.7
17.27	1.0	1.0	1.0	1.0	0.9	0.6
16.26	1.0	0.9	1.0	1.0	0.9	0.6
15.26	0.9	0.9	0.9	0.9	0.8	0.6
14.26	0.8	0.8	0.9	0.8	0.8	0.5
13.26	0.8	0.7	0.8	0.8	0.7	0.5
12.26	0.7	0.7	0.8	0.7	0.6	0.5
11.26	0.6	0.6	0.7	0.6	0.6	0.4
10.26	0.6	0.6	0.7	0.6	0.5	0.4
9.26	0.5	0.5	0.6	0.5	0.5	0.3
8.26	0.5	0.5	0.5	0.5	0.4	0.3
7.26	0.4	0.4	0.5	0.4	0.4	0.3
6.26	0.4	0.4	0.4	0.3	0.3	0.2
5.26	0.3	0.3	0.4	0.3	0.3	0.2
4.26	0.3	0.3	0.3	0.2	0.2	0.1
3.66	0.2	0.3	0.3	0.2	0.2	0.1

Transverse Current Magnitude (f = 300 MHz)

	SLOT NUMBER						
h (cm)	1	2	3	4	5	6	7
28.26	-175.0	-162.0	-155.0	-152.0	-150.0	-110.0	-104.0
27.26	-180.0	-165.0	-157.0	-155.0	-150.0	-110.0	-106.0
26.26	176.0	-167.0	-157.5	-155.0	-149.0	-111.0	-108.0
25.26	172.0	-170.0	-160.0	-156.0	-148.0	-111.0	-108.0
24.26	170.0	-170.0	-160.0	-154.0	-148.0	-111.0	-109.0
23.26	168.0	-172.5	-159.0	-153.0	-148.0	-112.5	-110.0
22.26	166.0	-175.0	-160.0	-153.0	-148.0	-112.5	-111.0
21.26	165.0	-175.0	-162.0	-152.0	-148.0	-112.5	-114.0
20.26	164.0	-176.0	-163.0	-154.0	-148.0	-113.0	-114.0
19.26	161.0	-176.5	-164.0	-154.0	-148.0	-113.0	-115.0
18.26	160.5	-179.0	-164.0	-154.0	-148.0	-115.0	-118.0
17.27	160.0	-180.0	-164.0	-154.0	-148.0	-124.0	-117.0
16.26	160.0	-180.0	-160.0	-154.0	-148.0	-120.0	-117.0
15.26	160.0	180.0	-160.0	-154.0	-148.0	-115.0	-117.0
14.26	159.0	180.0	-160.0	-154.0	-148.0	-110.0	-130.0
13.26	159.0	180.0	-165.0	-154.0	-148.0	-110.0	-134.0
12.26	159.0	179.0	-162.0	-154.0	-148.0	-114.0	-142.0
11.26	157.0	179.0	-162.0	-154.0	-148.0	-110.0	-150.0
10.26	155.0	179.0	-162.0	-154.0	-148.0	-115.0	-158.0
9.26	155.0	179.0	-162.5	-156.0	-148.0	-114.0	-156.0
8.26	166.0	179.0	-164.5	-156.0	-145.0	-115.0	-167.0
7.26	162.5	179.0	-165.0	-156.0	-144.0	-108.0	-170.0
6.26	160.0	179.0	-165.0	-157.0	-140.0	-125.0	-167.0
5.26	164.0	179.0	-165.0	-157.0	-145.0	-154.0	-175.0
4.26	164.0	179.0	-165.0	-159.0	-145.0	-154.0	-154.0
3.66	175.0	179.0	-165.0	-154.0	-144.0	-180.0	-140.0

Transverse Current Phase (f = 300 MHz)

	SLOT NUMBER						
h (cm)	8	9	10	11	12	13	14
28.26	- 88.0	- 71.0	92.0	90.0	65.0	49.0	16.0
27.26	- 89.0	- 71.0	88.0	86.0	64.0	46.0	16.0
26.26	- 90.0	- 75.0	85.0	85.0	61.0	44.0	15.5
25.26	- 90.0	- 75.0	75.0	84.0	61.0	42.0	14.0
24.26	- 92.0	- 75.0	70.0	82.0	57.0	40.5	12.5
23.26	- 94.0	- 76.0	63.0	80.0	56.0	40.0	11.0
22.26	- 94.0	- 76.0	54.0	76.0	56.0	37.0	10.5
21.26	- 94.0	- 77.5	50.0	74.0	54.0	36.0	10.0
20.26	- 94.0	- 76.0	42.0	72.0	51.0	34.0	9.0
19.26	-100.0	- 76.0	41.0	71.0	49.0	34.0	7.5
18.26	- 94.0	- 74.0	35.0	67.5	46.0	31.0	6.5
17.27	-104.0	- 70.0	28.0	66.0	45.0	31.0	5.5
16.26	-100.0	- 68.0	34.0	62.0	44.0	29.0	5.0
15.26	- 94.0	- 65.0	30.0	61.0	44.0	29.0	5.0
14.26	-102.0	- 60.0	55.0	60.0	41.0	29.0	4.0
13.26	- 99.0	- 60.0	54.0	58.0	41.0	30.0	3.5
12.26	-108.0	- 60.0	24.0	55.0	41.0	29.0	1.5
11.26	- 94.0	- 59.0	41.0	59.0	45.0	29.0	0.5
10.26	-140.0	- 57.0	70.0	54.0	50.0	25.5	0.5
9.26	-140.0	- 55.0	24.0	55.0	57.0	25.0	0.5
8.26	145.0	- 52.0	7.0	52.0	54.0	25.0	0.5
7.26	145.0	- 51.0	-18.0	51.0	49.0	24.0	0.5
6.26	127.0	176.0	-15.0	50.0	48.0	26.0	-0.5
5.26	145.0	162.0	-15.0	44.0	25.0	25.0	-0.5
4.26	175.0	80.0	-15.0	34.0	19.0	25.0	5.0
3.66	165.0	72.0	15.0	30.0	37.0	10.0	5.0

Transverse Current Phase (f = 300 MHz)

	SLOT NUMBER					
h (cm)	15	16	17	18	19	20
28.26	- 5.0	-44.0	-64.0	-80.0	-89.0	-105.0
27.26	- 6.0	-45.0	-65.0	-79.0	-88.0	-105.0
26.26	- 7.0	-44.0	-65.0	-80.0	-89.0	-105.0
25.26	- 8.0	-45.0	-65.0	-79.0	-89.0	-105.0
24.26	- 9.0	-44.0	-65.0	-78.0	-89.0	-105.0
23.26	-10.0	-44.0	-67.0	-77.0	-87.5	-105.0
22.26	-10.0	-46.0	-65.0	-78.0	-86.0	-105.0
21.26	-10.0	-45.5	-66.0	-79.0	-88.0	-105.0
20.26	-10.5	-44.0	-68.0	-77.5	-85.5	-105.0
19.26	-11.2	-45.0	-68.0	-78.0	-85.0	-105.0
18.26	-10.8	-45.0	-69.5	-77.0	-85.5	-105.0
17.27	-11.7	-45.0	-70.0	-76.0	-85.0	-105.0
16.26	-12.0	-45.0	-70.0	-75.0	-85.0	-105.0
15.26	-13.0	-45.0	-71.0	-76.0	-84.5	-105.0
14.26	-12.5	-44.0	-70.5	-77.5	-85.0	-105.0
13.26	-13.0	-44.0	-71.5	-77.0	-84.0	-105.0
12.26	-12.0	-44.0	-72.5	-77.0	-85.0	-105.0
11.26	-12.0	-43.0	-74.0	-77.0	-84.0	-105.0
10.26	-13.5	-42.0	-74.0	-77.0	-85.0	-105.0
9.26	-13.5	-41.0	-76.0	-77.0	-85.0	-105.0
8.26	-13.5	-40.0	-77.0	-79.0	-84.5	-105.0
7.26	-13.5	-40.0	-79.0	-78.0	-85.0	-105.0
6.26	-13.0	-37.5	-78.0	-77.5	-85.0	-105.0
5.26	-13.5	-35.0	-79.0	-78.0	-85.0	-105.0
4.26	-13.5	-35.0	-80.0	-75.0	-87.0	-105.0
3.66	-16.0	-32.0	-80.0	-84.0	-85.0	-105.0

Transverse Current Phase (f = 300 MHz)

	SLOT NUMBER						
h (cm)	1	2	3	4	5	6	7
28.26	0.5	0.5	0.7	0.8	1.0	0.5	0.5
27.26	0.4	0.4	0.6	0.7	0.8	0.4	0.3
26.26	0.3	0.3	0.4	0.5	0.7	0.4	0.3
25.26	0.2	0.2	0.3	0.4	0.6	0.5	0.2
24.26	0.2	0.2	0.3	0.4	0.5	0.5	0.2
23.26	0.2	0.2	0.3	0.4	0.5	0.6	0.2
22.26	0.3	0.2	0.3	0.4	0.5	0.6	0.2
21.26	0.4	0.2	0.3	0.4	0.5	0.5	0.2
20.26	0.5	0.3	0.3	0.4	0.6	0.5	0.2
19.26	0.5	0.3	0.4	0.4	0.6	0.8	0.3
18.26	0.6	0.4	0.4	0.5	0.7	0.9	0.4
17.27	0.7	0.4	0.5	0.5	0.8	0.9	0.4
16.26	0.8	0.5	0.5	0.6	0.9	1.1	0.4
15.26	0.9	0.5	0.6	0.6	0.9	1.1	0.5
14.26	1.0	0.6	0.7	0.7	1.0	1.2	0.5
13.26	1.0	0.6	0.7	0.7	1.1	1.3	0.4
12.26	1.1	0.7	0.8	0.8	1.1	1.3	0.4
11.26	1.1	0.7	0.8	0.8	1.2	1.4	0.4
10.26	1.2	0.8	0.8	0.8	1.3	1.5	0.3
9.26	1.3	0.8	0.9	0.9	1.3	1.5	0.5
8.26	1.3	0.8	0.9	0.9	1.3	1.5	0.5
7.26	1.4	0.9	1.0	1.0	1.4	1.7	0.6
6.26	1.4	0.9	1.0	1.0	1.5	1.7	0.7
5.26	1.4	0.9	1.0	1.0	1.5	1.7	1.0
4.26	1.5	1.0	1.0	1.0	1.5	1.6	1.3
3.66	1.5	1.0	1.0	1.0	1.5	1.7	1.0

Longitudinal Current Magnitude (f = 300 MHz)

	SLOT NUMBER						
h (cm)	8	9	10	11	12	13	14
28.26	0.8	1.6	1.8	1.2	0.4	0.5	0.3
27.26	0.8	1.4	1.4	1.0	0.5	0.4	0.3
26.26	0.7	1.3	1.2	0.8	0.5	0.3	0.3
25.26	0.7	1.1	1.0	0.9	0.6	0.4	0.2
24.26	0.6	0.9	0.9	0.8	0.6	0.4	0.2
23.26	0.5	0.8	0.9	0.7	0.6	0.3	0.2
22.26	0.5	0.7	0.9	0.7	0.5	0.4	0.3
21.26	0.5	0.6	0.9	0.7	0.5	0.4	0.3
20.26	0.5	0.5	0.8	0.7	0.5	0.4	0.3
19.26	0.5	0.5	0.8	0.6	0.5	0.4	0.3
18.26	0.5	0.4	0.7	0.6	0.5	0.4	0.4
17.27	0.5	0.4	0.7	0.6	0.4	0.5	0.4
16.26	0.5	0.5	0.7	0.6	0.5	0.4	0.4
15.26	0.4	0.6	0.7	0.6	0.5	0.5	0.4
14.26	0.5	0.6	0.7	0.4	0.6	0.5	0.4
13.26	0.5	0.6	0.6	0.4	0.6	0.5	0.4
12.26	0.5	0.7	0.6	0.4	0.4	0.5	0.5
11.26	0.5	0.7	0.5	0.5	0.4	0.5	0.5
10.26	0.4	0.7	0.5	0.4	0.7	0.5	0.5
9.26	0.4	0.7	0.5	0.6	0.7	0.6	0.5
8.26	0.4	0.7	0.6	0.6	0.7	0.6	0.5
7.26	0.2	0.6	0.6	0.7	0.7	0.6	0.5
6.26	0.5	0.7	0.7	0.6	0.7	0.6	0.5
5.26	0.0	0.6	0.5	0.7	0.7	0.6	0.5
4.26	0.0	0.9	0.5	0.6	0.7	0.6	0.5
3.66	0.0	0.9	0.5	0.5	0.7	0.7	0.5

Longitudinal Current Magnitude (f = 300 MHz)

	SLOT NUMBER					
h (cm)	15	16	17	18	19	20
28.26	0.2	0.2	0.3	0.3	0.1	0.2
27.26	0.2	0.1	0.3	0.2	0.1	0.2
26.26	0.3	0.2	0.2	0.1	0.1	0.2
25.26	0.3	0.2	0.2	0.1	0.1	0.2
24.26	0.3	0.2	0.3	0.0	0.1	0.2
23.26	0.3	0.2	0.3	0.0	0.1	0.3
22.26	0.3	0.3	0.3	0.1	0.1	0.3
21.26	0.3	0.3	0.3	0.1	0.1	0.3
20.26	0.3	0.2	0.3	0.1	0.1	0.4
19.26	0.4	0.2	0.3	0.1	0.1	0.4
18.26	0.4	0.2	0.3	0.1	0.2	0.4
17.27	0.4	0.3	0.3	0.2	0.2	0.4
16.26	0.4	0.3	0.4	0.1	0.2	0.5
15.26	0.4	0.3	0.4	0.1	0.2	0.5
14.26	0.5	0.3	0.4	0.2	0.2	0.5
13.26	0.4	0.3	0.4	0.2	0.2	0.5
12.26	0.5	0.3	0.4	0.2	0.2	0.5
11.26	0.5	0.3	0.4	0.2	0.2	0.6
10.26	0.5	0.3	0.3	0.2	0.2	0.6
9.26	0.5	0.4	0.3	0.2	0.2	0.6
8.26	0.5	0.4	0.3	0.2	0.2	0.6
7.26	0.5	0.4	0.3	0.2	0.2	0.6
6.26	0.5	0.4	0.4	0.2	0.2	0.6
5.26	0.5	0.4	0.4	0.3	0.2	0.7
4.26	0.6	0.5	0.3	0.2	0.3	0.7
3.66	0.6	0.4	0.3	0.2	0.3	0.7

Longitudinal Current Magnitude (f = 300 MHz)

	SLOT NUMBER						
h (cm)	1	2	3	4	5	6	7
28.26	54.0	65.0	75.0	70.0	67.5	112.0	134.0
27.26	45.0	62.5	66.0	62.0	60.0	77.0	132.5
26.26	30.0	47.5	60.0	54.0	50.0	84.0	112.0
25.26	8.0	30.0	45.0	40.0	40.0	64.0	100.0
24.26	-19.0	11.0	28.0	26.0	25.0	45.0	79.0
23.26	-50.0	-19.0	9.0	11.0	10.0	25.0	65.0
22.26	-69.0	-37.0	-15.0	0.0	-4.0	17.0	36.0
21.26	-80.0	-56.0	-35.0	-20.0	-15.0	4.0	21.0
20.26	-85.0	-72.0	-54.0	-33.0	-25.0	-1.0	1.0
19.26	-90.0	-80.0	-57.0	-44.0	-34.0	-10.0	-16.0
18.26	-95.0	-84.0	-65.0	-50.0	-41.0	-16.0	-23.0
17.27	-98.0	-88.0	-70.0	-55.0	-46.0	-20.0	-24.0
16.26	-100.0	-90.0	-73.0	-59.0	-50.0	-24.0	-29.0
15.26	-104.0	-94.0	-79.0	-62.0	-55.0	-27.0	-27.0
14.26	-104.0	-95.0	-80.0	-69.0	-57.5	-34.0	-20.0
13.26	-106.0	-95.0	-81.0	-67.0	-57.5	-35.0	-25.0
12.26	-106.0	-97.0	-84.0	-67.0	-60.0	-37.0	-51.0
11.26	-108.0	-98.0	-85.0	-70.0	-60.0	-39.0	-45.0
10.26	-109.0	-100.0	-85.0	-73.0	-62.5	-45.0	-59.0
9.26	-110.0	-100.0	-86.0	-74.0	-63.0	-50.0	-104.0
8.26	-110.0	-100.5	-86.0	-75.0	-65.0	-51.0	-97.0
7.26	-111.0	-101.0	-86.0	-75.0	-66.0	-54.0	-104.0
6.26	-111.0	-101.0	-86.0	-76.0	-66.0	-55.0	-126.0
5.26	-111.0	-101.5	-86.0	-76.0	-66.0	-58.0	-84.0
4.26	-111.0	-104.0	-86.0	-76.0	-66.0	-61.0	-76.0
3.66	-111.0	-104.0	-86.0	-76.0	-66.0	-68.0	-60.0

Longitudinal Current Phase (f = 300 MHz)

	SLOT NUMBER						
h (cm)	8	9	10	11	12	13	14
28.26	125.0	125.0	114.0	106.0	110.0	74.0	39.0
27.26	110.0	120.0	112.0	100.0	96.0	63.0	36.0
26.26	104.0	115.0	110.0	97.0	84.0	54.0	14.0
25.26	94.0	112.0	102.5	94.0	76.0	42.0	6.0
24.26	84.0	108.0	97.5	88.0	71.0	36.0	-11.0
23.26	84.0	104.0	90.0	84.0	58.0	29.0	-14.0
22.26	74.0	99.0	88.0	80.0	55.0	24.0	-14.0
21.26	62.5	94.0	80.0	69.0	52.0	15.0	-15.0
20.26	60.0	85.0	74.0	66.0	45.0	10.0	-19.0
19.26	46.0	76.0	71.0	60.0	41.0	5.0	-21.0
18.26	41.0	60.0	67.5	51.0	35.0	1.0	-24.0
17.27	35.0	44.0	66.0	46.0	34.0	-4.0	-25.5
16.26	25.0	28.0	65.0	45.0	31.0	-12.0	-27.5
15.26	16.0	20.0	74.0	40.0	34.0	-12.0	-29.5
14.26	9.0	16.0	75.0	47.0	15.0	-14.0	-30.5
13.26	7.0	16.0	58.0	41.0	11.0	-15.5	-32.0
12.26	7.0	14.0	50.0	40.0	30.0	-18.0	-34.0
11.26	4.0	11.0	55.0	35.0	32.0	-20.0	-35.0
10.26	-10.0	10.0	64.0	30.0	4.0	-21.5	-35.5
9.26	-24.0	8.5	62.0	26.0	1.0	-25.0	-41.0
8.26	-20.0	5.0	47.0	30.0	0.0	-27.0	-42.0
7.26	-29.0	155.0	30.0	30.0	-2.0	-27.0	-44.0
6.26	0.0	160.0	4.0	16.0	-4.0	-29.0	-44.0
5.26	0.0	158.0	40.0	25.0	-5.0	-30.0	-45.0
4.26	0.0	160.0	41.0	38.0	-5.0	-34.0	-47.0
3.66	0.0	152.0	67.0	48.0	-5.0	-49.0	-50.0

Longitudinal Current Phase (f = 300 MHz)

	SLOT NUMBER					
h (cm)	15	16	17	18	19	20
28.26	25.0	-10.0	-59.0	-85.0	-70.0	-101.0
27.26	4.0	-42.0	-64.0	-75.0	-100.0	-125.0
26.26	-6.0	-50.0	-65.0	-95.0	-104.0	-141.0
25.26	-15.0	-57.0	-75.0	-89.0	-119.0	-156.0
24.26	-20.0	-64.0	-75.0	0.0	-142.5	-177.5
23.26	-25.0	-70.0	-79.0	-165.0	-134.0	-179.0
22.26	-30.0	-75.0	-79.0	-150.0	-149.0	-180.0
21.26	-35.0	-78.0	-74.0	-108.0	-168.0	178.0
20.26	-37.0	-96.0	-75.0	-117.0	-172.0	174.0
19.26	-41.0	-100.0	-77.0	-120.0	-180.0	164.0
18.26	-41.0	-100.0	-77.5	-135.0	150.0	162.5
17.27	-42.0	-94.0	-77.0	-120.0	140.5	161.0
16.26	-44.0	-88.0	-76.0	-139.0	140.5	159.0
15.26	-46.0	-88.0	-76.0	-140.0	142.5	156.0
14.26	-47.0	-90.0	-76.0	-134.0	159.0	155.0
13.26	-48.0	-95.0	-75.0	-127.0	164.0	152.0
12.26	-49.0	-95.0	-75.0	-125.0	170.0	150.0
11.26	-50.5	-95.0	-73.0	-127.0	157.5	149.0
10.26	-52.0	-95.0	-74.0	-128.0	167.5	146.0
9.26	-53.0	-94.0	-72.0	-129.0	165.0	145.0
8.26	-54.0	-91.0	-67.5	-125.0	155.0	143.0
7.26	-56.0	-90.5	-69.0	-125.0	155.5	141.0
6.26	-56.0	-94.0	-67.0	-127.5	156.5	140.0
5.26	-57.0	-92.0	-67.0	-127.0	157.5	140.0
4.26	-57.0	-91.0	-65.0	-125.0	159.0	137.5
3.66	-57.0	-91.0	-58.0	-121.0	156.0	136.0

Longitudinal Current Phase (f = 300 MHz)

	SLOT NUMBER						
h (cm)	1	2	3	4	5	6	7
28.76	9.0	5.4	5.0	6.8	7.4	7.0	6.1
27.76	7.2	4.4	3.7	4.6	5.2	4.9	4.3
26.76	6.7	3.9	3.1	3.7	4.2	4.1	3.6
25.76	6.6	3.7	2.9	3.1	3.6	3.7	3.1
24.76	6.5	3.6	2.7	2.8	3.2	3.4	2.9
23.76	6.3	3.5	2.6	2.6	3.0	3.1	2.7
22.76	6.2	3.4	2.5	2.4	2.8	3.0	2.5
21.76	6.1	3.3	2.4	2.2	2.6	2.9	2.4
20.76	6.0	3.3	2.4	2.2	2.5	2.7	2.3
19.76	5.8	3.2	2.4	2.1	2.3	2.6	2.1
18.76	5.7	3.1	2.3	2.0	2.2	2.6	2.0
17.76	5.6	3.1	2.3	2.0	2.1	2.4	2.0
16.76	5.3	3.0	2.2	1.9	2.0	2.3	1.8
15.76	5.1	2.9	2.2	1.8	1.9	2.2	1.7
14.76	4.9	2.9	2.1	1.7	1.8	2.1	1.6
13.76	4.7	2.7	2.0	1.6	1.7	2.0	1.5
12.76	4.4	2.6	1.9	1.6	1.6	1.9	1.5
11.76	4.2	2.4	1.8	1.5	1.5	1.8	1.4
10.76	3.9	2.3	1.7	1.4	1.3	1.6	1.3
9.76	3.6	2.1	1.6	1.3	1.2	1.5	1.1
8.76	3.2	2.0	1.5	1.1	1.1	1.5	1.0
7.76	2.9	1.8	1.3	1.0	1.0	1.2	0.8
6.76	2.6	1.5	1.1	0.8	0.8	1.1	0.7
5.76	2.2	1.3	1.0	0.7	0.6	1.0	0.6
4.76	1.8	1.1	0.8	0.6	0.4	0.8	0.4
4.16	1.6	1.0	0.7	0.5	0.4	0.8	0.3

Charge Magnitude (f = 400 MHz)

	SLOT NUMBER						
h (cm)	8	9	10	11	12	13	14
28.76	5.5	5.5	5.2	5.0	4.5	3.8	3.4
27.76	4.1	4.1	4.3	3.6	3.4	3.0	2.6
26.76	3.5	3.6	3.4	3.0	2.9	2.6	2.3
25.76	3.2	3.2	3.2	2.8	2.6	2.3	2.0
24.76	3.0	3.0	2.9	2.6	2.4	2.1	1.8
23.76	2.8	2.9	2.7	2.5	2.2	1.9	1.7
22.76	2.7	2.7	2.6	2.3	2.0	1.8	1.6
21.76	2.5	2.6	2.4	2.2	1.9	1.6	1.5
20.76	2.5	2.5	2.3	2.1	1.8	1.5	1.4
19.76	2.4	2.4	2.2	2.0	1.7	1.5	1.3
18.76	2.3	2.3	2.0	1.9	1.6	1.4	1.3
17.76	2.2	2.2	1.9	1.9	1.5	1.3	1.2
16.76	2.1	2.1	1.8	1.8	1.4	1.2	1.1
15.76	2.0	2.0	1.8	1.7	1.4	1.1	1.0
14.76	1.9	1.9	1.6	1.6	1.3	1.1	1.0
13.76	1.8	1.8	1.5	1.5	1.2	1.0	0.9
12.76	1.7	1.6	1.4	1.5	1.1	0.9	0.9
11.76	1.6	1.5	1.3	1.3	1.0	0.9	0.8
10.76	1.5	1.4	1.2	1.2	0.9	0.8	0.7
9.76	1.4	1.3	1.1	1.2	0.9	0.7	0.6
8.76	1.2	1.2	1.0	1.1	0.8	0.7	0.6
7.76	1.1	1.0	0.9	1.0	0.7	0.6	0.5
6.76	1.0	1.0	0.7	1.0	0.6	0.5	0.4
5.76	0.9	0.8	0.6	0.7	0.5	0.5	0.4
4.76	0.7	0.7	0.6	0.8	0.4	0.4	0.3
4.16	0.7	0.7	0.7	0.7	0.4	0.3	0.3

Charge Magnitude (f = 400 MHz)

	SLOT NUMBER					
h (cm)	15	16	17	18	19	20
28.76	4.6	5.4	3.5	2.8	2.8	6.2
27.76	3.7	4.5	3.0	2.4	2.6	5.0
26.76	3.2	4.2	2.9	2.3	2.5	4.6
25.76	3.0	4.0	2.8	2.3	2.4	4.3
24.76	2.8	4.0	2.7	2.3	2.4	4.2
23.76	2.7	3.9	2.7	2.3	2.4	4.1
22.76	2.5	3.9	2.7	2.3	2.4	4.1
21.76	2.4	3.9	2.7	2.3	2.4	4.0
20.76	2.3	3.8	2.6	2.3	2.4	3.9
19.76	2.2	3.8	2.6	2.3	2.3	3.8
18.76	2.1	3.7	2.6	2.3	2.3	3.8
17.76	2.0	3.6	2.5	2.3	2.3	3.7
16.76	1.9	3.5	2.5	2.2	2.3	3.6
15.76	1.8	3.4	2.4	2.2	2.2	3.5
14.76	1.7	3.3	2.3	2.1	2.1	3.4
13.76	1.6	3.1	2.2	2.0	2.1	3.4
12.76	1.5	3.0	2.1	1.9	2.0	3.0
11.76	1.4	2.8	2.0	1.8	1.9	2.9
10.76	1.3	2.6	1.9	1.7	1.7	2.8
9.76	1.2	2.5	1.8	1.6	1.6	2.5
8.76	1.0	2.2	1.6	1.5	1.5	2.4
7.76	0.9	2.0	1.5	1.3	1.3	2.0
6.76	0.8	1.7	1.3	1.2	1.1	1.9
5.76	0.7	1.5	1.1	1.1	1.0	1.6
4.76	0.5	1.3	1.0	0.9	0.8	1.4
4.16	0.5	1.1	0.9	0.8	0.8	1.2

Charge Magnitude (f = 400 MHz)

	SLOT NUMBER						
h (cm)	1	2	3	4	5	6	7
28.76	162.5	177.0	-168.0	-152.0	-145.0	-135.0	-115.0
27.76	161.0	175.0	-170.0	-155.0	-146.0	-135.0	-115.0
26.76	160.5	175.0	-172.0	-157.0	-148.0	-130.0	-116.0
25.76	160.0	174.0	-174.0	-159.0	-150.0	-136.0	-118.0
24.76	160.0	172.0	-175.0	-160.0	-150.0	-137.0	-120.0
23.76	157.5	171.0	-175.5	-160.0	-150.5	-138.0	-120.0
22.76	157.0	170.0	-176.0	-160.0	-151.0	-139.0	-120.0
21.76	157.0	170.0	-177.0	-153.0	-152.0	-140.0	-120.0
20.76	157.5	170.0	-178.0	-164.0	-153.0	-140.5	-122.5
19.76	159.0	170.0	-179.0	-164.0	-154.0	-141.0	-124.0
18.76	159.0	170.0	-179.5	-165.0	-155.0	-142.0	-125.0
17.76	159.0	169.0	-180.0	-165.0	-155.0	-143.5	-125.0
16.76	159.0	169.0	-180.0	-165.0	-155.0	-144.5	-124.0
15.76	159.0	169.0	-180.0	-165.0	-155.0	-144.5	-124.0
14.76	158.5	168.0	-180.0	-165.0	-155.0	-145.0	-126.0
13.76	158.5	168.0	-180.0	-165.0	-156.0	-145.0	-126.0
12.76	158.0	168.0	-180.0	-165.0	-157.5	-145.5	-126.0
11.76	158.0	167.5	-180.0	-165.0	-157.5	-145.5	-127.0
10.76	158.0	167.5	-180.0	-165.0	-158.0	-146.5	-127.0
9.76	158.0	167.5	-180.0	-165.0	-158.0	-148.0	-127.5
8.76	158.0	167.5	-180.0	-166.0	-158.0	-149.0	-128.0
7.76	158.0	167.5	-180.0	-166.0	-158.0	-150.0	-129.0
6.76	158.0	167.5	-180.0	-167.0	-159.0	-150.0	-129.0
5.76	158.0	167.5	-180.0	-167.0	-159.0	-149.0	-129.0
4.76	157.5	167.5	-180.0	-167.0	-159.0	-149.0	-129.0
4.16	156.0	167.5	-180.0	-166.0	-159.0	-144.0	-129.0

Charge Phase (f = 400 MHz)

	SLOT NUMBER						
h (cm)	8	9	10	11	12	13	14
28.76	-85.0	-55.0	-58.0	-74.0	-95.0	-120.0	-142.0
27.76	-89.0	-60.0	-62.0	-75.0	-96.0	-121.0	-143.0
26.76	-90.0	-64.0	-67.0	-76.0	-97.0	-123.0	-144.0
25.76	-94.0	-66.0	-70.0	-78.0	-98.5	-123.0	-144.0
24.76	-95.0	-70.0	-74.0	-80.0	-99.0	-124.0	-144.5
23.76	-98.0	-74.0	-71.0	-84.0	-100.0	-124.0	-144.5
22.76	-100.0	-76.0	-74.0	-84.0	-100.0	-124.5	-144.5
21.76	-101.0	-79.0	-76.0	-86.0	-101.5	-125.0	-144.5
20.76	-104.0	-82.0	-78.0	-87.0	-104.0	-125.0	-144.5
19.76	-105.0	-84.0	-80.0	-89.0	-104.5	-125.0	-144.5
18.76	-105.0	-85.0	-82.0	-90.0	-105.0	-125.5	-144.5
17.76	-106.0	-86.0	-84.0	-91.0	-105.0	-126.0	-145.0
16.76	-108.0	-88.0	-85.0	-92.0	-105.5	-126.0	-145.0
15.76	-108.0	-89.0	-86.0	-94.0	-106.5	-126.0	-145.0
14.76	-108.5	-90.0	-88.0	-95.0	-107.0	-127.0	-145.0
13.76	-110.0	-90.0	-90.0	-96.0	-108.0	-127.5	-145.0
12.76	-110.0	-91.0	-91.0	-97.0	-109.0	-128.0	-145.0
11.76	-111.0	-92.0	-92.0	-98.0	-110.0	-129.0	-145.0
10.76	-111.0	-92.5	-95.0	-98.0	-110.0	-129.0	-145.0
9.76	-113.0	-94.5	-95.0	-100.0	-110.0	-129.0	-145.0
8.76	-114.0	-90.0	-95.0	-100.0	-111.0	-129.0	-145.0
7.76	-114.0	-92.0	-96.0	-100.0	-111.5	-130.0	-145.0
6.76	-115.0	-95.0	-97.0	-100.0	-114.0	-134.0	-145.0
5.76	-115.0	-96.0	-98.0	-100.0	-115.0	-131.0	-145.0
4.76	-115.0	-99.0	-100.0	-101.0	-116.0	-131.0	-143.0
4.16	-115.0	-104.0	-105.0	-101.0	-116.0	-128.0	-144.0

Charge Phase (f = 400 MHz)

	SLOT NUMBER					
h (cm)	15	16	17	18	19	20
28.76	-159.0	170.0	160.0	120.0	74.5	53.0
27.76	-159.0	166.0	160.0	120.0	75.0	53.0
26.76	-159.0	166.0	160.0	120.0	75.0	52.5
25.76	-160.0	165.5	160.0	120.0	75.0	51.5
24.76	-160.0	165.5	160.0	120.0	75.0	51.0
23.76	-160.0	165.5	160.0	119.5	75.0	50.5
22.76	-160.0	165.0	160.5	120.0	75.0	50.5
21.76	-160.0	165.0	160.5	120.0	74.0	50.0
20.76	-160.0	165.0	161.0	120.0	74.0	50.0
19.76	-160.0	165.0	161.0	120.0	74.0	50.0
18.76	-160.	164.0	162.5	120.0	74.0	50.0
17.76	-160.0	164.0	162.0	120.0	74.0	49.5
16.76	-160.0	164.0	163.0	120.0	74.0	49.0
15.76	-160.0	164.0	164.0	120.0	73.0	49.0
14.76	-160.0	162.5	164.0	121.0	73.0	49.0
13.76	-160.0	162.0	164.0	120.5	72.5	48.0
12.76	-160.0	161.0	164.5	121.0	72.5	48.0
11.76	-160.0	160.5	164.5	122.0	72.5	48.0
10.76	-160.0	160.5	164.5	122.0	72.5	48.0
9.76	-160.0	160.5	165.0	124.5	73.0	48.0
8.76	-160.0	165.0	162.5	125.0	73.0	48.0
7.76	-159.0	160.5	163.0	126.0	74.0	48.0
6.76	-160.0	160.0	165.0	127.5	74.0	48.0
5.76	-161.0	160.0	164.0	132.0	75.0	49.0
4.76	-161.0	160.0	165.0	137.5	75.0	50.0
4.16	-161.0	160.0	165.0	124.0	75.0	50.0

Charge Phase (f = 400 MHz)

	SLOT NUMBER						
h (cm)	1	2	3	4	5	6	7
28.26	1.5	2.9	3.7	2.5	2.7	4.4	7.5
27.26	0.9	2.5	3.2	2.0	2.6	3.5	6.5
26.26	0.7	2.1	2.9	1.9	2.4	3.1	5.2
25.26	0.6	1.8	2.6	1.6	2.4	2.9	4.6
24.26	0.5	1.6	2.4	1.5	2.2	2.6	4.0
23.26	0.4	1.5	2.1	1.4	2.1	2.3	3.5
22.26	0.3	1.4	2.1	1.3	2.0	2.1	3.1
21.26	0.4	1.4	2.0	1.1	2.0	2.0	2.9
20.26	0.3	1.2	1.9	1.1	1.9	1.9	2.6
19.26	0.4	1.1	1.7	1.0	1.8	1.8	2.4
18.26	0.4	1.1	1.7	1.0	1.7	1.7	2.2
17.27	0.4	1.0	1.1	1.0	1.6	1.6	1.9
16.26	0.4	0.9	1.5	0.9	1.4	1.5	1.7
15.26	0.4	0.9	1.4	0.8	1.5	1.4	1.7
14.26	0.4	0.8	1.3	0.8	1.3	1.3	1.6
13.26	0.3	0.8	1.2	0.7	1.2	1.2	1.4
12.26	0.3	0.7	1.1	0.7	1.2	1.1	1.3
11.26	0.3	0.7	1.1	0.6	1.2	1.1	1.2
10.26	0.3	0.6	1.0	0.5	1.0	1.0	1.1
9.26	0.3	0.6	0.8	0.5	0.9	0.9	1.0
8.26	0.3	0.5	0.8	0.4	0.8	0.8	0.9
7.26	0.2	0.4	0.7	0.4	0.8	0.7	0.8
6.26	0.2	0.4	0.6	0.3	0.7	0.6	0.7
5.26	0.2	0.4	0.6	0.3	0.6	0.5	0.6
4.26	0.2	0.3	0.4	0.2	0.5	0.4	0.5
3.66	0.1	0.3	0.4	0.2	0.6	0.4	0.5

Transverse Current Magnitude (f = 400 MHz)

	SLOT NUMBER						
h (cm)	8	9	10	11	12	13	14
28.26	7.1	3.7	3.0	6.0	7.5	8.0	6.6
27.26	5.5	3.0	2.4	4.9	6.2	6.6	5.5
26.26	4.6	2.7	1.9	3.9	5.2	5.5	4.9
25.26	4.1	2.2	1.5	3.2	4.6	4.5	4.5
24.26	3.6	1.9	1.1	2.8	4.1	4.4	3.9
23.26	3.2	1.7	1.0	2.3	3.5	3.9	3.4
22.26	2.9	1.6	0.9	2.1	3.1	3.4	3.2
21.26	2.6	1.4	0.7	1.8	2.8	3.4	3.0
20.26	2.4	1.4	0.6	1.7	2.6	3.0	2.8
19.26	2.2	1.2	0.5	1.5	2.4	2.8	2.5
18.26	2.0	1.1	0.5	1.4	2.1	2.5	2.4
17.27	1.9	1.0	0.4	1.3	2.0	2.3	2.3
16.26	1.7	1.0	0.3	1.1	1.8	2.2	2.2
15.26	1.6	0.9	0.3	1.1	1.7	2.1	2.0
14.26	1.4	0.9	0.3	1.0	1.5	2.0	1.8
13.26	1.3	0.9	0.3	0.9	1.3	1.8	1.8
12.26	1.2	0.8	0.3	0.9	1.2	1.6	1.6
11.26	1.1	0.7	0.2	0.8	1.1	1.4	1.5
10.26	1.0	0.6	0.2	0.7	0.9	1.3	1.3
9.26	1.0	0.6	0.2	0.6	0.8	1.1	1.2
8.26	0.8	0.5	0.2	0.5	0.7	1.0	1.0
7.26	0.8	0.5	0.2	0.5	0.6	0.9	0.9
6.26	0.7	0.4	0.3	0.4	0.5	0.8	0.8
5.26	0.6	0.4	0.3	0.4	0.5	0.7	0.7
4.26	0.6	0.3	0.3	0.4	0.4	0.6	0.6
3.66	0.5	0.3	0.3	0.3	0.3	0.5	0.5

Transverse Current Magnitude (f = 400 MHz)

	SLOT NUMBER					
h (cm)	15	16	17	18	19	20
28.26	6.2	5.3	5.6	5.7	5.3	3.2
27.26	5.3	4.7	4.7	4.7	4.5	3.0
26.26	4.3	4.1	4.2	4.5	3.8	2.5
25.26	4.2	3.6	3.6	4.0	3.3	2.3
24.26	3.8	3.2	3.4	3.5	3.3	2.1
23.26	3.4	2.8	3.2	3.1	2.8	2.0
22.26	3.0	2.6	2.9	3.0	2.8	1.9
21.26	2.9	2.4	2.7	2.8	2.5	1.8
20.26	2.6	2.2	2.6	2.6	2.3	1.7
19.26	2.5	2.1	2.3	2.5	2.2	1.6
18.26	2.4	2.0	2.3	2.2	2.0	1.5
17.27	2.3	1.9	2.0	2.1	1.9	1.4
16.26	2.0	1.8	2.0	2.0	1.9	1.3
15.26	1.9	1.7	1.7	1.8	1.7	1.3
14.26	1.8	1.5	1.6	1.6	1.6	1.2
13.26	1.7	1.4	1.6	1.6	1.5	1.1
12.26	1.5	1.3	1.3	1.5	1.4	1.0
11.26	1.3	1.3	1.3	1.3	1.3	1.0
10.26	1.2	1.1	1.2	1.2	1.1	0.9
9.26	1.2	1.0	1.0	1.1	1.0	0.8
8.26	1.1	1.0	1.0	1.0	0.9	0.7
7.26	1.0	1.0	0.9	0.8	0.8	0.7
6.26	0.9	0.9	0.8	0.7	0.7	0.6
5.26	0.5	0.8	0.6	0.6	0.6	0.5
4.26	0.6	0.9	0.5	0.5	0.5	0.3
3.66	0.5	0.7	0.4	0.5	0.4	0.3

Transverse Current Magnitude (f = 400 MHz)

	SLOT NUMBER						
h (cm)	1	2	3	4	5	6	7
28.26	115.0	108.0	94.0	91.0	80.0	153.0	175.0
27.26	107.0	100.0	90.0	105.0	82.0	149.0	171.0
26.26	98.0	95.0	87.5	90.0	84.0	146.0	168.5
25.26	90.0	95.0	85.0	104.0	85.0	143.0	167.0
24.26	80.0	90.5	84.0	100.0	86.5	140.0	165.0
23.26	67.5	89.0	80.0	96.0	86.0	136.0	164.0
22.26	61.0	85.0	80.0	96.0	86.0	135.0	160.5
21.26	54.0	81.0	78.0	95.0	88.0	132.5	158.0
20.26	46.0	81.0	76.0	101.0	86.0	130.0	157.5
19.26	46.0	80.0	75.0	100.0	87.5	129.0	155.0
18.26	42.0	80.0	75.0	99.0	87.0	126.5	152.5
17.27	40.0	77.5	74.0	88.0	85.0	125.0	151.0
16.26	36.0	75.0	72.0	90.0	85.0	123.0	150.5
15.26	36.0	75.0	71.0	94.0	84.0	122.0	150.0
14.26	32.0	74.0	70.0	91.0	82.5	120.0	147.0
13.26	35.0	71.0	70.0	94.0	80.0	119.0	145.5
12.26	38.0	70.0	70.0	88.0	80.0	115.0	145.0
11.26	34.0	70.0	70.0	87.5	80.0	115.5	144.0
10.26	34.0	70.0	70.0	87.5	78.0	116.0	142.5
9.26	29.0	70.0	70.0	84.0	77.0	118.0	142.0
8.26	30.0	69.0	70.0	75.0	74.0	114.0	140.5
7.26	29.0	69.0	70.0	76.0	70.0	118.0	140.0
6.26	35.0	72.0	70.0	65.0	63.0	109.0	140.0
5.26	42.0	74.0	70.0	70.0	54.0	109.0	141.0
4.26	46.0	71.0	70.0	67.0	37.0	107.0	144.0
3.66	44.0	70.0	70.0	70.0	37.0	106.0	145.0

Transverse Current Phase (f = 400 MHz)

	SLOT NUMBER						
h (cm)	8	9	10	11	12	13	14
28.26	-176.0	-168.0	32.0	6.0	-28.0	-52.5	-80.0
27.26	-176.0	-170.0	30.0	5.0	-30.0	-55.0	-81.0
26.26	-180.0	-175.0	30.0	-2.5	-32.0	-57.5	-84.5
25.26	178.5	-180.0	26.0	-8.0	-35.0	-60.0	-87.5
24.26	175.0	-180.0	24.0	-10.0	-37.0	-60.5	-89.0
23.26	174.0	178.0	19.0	-17.0	-40.0	-64.0	-90.0
22.26	168.0	172.5	17.0	-22.0	-41.0	-65.0	-94.0
21.26	166.0	170.0	14.0	-26.0	-45.0	-67.5	-95.0
20.26	164.0	167.5	13.0	-32.0	-47.0	-70.0	-96.0
19.26	161.0	166.0	10.0	-35.0	-49.0	-71.0	-97.5
18.26	158.0	164.0	10.0	-40.0	-50.0	-74.5	-100.0
17.27	156.0	162.0	8.0	-44.0	-54.0	-75.5	-101.0
16.26	156.0	161.0	8.0	-46.5	-55.0	-77.5	-102.5
15.26	155.0	160.0	7.0	-50.0	-55.0	-79.0	-104.0
14.26	152.0	158.0	7.0	-54.0	-57.0	-80.0	-104.0
13.26	151.0	156.0	10.0	-54.0	-58.0	-81.0	-105.0
12.26	150.0	155.0	11.0	-58.0	-59.0	-82.5	-106.5
11.26	149.0	156.0	18.0	-60.0	-59.0	-84.0	-107.5
10.26	147.5	157.0	20.0	-64.0	-60.0	-85.0	-110.0
9.26	147.0	155.0	30.0	-64.0	-60.0	-85.0	-110.0
8.26	145.0	148.0	35.0	-65.0	-55.0	-87.5	-111.0
7.26	144.0	144.0	30.0	-67.0	-60.0	-85.0	-111.0
6.26	145.0	145.0	33.0	-67.0	-55.0	-89.0	-114.0
5.26	147.0	145.0	33.0	-65.0	-75.0	-90.0	-113.0
4.26	149.0	140.0	31.0	-67.0	-74.0	-90.0	-116.0
3.66	147.0	140.0	30.0	-67.0	-70.0	-91.0	-118.0

Transverse Current Phase (f = 400 MHz)

	SLOT NUMBER					
h (cm)	15	16	17	18	19	20
28.26	110.0	-112.0	-141.0	-170.0	125.0	102.5
27.26	112.5	-115.0	-142.5	-171.0	127.5	101.0
26.26	110.0	-117.5	-142.5	-170.0	125.0	102.5
25.26	116.0	-120.0	-144.0	-170.0	125.0	102.5
24.26	119.0	-121.0	-145.0	-170.0	126.0	102.5
23.26	120.0	-121.0	-145.0	-170.0	125.0	102.5
22.26	120.5	-122.0	-145.0	-170.0	125.0	101.0
21.26	124.0	-124.0	-145.0	-170.0	127.5	101.0
20.26	120.0	-126.0	-146.0	-170.0	127.5	100.0
19.26	121.0	-130.0	-146.0	-170.0	127.5	100.0
18.26	124.0	-130.0	-147.5	-171.0	127.5	102.5
17.27	125.0	-134.0	-146.0	-171.0	127.5	102.5
16.26	125.0	-133.0	-148.0	-171.0	125.0	101.0
15.26	125.0	-136.0	-147.0	-171.0	128.0	100.0
14.26	127.0	-136.0	-147.0	-171.0	128.0	100.0
13.26	130.0	-140.0	-150.0	-171.0	130.0	101.0
12.26	129.0	-142.5	-150.0	-172.5	129.0	101.0
11.26	125.0	-144.5	-150.0	-172.5	129.0	101.0
10.26	126.0	-145.0	-150.0	-172.5	129.0	100.0
9.26	134.0	-147.5	-150.0	-172.5	129.0	100.0
8.26	134.0	-150.0	-151.0	-175.0	129.0	100.0
7.26	134.0	-160.0	-152.5	-175.0	127.5	97.5
6.26	135.0	-165.0	-155.0	-175.0	125.0	98.0
5.26	134.0	-172.5	-155.0	-177.5	125.0	97.5
4.26	134.0	180.0	-155.0	-179.0	125.0	94.0
3.66	140.0	180.0	-157.0	-180.0	125.0	95.0

Transverse Current Phase (f = 400 MHz)

	SLOT NUMBER						
h (cm)	1	2	3	4	5	6	7
28.26	1.0	1.3	1.4	1.8	1.8	1.2	1.5
27.26	1.0	1.0	1.2	1.5	1.6	1.3	0.9
26.26	0.8	0.9	1.0	0.9	1.4	1.3	1.0
25.26	0.7	0.7	0.9	0.8	1.2	1.2	0.8
24.26	0.5	0.6	0.8	0.6	1.0	1.0	0.7
23.26	0.4	0.4	0.6	0.5	0.9	0.8	0.7
22.26	0.2	0.3	0.5	0.4	0.7	0.9	0.5
21.26	0.0	0.1	0.3	0.5	0.6	0.8	0.5
20.26	0.2	0.1	0.2	0.4	0.5	0.8	0.5
19.26	0.4	0.2	0.1	0.3	0.5	1.0	0.4
18.26	0.6	0.4	0.2	0.3	0.6	1.1	0.5
17.27	0.8	0.5	0.3	0.4	0.7	1.4	0.6
16.26	1.0	0.6	0.5	0.5	0.8	1.6	0.8
15.26	1.1	0.8	0.6	0.6	1.0	1.8	0.9
14.26	0.3	0.9	0.7	0.7	1.1	2.0	1.0
13.26	1.5	1.0	0.8	0.8	1.2	2.3	1.1
12.26	1.6	1.2	1.0	0.9	1.1	2.4	1.2
11.26	1.8	1.3	1.0	1.0	1.6	2.7	1.3
10.26	1.9	1.4	1.1	1.1	1.9	2.8	1.4
9.26	2.0	1.5	1.2	1.2	1.9	3.0	1.5
8.26	2.2	1.5	1.3	1.3	2.2	3.1	1.6
7.26	2.2	1.6	1.4	1.4	2.2	3.2	1.7
6.26	2.2	1.7	1.4	1.4	2.2	3.2	1.7
5.26	2.3	1.7	1.5	1.5	2.2	3.3	1.8
4.26	2.3	1.7	1.5	1.5	3.2	3.4	1.8
3.66	1.8	1.8	1.5	0.9	2.1	3.5	2.0

Longitudinal Current Magnitude (f = 400 MHz)

	SLOT NUMBER						
h (cm)	8	9	10	11	12	13	14
28.26	2.2	3.2	2.7	1.9	0.4	0.6	0.0
27.26	2.2	2.8	2.5	1.8	0.7	0.5	0.2
26.26	1.8	2.4	2.3	1.5	0.9	0.4	0.2
25.26	1.5	2.2	2.1	1.4	1.0	0.3	0.1
24.26	1.4	2.0	1.8	1.3	1.0	0.3	0.2
23.26	1.2	1.7	1.7	1.2	0.9	0.4	0.3
22.26	1.0	1.5	1.6	1.1	0.8	0.4	0.3
21.26	0.8	1.3	1.5	1.0	0.7	0.4	0.3
20.26	0.7	1.2	1.3	1.0	0.7	0.4	0.4
19.26	0.6	1.1	1.2	0.9	0.6	0.4	0.4
18.26	0.6	0.9	1.1	0.9	0.6	0.4	0.5
17.27	0.5	0.8	1.0	0.9	0.6	0.4	0.6
16.26	0.5	0.8	1.0	0.9	0.6	0.5	0.6
15.26	0.6	0.7	0.9	0.9	0.7	0.6	0.7
14.26	0.7	0.7	0.9	0.9	0.7	0.7	0.7
13.26	0.7	0.7	0.9	1.0	0.7	0.8	0.8
12.26	0.9	0.7	0.9	1.1	0.7	0.8	0.9
11.26	0.9	0.8	1.0	1.1	0.7	0.9	0.9
10.26	1.0	0.8	1.0	1.1	0.8	0.9	0.9
9.26	1.1	0.9	1.0	1.2	0.8	1.0	1.0
8.26	1.2	1.0	1.0	1.3	0.9	1.0	1.0
7.26	1.3	1.0	1.0	1.3	0.9	1.0	1.0
6.26	1.3	1.0	1.1	1.3	0.9	1.1	1.0
5.26	1.4	1.0	1.1	1.3	0.9	1.1	1.2
4.26	1.4	1.1	1.0	1.3	0.9	1.1	1.1
3.66	1.5	1.1	1.0	1.4	0.9	1.2	1.5

Longitudinal Current Magnitude (f = 400 MHz)

	SLOT NUMBER					
h (cm)	15	16	17	18	19	20
28.26	0.2	0.3	0.4	0.4	0.3	0.4
27.26	0.1	0.3	0.3	0.3	0.3	0.3
26.26	0.0	0.2	0.3	0.3	0.2	0.4
25.26	0.1	0.2	0.3	0.3	0.3	0.4
24.26	0.3	0.2	0.3	0.3	0.3	0.4
23.26	0.3	0.2	0.3	0.4	0.3	0.5
22.26	0.3	0.3	0.3	0.3	0.3	0.5
21.26	0.3	0.4	0.3	0.3	0.3	0.6
20.26	0.4	0.4	0.4	0.4	0.3	0.6
19.26	0.4	0.5	0.4	0.4	0.4	0.6
18.26	0.4	0.5	0.4	0.4	0.4	0.5
17.27	0.5	0.6	0.4	0.4	0.4	0.7
16.26	0.5	0.6	0.5	0.4	0.4	0.7
15.26	0.6	0.7	0.5	0.4	0.4	0.7
14.26	0.6	0.7	0.5	0.4	0.4	0.7
13.26	0.6	0.7	0.5	0.5	0.4	0.7
12.26	0.6	0.8	0.5	0.5	0.4	0.8
11.26	0.7	0.9	0.5	0.5	0.6	0.8
10.26	0.7	1.0	0.5	0.5	0.5	0.8
9.26	0.9	1.1	0.6	0.5	0.5	0.9
8.26	0.8	1.0	0.6	0.5	0.5	1.0
7.26	0.9	1.2	0.6	0.5	0.5	1.0
6.26	0.9	1.2	0.6	0.5	0.5	1.0
5.26	0.9	1.3	0.6	0.5	0.5	1.0
4.26	1.0	1.4	0.6	0.5	0.5	1.0
3.66	1.2	1.5	0.6	0.5	0.5	1.1

Longitudinal Current Magnitude (f = 400 MHz)

	SLOT NUMBER						
h (cm)	1	2	3	4	5	6	7
28.26	-42.0	-27.0	-23.0	-19.0	-22.0	-10.0	10.0
27.26	-44.5	-20.0	-22.5	-16.0	-17.0	-15.0	18.0
26.26	-46.0	-22.0	-24.0	-3.0	-21.0	-20.0	13.0
25.26	-48.0	-18.0	-39.0	-3.0	-29.0	-25.0	8.0
24.26	-45.0	-16.0	-30.0	-10.0	-30.0	-32.0	2.0
23.26	-42.0	-12.0	-32.0	-18.0	-44.0	-44.0	-2.0
22.26	-50.0	-6.0	-36.0	-20.0	-47.0	-60.0	-19.0
21.26	0.0	8.0	-41.0	-38.0	-62.0	-80.0	-32.0
20.26	145.0	88.0	-55.0	-70.0	-85.0	-97.0	-48.0
19.26	140.0	118.0	-116.0	-90.0	-104.0	-112.0	-80.0
18.26	136.0	129.0	-165.0	-120.0	-120.0	-122.0	-97.0
17.27	136.0	135.0	180.0	-146.0	-137.0	-132.0	-106.0
16.26	136.0	135.0	172.0	-155.0	-149.0	-139.0	-110.0
15.26	135.0	137.5	166.0	-165.0	-155.0	-144.0	-117.5
14.26	135.0	139.0	165.0	-171.0	-159.0	-147.0	-125.0
13.26	134.0	140.0	161.0	-176.0	-174.0	-150.0	-130.0
12.26	134.0	141.0	160.0	-179.5	-174.0	-151.0	-130.0
11.26	134.0	140.0	160.0	180.0	-174.0	-154.0	-134.0
10.26	133.0	140.0	160.0	176.0	-180.0	-155.0	-137.0
9.26	133.0	140.0	160.0	175.0	179.0	-155.0	-137.0
8.26	134.0	140.0	158.0	175.0	175.0	-156.0	-138.0
7.26	134.0	140.0	156.0	172.5	176.0	-157.0	-140.0
6.26	132.5	140.0	155.0	172.5	172.0	-157.0	-140.0
5.26	132.0	140.0	155.0	171.0	175.0	-158.0	-142.5
4.26	130.5	140.0	154.0	175.0	174.0	-159.0	-142.5
3.66	139.0	140.0	152.5	170.0	-179.0	-159.0	-147.0

Longitudinal Current Phase (f = 400 MHz)

	SLOT NUMBER						
h (cm)	8	9	10	11	12	13	14
28.26	18.0	30.0	32.0	14.5	-5.0	-31.0	0.0
27.26	20.0	30.0	29.0	15.4	-5.0	-26.0	-68.0
26.26	17.0	27.0	25.0	11.5	-5.0	-32.0	-76.0
25.26	16.0	24.0	21.0	7.0	-9.0	-39.0	-100.0
24.26	14.0	20.0	16.0	1.5	-14.0	-36.0	-107.5
23.26	8.0	17.0	13.0	-5.5	-17.0	-50.0	-120.0
22.26	4.0	14.0	8.0	-10.5	-21.0	-64.0	-130.0
21.26	-1.0	9.0	4.0	-17.5	-27.0	-76.0	-135.0
20.26	-8.0	2.5	-2.0	-25.0	-35.0	-89.0	-137.5
19.26	-20.0	-4.0	-9.0	-34.0	-42.0	-99.0	-146.0
18.26	-34.0	-12.0	-16.0	-44.0	-51.0	-125.0	-150.0
17.27	-52.0	-23.0	-24.0	-52.0	-62.5	-130.0	-154.0
16.26	-70.0	-36.0	-33.0	-61.0	-70.0	-130.0	-156.0
15.26	-80.0	-48.0	-42.0	-71.0	-77.5	-130.0	-160.0
14.26	-95.0	-58.0	-50.0	-78.0	-86.0	-131.0	-160.0
13.26	-105.0	-70.0	-59.0	-85.0	-94.0	-135.0	-160.0
12.26	-110.0	-85.0	-65.0	-90.0	-100.0	-138.0	-161.0
11.26	-115.0	-95.0	-72.5	-94.0	-106.0	-140.0	-165.0
10.26	-120.0	-100.0	-80.0	-96.0	-110.0	-145.0	-165.0
9.26	-121.0	-105.0	-84.0	-100.0	-114.0	-145.0	-165.0
8.26	-124.0	-110.0	-86.0	-101.0	-116.0	-145.0	-168.0
7.26	-125.0	-115.0	-88.0	-105.0	-119.0	-145.0	-167.5
6.26	-127.5	-120.0	-91.0	-106.0	-120.0	-145.0	-165.0
5.26	-130.0	-120.0	-92.5	-106.0	-124.0	-145.0	-165.0
4.26	-132.0	-124.0	-94.0	-107.0	-120.0	-145.0	-165.0
3.66	-134.0	-126.0	-92.0	-107.0	-120.0	-145.0	-165.0

Longitudinal Current Phase (f = 400 MHz)

	SLOT NUMBER					
h (cm)	15	16	17	18	19	20
28.26	100.0	-180.0	155.0	96.0	-4.0	-11.0
27.26	90.0	135.0	136.0	75.0	-4.0	11.0
26.26	0.0	180.0	118.0	70.0	-6.0	10.0
25.26	170.0	160.0	120.0	70.0	3.0	5.0
24.26	-175.0	157.5	150.0	65.0	18.0	5.0
23.26	-180.0	155.0	155.0	51.0	42.0	10.0
22.26	-180.0	150.0	155.0	62.5	38.0	16.0
21.26	-174.0	150.0	150.0	65.0	32.0	15.0
20.26	170.0	140.0	161.0	75.0	42.0	12.0
19.26	170.0	140.0	161.0	75.0	14.0	-1.0
18.26	175.0	145.0	155.0	67.5	14.0	-8.0
17.27	172.5	150.0	160.0	76.0	15.0	-6.0
16.26	170.0	155.0	161.0	80.0	15.0	-6.0
15.26	171.0	159.0	161.0	70.0	22.0	-9.0
14.26	170.0	159.0	160.0	72.5	23.0	-10.0
13.26	170.0	152.0	158.0	77.5	30.0	-10.0
12.26	161.0	155.0	150.0	80.0	36.0	-18.0
11.26	165.0	155.0	151.0	85.0	37.0	-16.0
10.26	171.0	157.5	152.5	86.0	31.0	-17.0
9.26	171.0	159.0	151.0	86.0	30.0	-15.0
8.26	170.0	160.0	152.5	86.0	30.0	-12.0
7.26	171.0	160.0	154.0	86.0	32.0	-12.0
6.26	175.0	160.0	157.5	85.0	37.0	-12.0
5.26	175.0	160.0	157.0	84.0	41.0	-14.0
4.26	176.0	160.0	155.0	81.0	39.0	-14.0
3.66	-180.0	160.0	155.0	84.0	39.0	-18.0

Longitudinal Current Phase (f = 400 MHz)

BIBLIOGRAPHY

1. Jane's Fighting Ships, 1971-1972, Sampson Low, Matson & Company, Ltd, London.

2. King, Ronold W.P., The Theory of Linear Antennas, Harvard University Press, Cambridge, Massachusetts, 1956.

3. Cruft Laboratory, Harvard University Report Number 377, Electromagnetic Field Probes, by Haven Whiteside, Oct. 1962.

4. King, Ronold W.P., Tables of Antenna Characteristics, IFI/Plenum, New York - Washington - London, 1971.

5. Dearholt D.W., and Mc Spadden W.R., Electromagnetic Wave Propagation, McGraw-Hill Book Company, New York, 1973.

6. Harvard University Report Number 660, Monopole Antennas On Electrically Thick Conducting Cylinders, by Lee J. Cooper, July 1975.

INITIAL DISTRIBUTION LIST

		No. Copies
1.	Defense Documentation Center Cameron Station Alexandria, Virginia 22314	2
2.	Library, Code 0212 Naval Postgraduate School Monterey, California 93940	2
3.	Assoc. Prof. Richard W. Adler, Code 52Ab Department of Electrical Engineering Naval Postgraduate School Monterey, California 93940	15
4.	Assoc. Prof. Robert W. Burton, LTCOL, USAF Code 52Zn Department of Electrical Engineering Naval Postgraduate School Monterey, California 93940	5
5.	Chairman, Code 52 Department of Electrical Engineering Naval Postgraduate School Monterey, California 93940	1
6.	LT Charles Ristorcelli Commanding Officer USS EXULTANT (MSO-441) FPO New York, N.Y. 02515	3
7.	LT R. B. Burchfield Naval Materiel Command Code MAT034 Washington, D.C. 20360	1
8.	Ray P. Bouchard General Electric Space Division P.O. Box 2500 Daytona Beach, Florida 32015	1
9.	Dr. C. M. Butler Electrical Engineering Department University of Mississippi University, Mississippe 38677	1

10. Walter Curtis — 1
Boeing Aerospace Company
P.O. Box 3999
Seattle, WA 98124

11. Hank DeMattia — 1
Code SEA034
Naval Sea Systems Command
Washington, D.C.

12. Dr. Don Dudley — 1
Electrical Engineering Department
University of Arizona
Tucson, Arizona 87521

13. CDR USACEEIA — 1
ATTN: ACCC-CED-RP
(Edwin F. Bramel)
Ft. Huachuca, Arizona 85613

14. Dennis E. Fessenden — 1
Code SA32
U.S. Naval Underwater Systems Center
New London, CONN 06320

15. Richard G. Fitzgerrell — 1
OT ITS
Boulder, Colorado 80302

16. Dr. R. C. Hansen — 1
17100 Ventura Blvd. (Suite 218)
Encino, California 91316

17. John M. Horn — 1
Naval Electronic Laboratory Center
San Diego, CA 92152

18. CDR E. G. Neely III — 1
Naval Electronic Systems Command
Code PME 108
Washington, D.C. 20360

19. Carmen S. Malagasi — 1
OCTS
Rome Air Development Center
Griffiss AFB, N.Y. 13441

20. MAJ. Anthony Martinez — 1
(LZR) AFCRL
Hanscom Field, MASS 01730

21. J.C.P. McEachen — 1
Naval Sea Systems Command
Code SEA06T
Washington, D.C. 20360

22. L. N. Medgysei-Mitschang — 1
McDonnel Douglas Research Labs
Box 516
St. Louis, MO 63166

23. Dr. E. K. Miller — 1
(L158)
Lawrence Livermore Lab
P.O. Box 808
Livermore, CA 94550

24. Dr. Raj Mittra — 1
Electrical Engineering Department
University of Illinois
Urbana, ILL 61801

25. Ronald Prehoda — 1
Code FVR
Naval Surface Weapons Center
Dahlgren, VA 22448

26. Dr. Jose Perini — 1
Electrical Engineering Department
111 Link Hall
Syracuse University
Syracuse, N.Y. 13210

27. John Potenza — 1
OCTS
Rome Air Development Center
Griffiss AFB, N.Y. 13441

28. Dr. Chuck Ryan — 1
Georgia Institute of Technology
Electrical Engineering Department
Atlanta, GA

29. Dr. John W. Rockway — 3
Naval Electronic Laboratory Center
Code 2120
San Diego, CA 92152

30. Dr. J. H. Richmond — 1
Electroscience Lab
Ohio State University
1320 Kinnear Road
Columbus, Ohio 43212

31. Dr. R. Tanner — 1
Technology for Communications International
1625 Stierlin Road
Mountain View, CA 94043

32. Dr. Fred Tesche — 1
Science Applications, Inc.
P.O. Box 277
Berkeley, CA 94701

33. CDR R. C. Todaro — 1
Naval Electronic Systems Command
Code PME-107
Washington, D.C. 20360

34. Dr. A. Sankar — 1
MS R-1 1144
TRW Systems
1 Space Park
Redondo Beach, CA 90278

35. Carlyle J. Sletten — 1
Code LZ
AF Cambridge Research Lab
Bedford, MASS 91730

36. Dr. B. Strait — 1
Electrical Engineering Department
111 Link Hall
Syracuse University
Syracuse, N.Y. 13210

37. Al Mink (Code 6179) — 1
Naval Ship Engineering Center
Hyattsville, MD 20784

38. Fran Prout (Code 6174) — 1
Naval Ship Engineering Center
Hyattsville, MD 20784

39. Dr. S. Siahtgar (Code 6174) — 1
Naval Ship Engineering Center
Hyattsville, MD 20784

40. Tony Testa — 3
Naval Ship Engineering Center
Hyattsville, MD 20784